#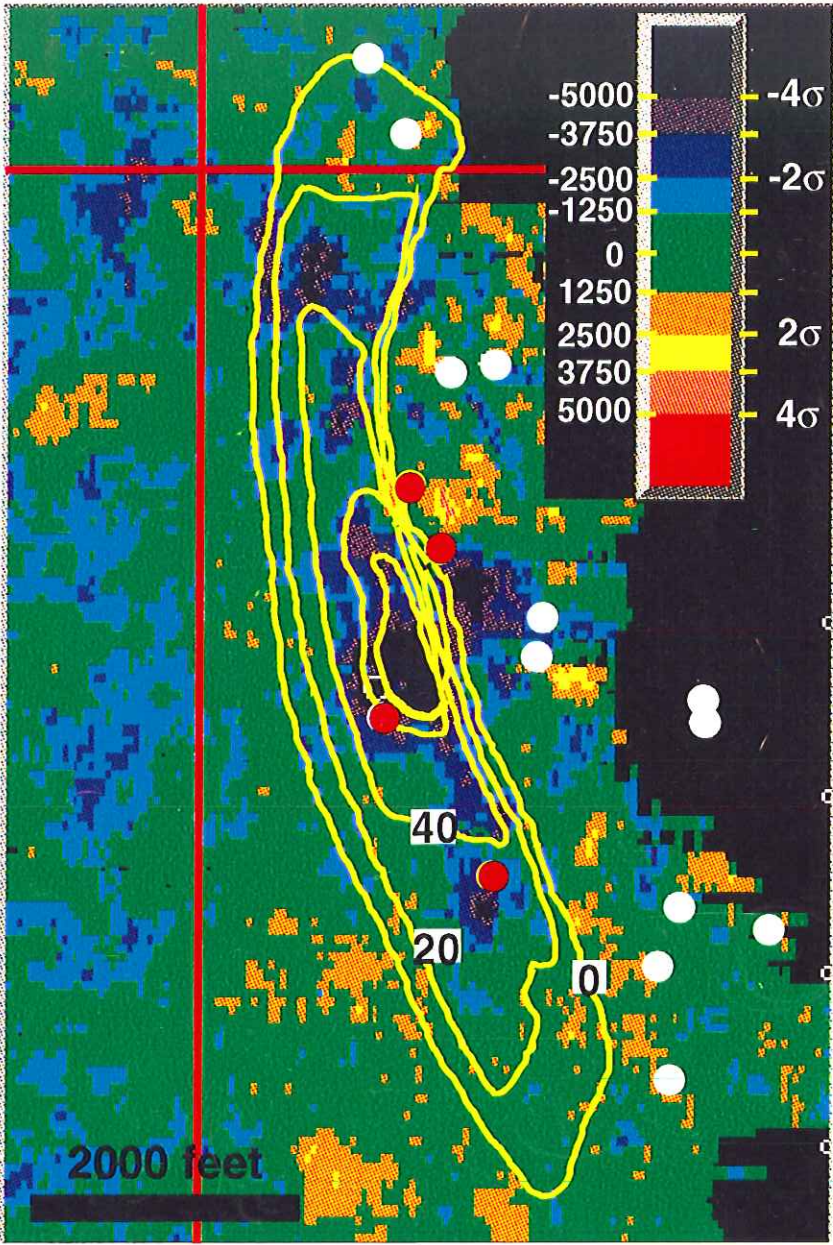 RESERVOIR AND PRODUCTION CHARACTERISTICS OF THE SOUTH TIMBALIER 295 FIELD, OFFSHORE LOUISIANA, WITH COMPARISON TO OUTCROP ANALOGUE AND 4-D SEISMIC RESULTS

ANDREW R. HOOVER

PENNSYLVANIA STATE UNIVERSITY

DECEMBER, 1997

The Pennsylvania State University

The Graduate School

College of Earth and Mineral Sciences

RESERVOIR AND PRODUCTION CHARACTERISTICS OF THE SOUTH

TIMBALIER 295 FIELD, OFFSHORE LOUISIANA, WITH COMPARISON TO

OUTCROP ANALOGUE AND 4-D SEISMIC RESULTS

A Thesis in

Geosciences

by

Andrew R. Hoover

Submitted in Partial Fulfillment
of the Requirements
for the Degree of

Master of Science

December 1997

We approve the thesis of Andrew R. Hoover.

Date of Signature

_____   _____

Peter B. Flemings
Associate Professor of Geosciences
Thesis Advisor

_____   _____

Rudy L. Slingerland
Professor of Geology

_____   _____

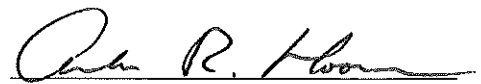Sridhar Anandakrishnan
Research Associate

_____   _____

Paul J. Hicks, Jr.
Assistant Professor of Petroleum and Natural Gas Engineering

_____   _____

James A. Beer
Senior Geologist
Shell Offshore, Inc.
Special Signatory

_____   _____

Lee R. Kump
Professor of Geosciences
Associate Head for Graduate Programs and Research

I grant The Pennsylvania State University the nonexclusive right to use this work for the University's own purposes and to make single copies of the work available to the public on a not-for-profit basis if copies are not otherwise available.

Andrew R. Hoover

Abstract

I characterize a turbidite sand reservoir in South Timbalier block 295, offshore Louisiana, and relate the geologic model to differences between 1994 and 1988 3-D seismic surveys. A field analogue from the Brushy Canyon Formation, west Texas, gives insight toward facies architecture, lateral variability of lithofacies, and development of a turbidite channel complex.

Reservoir and production characteristics of the K40 sand suggest a simple drainage history where a nearly horizontal oil-water contact has moved vertically 80 m between 1988 and 1994. The zone of drainage is associated with strong decreases in seismic amplitude observed from 3-D surveys shot before production (1988) and during production (1994). However, a zone of seismic dimming updip from the inferred oil water contact cannot be explained with the simple drainage model proposed. The K40 sand is an overpressured (0.80 psi/ft.) turbidite reservoir deposited in a slope minibasin in Pliocene time. Wireline and seismic data are used to develop a geologic model for this reservoir. This analysis, combined with production history and log data, indicates that relatively even water sweep was effectively imaged by 4-D seismic in the thickest portion of the reservoir. Swept zones with less than 10 meters of original net pay yield weak difference results, suggesting a threshold of detection.

The Salt Flat Bench outcrop of the uppermost Brushy Canyon Formation is an outcrop that has macro-scale geometry similar to the K40 reservoir. This analogue provides insight into finer-scale variation not imaged with geophysical data. Channel elements include erosional surfaces, silt drapes, and initial and subsequent fill. Sands thicken and

coarsen toward the axis of the channel complex where they are very thickly bedded and medium-grained with large rip-up clasts. Channel margins preserve silts and medium to very fine sands displaying complete Bouma sequences. Topography controlled distribution of sands and steered channels toward the axis of the depositional low where coarser amalgamated sands accumulated. Flanks of the depositional low preserved less energetic events and were less prone to amalgamation by subsequent turbidite events. South Timbalier 295 turbidite sands deposited in a salt-withdrawal minibasin are thicker and amalgamated downdip with levee and channel margin deposits of thinner sands preserved on the flank of the minibasin. From outcrop observations, we predict good lateral and vertical permeability with even water sweep in axial (basinward) sands. Marginal sands with limited vertical permeability due to interbedded shales will have variable water sweep influenced by proximity to producing wells.

Table of Contents

List of Figures

List of Tables

Preface

This thesis characterizes amalgamated turbidite channel reservoirs with the goals of interpreting and evaluating time-lapse (4-D) seismic differences and gaining insight into the control of facies architecture on subsurface fluid flow. The first chapter gives an introduction to 4-D seismic analysis and describes the motivation and reasoning behind the study. The second chapter is a subsurface study of the K40 reservoir, offshore Louisiana, that relates observed seismic differences to a drainage model to evaluate the effectiveness of time-lapse seismic analysis.

Chapter 3 is an outcrop study of the middle Permian Brushy Canyon Formation exposed in the Delaware Basin of west Texas. Investigation of an outcrop analogue to the K40 sand gives insight into facies architecture, depositional processes, and development of turbidite channel complexes.

The appendix to this thesis records work characterizing the K8 sand and relating geologic models to observed seismic differences.

Acknowledgments

There are numerous people and organizations without whom this project could not have happened. I am indebted to Tucker Burkhart, who has been a nearly constant companion over two years as a lab partner and coworker, but also as a roommate and friend. I have leaned on other members of the Penn State Basin Research Group at one time or another throughout my work: Beth Bishop Stump, Amanda Shaw, Steve Nelson, Anil Deshpande, John Metzger, Joe Comisky, Pat Walsh, and John Miley.

I am most grateful to Peter Flemings, who introduced petroleum geology as a world of exciting opportunities. As an advisor, his energy and enthusiasm will be a model for years to come. His confidence in me gave me the confidence to present my research at a national meeting and several industry consortia. I greatly appreciate the time and effort he dedicated to this research.

Jim Beer took a chance and gave me the opportunity to spend a summer with Shell Offshore Inc. in New Orleans as a summer intern. His patience and encouragement as a mentor and friend made my summer experience great. Paul Hicks could always be depended on to provide a pragmatic engineering viewpoint. His insight kept us from fooling him and fooling ourselves.

I thank my wife, Alexa, for her love, support, and encouragement from across campus and from across the country. I am also grateful to my parents and grandparents for allowing

me to follow whatever path I chose, though they may not have known where I was going.

September 2, 1997

Chapter 1

INTRODUCTION

As part of a research initiative to evaluate the feasibility of time-lapse (4-D) seismic analysis, this study characterizes a turbidite water drive reservoir and relates time-lapse seismic differences to a geologic model. 4-D seismic analysis monitors changes in a producing oil reservoir through comparison of multiple 3-D seismic datasets acquired during hydrocarbon production. The principle is that reservoir impedance changes during hydrocarbon production due to water sweep, gas exsolution, and compaction. Time-lapse seismic identifies changes in reflectivity due to these changing fluid saturations.

The second chapter of this thesis describes a complementary study that relates the subsurface characterization of the K40 sand to an outcrop analogue in the west Texas Brushy Canyon Formation. This approach allows us to analyze facies architecture of a turbidite channel complex and see fine-scale variations not resolvable with subsurface data. By observing facies architecture and lateral variations we gain insight into development and geometry of topographically-controlled turbidite channel complexes such as the K40 sand. Understanding facies architecture promotes understanding of reservoir connectivity and drainage patterns.

The 4-D seismic technique has been successfully used to monitor enhanced oil recovery (EOR) projects (Eastwood, 1994; Greaves and Fulp, 1987), but only recently have attempts been made to image water sweep within a reservoir (Anderson et al., 1996). Imaging the seismic response to changing fluid saturations helps geologists and engineers understand producing fields better. Effective monitoring can optimize redevelopment well locations and increase ultimate recovery by identifying zones of bypassed oil and gas.

Understanding initial reservoir geometry and fluid distribution aids 4-D seismic interpretation by identifying regions where production effects can cause seismic changes. Understanding reservoir connectivity, thickness, and structure are basic elements of any reservoir characterization. Production and pressure history record reservoir fluid changes that may cause impedance changes during production. Relating seismic difference results to a sound geologic model is a key to evaluating the effectiveness of time-lapse seismic analysis.

The K40 sand, in the South Timbalier Block 295 field, offshore Louisiana, serves as an excellent subject for a case study that evaluates strengths and limitations of 4-D sesimic. A baseline survey acquired before production (1988) captured initial reservoir conditions. A second survey acquired during production (1994) imaged the reservoir after production of 3.4 million barrels of oil. The K40 sand is a laterally continuous reservoir with strong water drive. These conditions allow us to evaluate the effectiveness of 4-D seismic imaging of water sweep without complications associated with significant pressure decline (see Appendix) and production prior to baseline survey acquisition.

The 3-D seismic surveys used for the K40 study were not acquired with the intention of performing 4-D analysis. As a result, they have different acquisition and processing parameters. In this sense, they are "legacy" datasets. The advantage of legacy datasets is their cost-effectiveness. Data formerly considered out-of-date relative to numerous extensive speculative seismic surveys acquired by geophysical service companies can be re-analyzed and may potentially serve as baseline surveys.

The companion study by Burkhart (1997) uses data from ST295 to investigate normalization methodologies for meaningful comparison of seismic datasets, and characterize signal-to-noise to distinguish meaningful differences. Burkhart (1997) also models the effects of fluid saturations, porosity, and pressure on impedance and compares model results to observed seismic differences.

Communication and understanding between the numerous disciplines related to petroleum geology is a necessity as specialized geophysical techniques such as 4-D seismic influence other disciplines. This thesis incorporates subsurface well log and seismic data, reservoir engineering data, sidewall core analyses, and field work to evaluate a 4-D seismic case study. It has given me the opportunity to think as a geophysicist, reservoir engineer, petroleum geologist, petrophysicist, stratigrapher, and hydrogeologist.

References

Anderson, R.N., A. Boulanger, W. He, Y.F. Sun, L. Xu, and B. Hart, 1996, 4-D seismic monitoring of reservoir production in the Eugene Island 330 Field, Gulf of Mexico, *in* P. Weimer and T.L. Davis, eds., Applications of 3-D seismic data to exploration and production, AAPG Studies in Geology, No. 42 and SEG Geophysical Developments Series, No. 5: AAPG/SEG, Tulsa, p. 9-20.

Burkhart, T., 1997, Time-lapse seismic monitoring of the South Timbalier 295 field, offshore Louisiana: Pennsylvania State University, master's thesis.

Eastwood, J., P. Lebel, A. Dilay, and S. Blakeslee, 1994, Seismic monitoring of steam-based recovery of bitumen: The Leading Edge, p. 242-251.

Greaves, R.J., T.J. Fulp, 1987, Three-dimensional seismic monitoring of an enhanced oil recovery process: Geophysics, v. 52, p. 1175-1187.

Chapter 2

RESERVOIR AND PRODUCTION ANALYSIS OF THE K40 SAND, SOUTH TIMBALIER 295, OFFSHORE LOUISIANA, WITH COMPARISON TO TIME-LAPSE (4-D) SEISMIC RESULTS

Abstract

An integrated analysis of reservoir and production characteristics of the K40 sand (South Timbalier Block 295, offshore Louisiana) tracks the position of a nearly horizontal oil-water contact which moved vertically 80 meters between 1988 and 1994. The zone of drainage is associated with a strong decrease in seismic amplitudes apparent from 3-D surveys shot before production (1988) and during production (1994). However, a zone of seismic dimming updip from the inferred oil-water contact cannot be explained with the simple drainage model proposed. The K40 sand is an overpressured (0.80 psi/ft.) turbidite reservoir deposited in a slope minibasin in Pliocene time. Wireline and seismic data are used to develop a geologic model for this reservoir. This analysis, combined with production history and log data, indicates that relatively even water sweep was effectively imaged by 4-D seismic over most of the reservoir. Zones that are interpreted to have less than 10 meters of original net pay do not record seismic differences. These zones may be bypassed pay or may be below the detection limit.

Introduction

Time-lapse seismic analysis ('4-D' seismic analysis) is a potential reservoir monitoring tool whereby multiple seismic surveys, taken over the life of a producing field, can be used to image fluid movements (Lumley, 1995; King, 1996). This approach aims to resolve changes in seismic amplitude through time that result from impedance changes associated with production. In typical low-impedance Gulf of Mexico sands, decreases in amplitude may result from water sweep or reservoir compaction, while gas exsolution may cause increases in amplitude.

Although there is great interest in time-lapse seismic as a potential industry tool, there have been few case-studies examining its utility. Sibley and Mastoris (1994) used bright spots in a single 3-D survey to detect bypassed reserves in two oil reservoirs of a mature Gulf of Mexico field. They related water swept portions of reservoirs to low seismic amplitudes, and a successful drilling program was based on the correlation of high amplitude zones to areas of undrained pay. Time-lapse 3-D surveys have been performed in Alberta (Eastwood et al., 1994), the North Sea (Johnstad et al., 1993, 1995; Kristiansen et al., 1996), north-central Texas (Greaves and Fulp, 1987), and the Gulf of Mexico (Anderson et al., 1996).

This paper is part of a case study of a Gulf of Mexico reservoir in the South Timbalier Block 295 field (Figure 2.1). Burkhart et al. (1997) present a detailed analysis of changes observed between two seismic surveys and the methodology by which these changes are

imaged. This paper establishes the initial reservoir conditions, describes the reservoir characteristics, and presents a drainage model to predict how the fluid distribution has changed in the subsurface. We then compare our predicted drainage with observations of amplitude change through time in the K40 reservoir. Other time-lapse studies of the ST295 field evaluate seismic differences and relate observed changes to production (Berni et al., 1997; Huang et al., 1997).

We propose a simple drainage history of a horizontal oil-water contact that moves vertically 80 m between 1988 and 1994. Comparison of a 3-D seismic survey shot before production (1988) with one shot during production (April, 1994) reveals a strong decrease in seismic amplitude downdip of producing oil wells. The results of observed seismic differences are consistent to a first-order with predictions from our proposed drainage model, and we evaluate inconsistencies between modeled drainage and seismic differences.

South Timbalier 295 is an excellent location for such a study because there was a 3-D seismic survey shot prior to production (1988) and one after significant production (1994), and there is an extensive log, core, and production data base. In addition this field is over-pressured; consequently the sands are poorly compacted, ideal conditions for amplitude bright spots associated with oil-saturated sands (Clark, 1992). However, these conditions are not atypical; the Gulf of Mexico as a whole is a good location for studies of this fashion. There is extensive historical 3-D seismic coverage and new surveys are being acquired. As a result, the methodologies and results presented here may have broad application.

Background

Mason (1992) provides a detailed history of the field discovery and development which is summarized here. The South Timbalier Block 295 field is located in the Gulf of Mexico 120 miles south of New Orleans (Figure 2.1) in 290 feet of water. This field was discovered in 1984 and limited production began in May, 1989. Total estimated reserves are 25 million barrels of oil and 125 billion cubic feet of gas. Hydrocarbons occur in over 40 pay sands and the main producing reservoirs are the overpressured (pressure gradient = 0.8 psi/ft) late Pliocene-age (c. 3.5Ma) K8, K16, and K40 turbidite sands at depths 3100-3600 m below sea level (Figure 2.2). These reservoirs contain 60% of the field reserves with other reserves mainly in the deeper L and M sands.

The oil-charged K8, K16, K24, and K40 sands each have lower velocity and density than their bounding shales. A 13 Hz synthetic seismogram predicts strong negative amplitudes corresponding to the top of these pay sands (Figure 2.2). The K8 sand, the uppermost of the main reservoirs, is a shaley sand showing a variable blocky to fining-upward gamma ray character in the field. A strong velocity contrast at the top of the interval between poorer quality sands (as judged from the gamma ray response) and overlying shale produces a strong negative seismic amplitude (trough) in the synthetic, matching the response from the actual seismic trace. A prominent underlying peak marks the base of the sand. The K16 sand is the most prolific reservoir in the field with a blocky log character and net sand thickness of 86 feet in the A-13 well. As with the K8, a strong negative seismic

amplitude corresponds to the sand top, which correlates to a point slightly below the maximum negative amplitude in the synthetic.

The K40 sand, consisting of two sand lobes in the downdip part of the field area, produces the third major trough-peak pair. The individual sand lobes are not resolved in the seismic data. The underlying L sands contain oil in some updip wells, but are volumetrically less significant than the K8, K16, and K40 sands. L sands show very weak seismic response, primarily responding to a strong density contrast at the sand top. Virtually no velocity contrast exists at the L sand top; velocities throughout much of the sand are equivalent to the over- and underlying shale.

An east-west seismic line shows pay horizons (K8, K16, K40) and the underlying wet L sands mapped on the seismic troughs (Figure 2.3). Lateral continuity of the reflectors decreases vertically upward. The high degree of lateral seismic continuity of the K40 implies a sheet-like character to the downdip sands. In contrast, the overlying K8 and K16 reservoirs are discontinuous, high-amplitude events, with highly variable log character over distances of 200 meters. We interpret these signals as indicators of channelized deposition. The high amplitudes associated with the K8 masks the underlying K16 in places. Each of the K through L horizons onlap the structural high to the east.

The K sands illustrated in the type log share characteristics common to other turbidite reservoir sands deposited in slope minibasins (Pratson and Ryan, 1994; Balinski et al., 1995; Lund et al., 1978; Holman and Robertson, 1994; and Mahaffie, 1994). A series of high

reservoir quality (30% porosity, 500+ mD permeability) updip-thinning pay sands change upward from laterally continuous amalgamated sands to more discontinuous channelized sands and are capped by a thick bathyal shale. Biostratigraphic markers within the type log interval are dated at 3.64 and 3.47Ma and correlate to a significant (140m) sea level fall (Styzen, 1996). Benthic foraminifera indicate deposition of the K8 through L sands in bathyal to upper bathyal water depths. Holman and Robertson (1994) describe a similar upward trend in sand distribution of the Bullwinkle field (Green Canyon 65) where deeper sands are ponded, internally amalgamated sheets and upper sands are channelized and capped by a bypass section. Accommodation space was likely controlled by sediment loading of the ST296 minibasin and associated salt withdrawal in a manner similar to that described by Pulham (1993). As the basin fills, channels becomes prevalent until accommodation space is filled and sediment bypass occurs (Figure 2.4).

K40 Sand

The goal of this study is to characterize the K40 sand and evaluate how a model of simple drainage history compares with observed seismic amplitude decreases between 1988 and 1994. Seismic data, wireline logs, and sidewall cores are integrated to construct structure maps and net pay maps, predict aquifer distribution, and to delineate the original oil-water contact. With these constraints on reservoir geometry (structure and original net pay) and an assumption of a horizontal oil-water contact, we identify water swept areas for a given position of the contact.

The K40 sand is an excellent reservoir. Sidewall core in the A-22 well shows the K40 to be a silty fine-to-very fine sand (Figure 2.5a). The cleanest, most porous sands contain approximately 5% medium sand, 35% fine and 25% very fine sand. Clay fractions range from 5-10% in these high quality sands. Generally, K40 sands are made up of approximately 20% fine sand, and 30% very fine sand, with silt and clay fractions making up the balance of the distribution. Channel sands have 30% porosity and permeabilities averaging 500mD at producing well locations, and sand quality decreases updip (east) and to the north and south due to the lateral facies variations. The A-28 well, which was drilled downdip through the water leg, demonstrates amalgamation of the K40 sand lobes closer to the basin axis (Figure 2.5b).

Structure maps derived from time-depth conversion of the K40 seismic trough and constrained by well data show 425 m (1400 ft.) of relief from the basin floor to the updip extent of the K40 in the South Timbalier 295 field on the west flank of the structural high (Figures 2.6a, 2.6b). Fault displacement is not evident at the K40 level in the field area, although N-S trending faults occur north of the field in ST275. South of the field is a saddle extending southeast into ST304.

A regional seismic amplitude map (Figure 2.6c), extracted along the K40 trough, reveals lateral variation in seismic response. A prominent lobe of high amplitudes (oriented north-south) in Block 296 corresponds to the thickest portions of the L-K40 isochron (Figure 2.7) which are present in the structural low of the minibasin. The zone of high amplitudes in the western portion of Block 295 corresponds to oil-saturated sands in the field

area. Low amplitudes occur in Block 295 southwest of the field and in the southeast quadrant of Block 296.

The distribution of high seismic amplitude shows variation both along strike (N-S) and in a dip-parallel (E-W) direction (Figure 2.8a). In a dip section, the K40 trough is a laterally-continuous horizon with low seismic amplitude updip of the pay sands (where they are shaled out), high amplitudes in the region of pay sands, and variable moderate-to-low amplitude downdip of the oil-water contact (Figure 2.3). Along strike, low amplitude response is due to shale-out of the K40 north and south of the field. The downdip fit of high amplitudes to structure implies that the seismic data are imaging the oil-water contact at 3468m (11,375 ft.) and that there was an initial column height of approximately 180 m (600 ft.); no wells penetrate this original contact.

We attribute the variation in K40 amplitude to changes in sand thickness and sand quality in downdip regions and to changes in net pay thickness in the field area. We hypothesize that where there are no hydrocarbons present, and the sand has a dual-lobed structure similar to that observed in the producing wells (e.g. A-5, A-25, A-27), there is little or no amplitude response because the water sands of the K40 have approximately the same impedance as their bounding shales. In contrast, further downdip where the lobes thicken, amalgamate, and are cleaner, the impedance of the sand is lower than its bounding shale, and it is imaged as a seismic trough (Figure 2.8a,b). To test this hypothesis, we use seismic modeling to calculate the K40 acoustic response at the A-5 penetration if no hydrocarbons were present. We compare modeled wet sand response from the A-5 well to the oil-

saturated sand response at the A-5 and to the observed wet sand amplitude response at the recently drilled (January 1997) A-28 well (Figure 2.8a).

Fluid substitution uses rock and fluid properties from core analyses, PVT reports, and water analyses in conjunction with Gassmann-Biot relationships (Gassmann, 1951; Biot, 1956) to calculate reservoir velocity and density at different fluid saturations (Flemings et al., 1997). Substitution of 100% water saturation for original oil saturations in the A-5 well and subsequent 1-D seismic modeling using a 13 Hz zero-phase ricker wavelet shows that the K40 top is imaged with very low amplitude where the sand is wet (Figure 2.9). The velocity contrast is eliminated, the density contrast is reduced by 50%. The significance is twofold: first, sands of similar proportion to those found in the producing wells may be present in low-amplitude downdip regions; second, amplitude response is strongly correlated to pay and weakly correlated to sand thickness and/or quality. For these reasons, we judge the amplitude decrease at 3468 m (11,375 ft.) to be the oil-water contact. The prediction of sand in the low amplitude region downdip of high amplitude response is consistent with observations of an apparent seismically-imaged oil-water contact and with the strong water drive that implies a large downdip aquifer.

We next address the question of what causes the moderate amplitudes in the downdip region such as penetrated by the A-28 well (Figure 2.8a). This well drilled through the water leg of the K40 in a region of moderate amplitude (Figure 2.8). In this location, the K40 net sand is 108 feet (twice as thick as the updip A-5), and a blocky gamma ray character indicates a single lobe (Figure 2.8).

Like the K40, the L sand ties to a laterally continuous seismic event across the basin. The A-5 well clearly illustrates a lower impedance (i.e. lower velocity and density) than its bounding shales even though it is water saturated (Figure 2.9). Seismic modeling of the thick (100+ feet) wet, L sands suggests that this impedance contrast will result in a strong amplitude response. Thus, based on the analogy with the underlying L sands, the large downdip amplitudes of the K40 (e.g. at the A-28 well) are interpreted to record thicker and sandier intervals than those present on the basin flank.

K40 Depositional Model

The K40 sand was deposited by gravity driven currents (i.e. turbidites and debris flows) delivering sand from the shelf to a subsiding minibasin centered in Block 296. A facies model of submarine channel deposition dominated by amalgamated channel fill sands and thinly-bedded overbank and levee deposits is used to interpret subfacies of K40 sands interpreted from well logs (Figure 2.10).

Structural influence on sand deposition is evident from the K40 pinch-out against structure to the east. Key observations toward developing a depositional model are: 1) preserved channel and levee-overbank facies in the field area, 2) downdip continuity of seismic horizons, 3) significant downdip amalgamation, and 4) the ease of correlation between downdip sands in the field.

Amalgamation of channel sands was common downdip while paleotopography and decreased local accommodation limited accumulation of sands on basin flanks. This trend results in improved reservoir quality downdip (Figure 2.10). The A-5, A-22, A-25, and A-27 wells penetrate a two-lobe K40 sand in the field area; the downdip A-28 penetrates a single sand with no substantial interbedded shale. Downdip amalgamation of two lobes would lead to pressure communication and strong aquifer support. On the flanks of the minibasin, amalgamation of sands was rare and thinner sands and channel levee facies were preserved.

We propose a conceptual model of the evolution of minibasin sedimentation (Figure 2.4). In early stages of basin filling (equivalent to L and K40 time) the enclosed basin trapped sands and sheet-like sand geometries resulted from extensive channel amalgamation downdip. As the basin filled, channel incision and bypass restricted sand distribution (Figure 2.4).

This model is similar to those of other Plio-Pleistocene turbidite reservoirs in salt-with-drawal minibasins of the Gulf of Mexico where thick reservoir sands in paleo-lows thin and pinch out against structural highs (Holman and Robertson, 1994; McGee et al., 1994; and Mahaffie, 1994). Interpreted subfacies have different sand/shale ratios, permeability, lateral continuity, and grain size characteristics that should strongly influence production rates.

Drainage Model

We observed a linear relationship between 1988 maximum absolute seismic amplitude and net pay thickness observed in well logs (Figure 2.11). We believe this relationship results from the tuning effect (constructive interference in seismic response - Figure 2.11), and we used this to construct a pre-production net pay map. All pay thicknesses are below the tuning thickness for the dominant frequency of 13 Hz at the K40 level (30 m, 100 ft.) and thus lie on the linear portion of the tuning curve. We constrain pay thickness between wells with the correlation, honoring measured pay thicknesses at well locations (Figure 2.13a). The thickest portion of the reservoir lies between the A-5 and A-22 wells. We recognize the presence of error associated with this method of net pay mapping (scatter in Figure 2.11), but seismic data provide the only information on net pay thickness between wells.

We assume a horizontal oil-water contact and use available data to plot the vertical movement of the contact through time (Figure 2.14). The original oil-water contact, defined seismically at 3468 m, begins moving upward in October, 1989 when the A-5 begins limited production. The A-22 well, drilled in June, 1991, images the contact at 3445 m. A 50% water cut in producing wells is used to time the water breakthrough at the A-25, A-27, and A-5 (Figure 2.15a). These observations allow us to develop time-dependent net pay maps as a basis for comparison with seismic difference results (Figure 2.14). The upward movement of the oil-water contact is coincident with decreasing reservoir pressure

and two distinct production rates (Figure 2.14b). The A-25 and A-27 wells, completed in summer 1992, increased production rate and pressure decline for the K40.

The 1994 net pay map (Figure 2.13c) was produced by modifying the original net pay map assuming a flat oil-water contact positioned at 3387 m (11108 ft.), the depth to the base of the perforations in the A-5 well. At the time of the 1994 survey, water breakthrough had begun at updip producing wells (A-5 and A-27) but production rates remained high (>1500 bbls/day). Cased hole log analysis (PDK-100 and TMD) at the A-5 well shows that both lobes of the K40 sand watered out by 1996. A map of drained net pay thickness (Figure 2.13d), obtained by subtracting the 1994 net pay (Figure 2.13c) from the 1988 net pay (Figure 2.13a), shows the volume of reservoir affected by water sweep.

Comparison of Seismic Difference with Drainage Model

The seismic difference map shows amplitude change with green representing little positive or negative change (equivalent to one standard deviation of the differenced seismic volume), blues representing increasingly significant dimming (decreases in seismic amplitude), and yellow and red indicating brightening (increases in seismic amplitude) (Figure 2.16). The green region comprises those data with amplitude changes within one standard deviation (1σ) of the mean (66% of the population). Standard deviation units are used as a measure of signal-to-noise because they represent the statistical significance of the amplitude change at a chosen location (see Burkhart (1997) for more detailed discussion of difference maps).

A coherent zone of significant dimming (>3σ) trends along strike downdip of producing wells. An overlay of the contoured water-swept volume indicates that the thickest portions of the reservoir south and west of the A-27 and A-5 producing wells were swept by 1994 (Figure 2.16). Dimming is strongest where sands are thick. Of the two well penetrations within the dimmed zone, the A-22 well (original 18 m of net pay) shows dimming of -4σ, while the A-25 (11 m of net pay) exhibits change of -3σ. Porosity and initial water saturation in the A-22 and A-25 are similar, so we conclude that the strength of the dimming signal is related to thickness of drained pay sands. The lateral extent of dimming does not match the extent of the swept volume. To the north, dimming follows facies trends rather than original net pay (Figures 2.10e, 2.16). However, with the exception of the anomalous zone southeast of the A-5, most dimming is restricted to the water-swept region. In the discussion we return to the possible origin of updip dimming and address inconsistencies between observed dimming and predicted water sweep.

To evaluate 4-D results, we compare the volume of produced oil with estimated oil volumes for the dimmed area and the water swept region. Recovery factors with assumed porosity and saturation change in turbidite channel facies are displayed in Table 2.1. At the A-22 well, the K40 sand has approximately 32% porosity and 58% recovery based on calculated initial saturations and residual oil saturation measured from sidewall core of the waterswept interval. This results in a recovery factor of 813 bbls/acre-ft (based on the formation volume factor in Table 2.1). This value overestimates overall recovery from the reservoir; we propose recovery factors in Table 2.1 that assume a range of porosity and saturation change for channel sands. Three drainage cases were considered: 1) entire vol-

ume drained with single recovery factor reflecting average recovery across the reservoir, 2)

preferential drainage from channel facies, and 3) drainage restricted to the region of seis-

mic dimming. We justify the facies-specific approach with analysis of the A-10 well, a

K40 producer from the interbedded sand and shale of the levee subfacies (Figure 2.10c).

The first drainage scenario uses a single recovery factor of 740 bbls/acre-ft. for the entire

swept reservoir volume and calculates a volume of 4.142 MMbbls, 20% greater than the

actual produced volume of 3.442 MMbbls through April, 1994 (Table 2.2). Scenario 2

assumes that only highest permeability sands (amalgamated channel facies) are swept dur-

ing production. We assign recovery factors of 842 bbls/acre-ft. to the cleanest (high seis-

mic amplitude) sands and 657 bbls/acre-ft. to other amalgamated channel sands,

calculating a volume of 3.437 MMbbls, very close to actual production. The final drain-

age scenario is based solely on 4-D seismic results and assumes 740 bbls/acre-ft. recovery

for all water-swept sands within the region of seismic dimming (defined as coherent dim-

ming of 2σ or greater) downdip of the A-5 well (shaded area in Figure 2.17). This method

calculates 2.764 MMbbls of produced oil, 20% less than actual production. The calcu-

lated recovery volumes bracket the actual production volume, and indicate that the recov-

ery factors and drainage scenarios approximate drainage in the reservoir between 1988

and 1994 (Figure 2.17). Obviously, this analysis is subject to assumed recovery factors in

the reservoir. Another source of error is uncertainty associated with the seismic delinea-

tion of original net pay.

Oil and water production data from the A-10 well demonstrate the drainage behavior of thin levee sands and illustrate the importance of facies-dependent volumetric analysis for the K40 (scenarios 2 and 3). In 1994 the inferred oil-water contact was at a depth of 3380 m, above the top of the K40 in the A-10 well. Yet, production from these thin levee sands yielded 70,000 barrels of oil at average daily rates of 159 bbls/day before watering out. Initial water cut was 2%, increasing to 40% after five months of A-10 production. These data contrast with producers from K40 amalgamated channel sands that produce at average rates of 1060 bbls/day (A-5), 1200 bbls/day (A-27), and 750 bbls/day (A-25).

Low initial water cut at the A-10 and the ultimate recovery of 70,000 barrels from thin levee sands suggest the model of a horizontal oil-water contact is not applicable in lower-permeability sands. Vertical relief between the base of the A-10 sand and the inferred 1994 oil-water contact is 49 m (160 ft.). The oil-water contact at the onset of A-10 prduction may have been slightly below the base of the perforations, or else the well may penetrate a different compartment of the K40 sand. Either possibility is consistent with the lack of seismic dimming observed around the A-10 well, and both sugest that volumetric calculations should assume preferential drainage from amalgamated channel sands.

Discussion

Comparison of our model of reservoir drainage to observed seismic changes is, to a first order, successful. Dimming is correlated to structure and is compatible with inferred drainage in the higher-quality reservoir sands. Yet, there are several areas where the

observed amplitude changes are not in agreement with our production analysis. These differences may tell us of reservoir behavior not predicted by our reservoir model, or they may reflect limitations in our ability to image drainage. We address three issues: first, dimming updip of production wells; second, the lack of significant dimming in sands thinner than 10 meters; third, significant dimming present in the downdip water leg.

The anomalous updip dimming southeast of the A-5 well is not accounted for by our reservoir model and would require an extraordinary model to pull oil from 50 m (vertical distance) updip of the producing A-5 well (Figure 2.18a). This becomes even less plausible when we see that A-5 water cut is less than 20% at the time of the second survey (April, 1994 - Figure 2.15a). While the geologic model does not provide a reasonable explanation for updip dimming, Burkhart (1997) shows that the overlying K8 sand is a zone of dramatic brightening which may result from gas exsolution. Thus, one possible interpretation is that the dimming observed at the K40 level is due to attenuation of K40 seismic response by gas exsolution within the overlying K8 reservoir (Figure 2.18b).

The absence of significant dimming in sands thinner than 10 meters suggests either that bypassed pay is present in lower permeability facies away from producing wells, or drainage in sands thinner than 10 m is below the detection limit of 4-D seismic. In the former case, producing wells may not be draining lower permeability facies in thin sands at the north and south limits of the reservoir, and 4-D seismic is identifying bypassed pay. This hypothesis is supported by the correlation of dimming with facies distributions (Figures 2.10e, 2.16) and by the A-10 well that produced 70,000 bbls of oil despite being structur-

ally below the 1994 oil-water contact inferred from A-5 and A-27 production data. However, unchanged areas along the narrow band of net pay trending along strike are closer to producing wells, have better sand quality and may be drained.

If some of these thin sands are drained, this implies water sweep in sands less than 10 meters thick may be below the detection limit of these 4-D seismic data. Specifically, in sands less than 10 m thick, the observeable change in amplitude due to water sweep may be too small to be resolveable relative to the noise present between in the differenced data. This is shown schematically in Figure 2.18 where the change in amplitude due to water sweep is modeled for progressively thinner sands. Burkhart (1997) discusses methods of quantifying the detection limit for 4-D seismic datasets.

We emphasize that these thinner sands are within the resolution of the seismic data used to delineate net pay (Figure 2.13a). Error associated with our method of net pay mapping should also be considered when interpreting volumetric calculations and seismic differences in thin sands.

While we see no seismic change in some areas of the reservoir thought to be water swept, we also observe significant amplitude decreases in the K40 water leg where production-related changes should be minimal (Figure 2.15). Dimming may occur where reduced fluid pressure causes reservoir compaction; however, we are not satisfied with this explanation in the case of the K40 sand, strongly supported by an extensive aquifer. Other possible causes for dimming in the water leg include shadowing effects from overlying

reservoirs or a fundamental difference between imaged reflections in the two 3-D surveys. Although these possiblities may be factors in the K40 water leg, Burkhart (1997) uses statistical methods to filter seismic difference data and shows that K40 differences outside the reservoir are not meaningful.

The K40 shows a strong drainage signal in seismic difference results (Figure 2.15). However, because acquisition, processing, and attenuation effects of overlying reservoirs may contribute to seismic differences, further work is needed to analyze and isolate the influence of these effects. Careful 4-D analysis of all stacked pay sands can aid in distinguishing contributing reservoir effects, and reprocessing of original seismic data sets may eliminate acquisition and processing effects on seismic differences. In general, more comprehensive seismic modeling may address poorly-understood seismic differences, and refine 4-D seismic interpretations. These methods, however, are beyond the scope of this study.

Any caveats concerning 4-D seismic analysis should not overshadow observations of very significant seismic amplitude decreases observed in the K40 downdip of producing wells and the possible identification of bypassed pay in lower permeability sands. These results indicate that pre-production seismic surveys, not originally intended for use in 4-D seismic analysis, have value as baselines for seismic monitoring studies without costly reprocessing. Further advances in normalization techniques may eventually make such monitoring routine and highly cost-effective.

Conclusions

The K40 sand is a turbidite reservoir that demonstrates remarkable compatibility between seismic amplitude decreases and predicted water sweep after five years of production. The drainage model assuming a horizontal oil-water contact and even sweep of the reservoir is consistent with seismic amplitude changes from 1988 and 1994. Dimming is most significant where the thickest sands have been drained. Unchanged amplitudes in reservoir sands indicate the presence of bypassed pay or alternatively reflect the detection limit of the 4-D tool in this field. Overall, the K40 demonstrates the potential of 4-D seismic analysis, although questions remain regarding the influence of overlying horizons.

References

Anderson, R.N., A. Boulanger, W. He, Y.F. Sun, L. Xu, and B. Hart, 1996, 4-D seismic monitoring of reservoir production in the Eugene Island 330 Field, Gulf of Mexico, *in* P. Weimer and T.L. Davis, eds., Applications of 3-D seismic data to exploration and production, AAPG Studies in Geology, No. 42 and SEG Geophysical Developments Series, No. 5: AAPG/SEG, Tulsa, p. 9-20.

Balinski, P.W., D.T. McGee, D.S. Pfeiffer, and R.D. Shew, 1995, Reservoir characterization of the "S" Sand Auger Field, Garden Banks 426, 427, 470, and 471, *in* R.D. Winn Jr., and J.M. Armentrout, eds., Turbidites and associated deep-water facies: SEPM Core Workshop No. 20, p. 75-93.

Berni, A.J., J.C. Barros, M. Kohli, T.A. Stellman, and G.E. Purdy, 1997, On the use of data transformation filters in time-lapse imagery: OTC paper 8291 in 1997 Offshore Technology Conference p. 153-160.

Biot, M.A., 1956, Theory of propagation of elastic waves in a fluid-saturated porous solid, 1. Low-frequency range, 2. Higher frequency range: Acoust. Soc. America Journal., v. 28, p. 168-191.

Burkhart, T., A. R. Hoover, and P.B. Flemings, 1997, Time-lapse seismic monitoring of the South Timbalier 295 field, offshore Louisiana: Society of Exploration Geophysicists 67th Annual Meeting, Dallas, expanded abstract.

Burkhart, T., 1997, Time-lapse seismic monitoring of the South Timbalier 295 field, offshore Louisiana: Pennsylvania State University, M.S. thesis.

Clark, V. A., 1992, The effect of oil under in-situ conditions on the seismic properties of rocks: Geophysics, v. 57, p. 894-901.

Eastwood, J., P. Lebel, A. Dilay, and S. Blakeslee, 1994, Seismic monitoring of steam-based recovery of bitumen: The Leading Edge, p. 242-251.

Flemings, P.B., T. Burkhart, A.R. Hoover, P.J. Hicks, 1997, Impedance change in the K40 sand, South Timbalier 295, offshore Louisiana: Applications to 4-D seismic analysis: Society of Exploration Geophysicists 67th Annual Meeting, Dallas, expanded abstract.

Gassmann, F., 1951, Elastic Waves Through a Packing of Spheres: Geophysics, v. 16, 673-685.

Greaves, R.J., T.J. Fulp, 1987, Three-dimensional seismic monitoring of an enhanced oil recovery process: Geophysics, v. 52, p. 1175-1187.

Holman, W.E., S.S. Robertson, 1994, Field Development, depositional model, and production performance of the turbiditic "J" sands at prospect Bullwinkle, Green Canyon 65 Field, outer-shelf Gulf of Mexico, in P. Weimer, A.H. Bouma, and B.F. Perkins, eds., Submarine Fans and Turbidite Systems: GCSSEPM Foundation 15th Annual Research Conference, p. 139-150.

Huang, X., L. Meister, and R. Workman, 1997, Reservoir characterization by integration of time-lapse seismic and production data: SPE paper 38695 in SPE Annual Technical Conference and Exhibition, San Antonio, TX.

Johnstad, S.E., R.C. Uden, and K.N.B. Dunlop, 1993, Seismic reservoir monitoring over the Osberg Field: First Break, v. 11, p. 177-185.

Johnstad, S.E., R.H. Seymour, and P.J. Smith, 1995, Seismic reservoir monitoring over the Oseburg Field during the period 1989-1992: First Break, v. 11, p. 169-183.

King, G.A., 1996, 4-D seismic improves reservoir management decisions: World Oil, v. 217, p. 1-8.

Kristiansen, P., O. Holberg, and D. Ireson, 1996, Reservoir characterization and monitoring utilizing seismic methods: a flexible multi-disciplinary approach, in J.A.

Pacht, R.E. Sheriff, and R.F. Perkins, eds., Stratgraphic Analysis Utilizing Advanced Geophysical, Wireline and Borehole Technology for Petroleum Exploration and Production: GCSSEPM Foundation 17th Annual Research Conference, p. 167-174.

Lumley, D.E., 1995, Seismic time-lapse monitoring of subsurface fluid flow: Dissertation, Stanford University.

Lund, J.W., J.S. King, R. Berlitz, and J.A. Gilreath, 1978, Pre-platform exploration of High Island Blocks A-560 and A-561: Transactions of the 28th annual GCAGS convention, v. 28, p. 273-294.

Mahaffie, M.J., 1994, Reservoir classification for turbidite intervals at the Mars discovery, Mississippi Canyon 807, Gulf of Mexico, in P. Weimer, A.H. Bouma, and B.F. Perkins, eds., Submarine Fans and Turbidite Systems: GCSSEPM Foundation 15th annual research conference, p. 233-244.

Mason, E.P., 1992, Reservoir geology and production performance of turbidite sands at South Timbalier 295 Field, offshore Louisiana: Transactions of the 42nd annual GCAGS convention, Jackson, MS, v. 42, p. 267-278.

Pratson, L.F., and W.B.F. Ryan, 1994, Pliocene to recent infilling and subsidence of intraslope basins offshore Louisiana: AAPG Bulletin, v. 78, p. 1483-1506.

Pulham, A.J., 1993, Variations in slope deposition, Pliocene-Pleistocene, offshore Louisiana, northeast Gulf of Mexico, in P. Weimer, and H. Posamentier, eds., Siliciclastic Sequence Stratigraphy: AAPG Memoir 58, p. 199-233.

Sibley, D.M., 1994, Rethinking conventional field development: 3D shows direct detection of bypassed oil reserves: SPE paper 28719 in SPE International Petroleum Conference & Exhibition of Mexico, Veracruz, Mexico.

Styzen, M.J., 1996, Late Cenozoic chronostratigraphy of the Gulf of Mexico: Gulf Coast Section SEPM, chart.
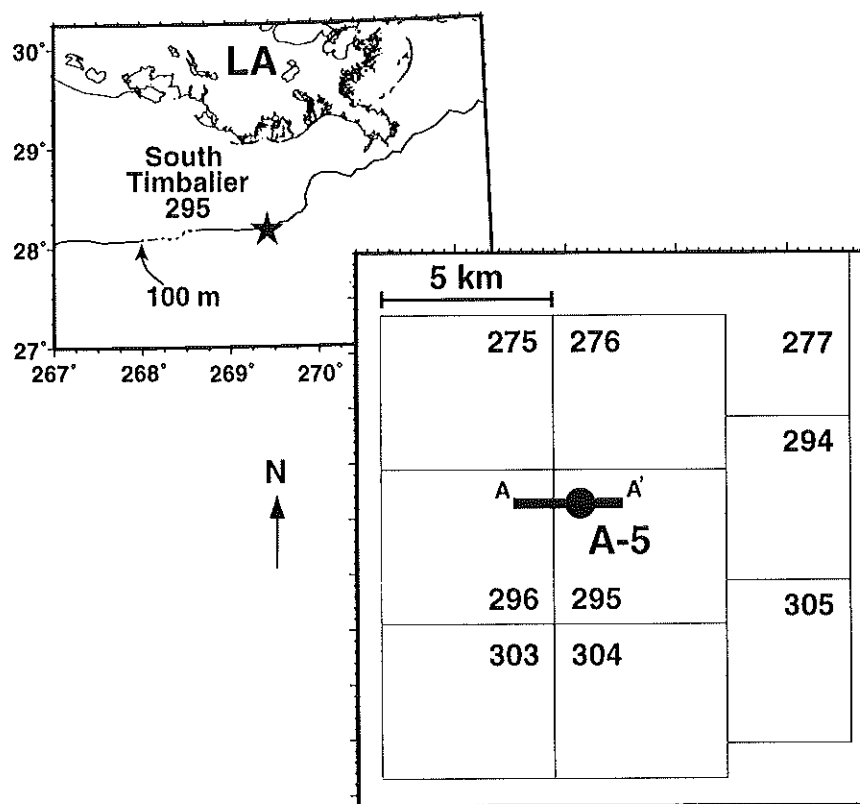
Figure 2.1. Basemap of South Timbalier block 295 field area, located 120 miles south of New Orleans in 290 feet of water. Operated by Shell Offshore, production is from blocks 295 and 276. Line A-A' is seismic line displayed in Figure 3; the circle marks the location of the A-5 well penetration of the K40 sand.

SHELL A-5
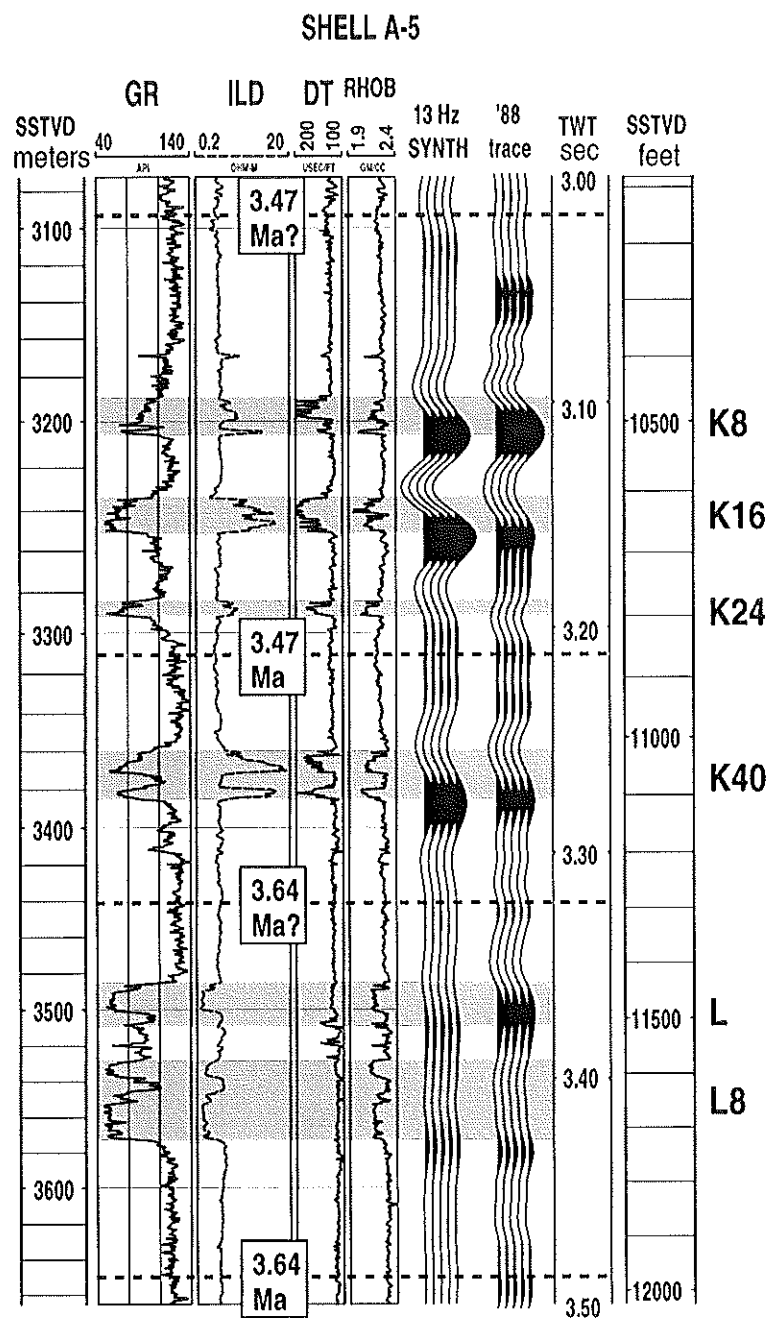
Figure 2.2. Type log of main pay sands, K8, K16, and K40, from the A-5 well shows stacked turbidite sands at 3200-3600 m subsea depth (10000-12000 ft.). Open hole logs, from left to right, are gamma ray, deep induction, sonic, and density. A 13 Hz synthetic seismogram ties to the 1988 seismic data trace extracted along A-5 well path and sand tops correspond to seismic troughs.
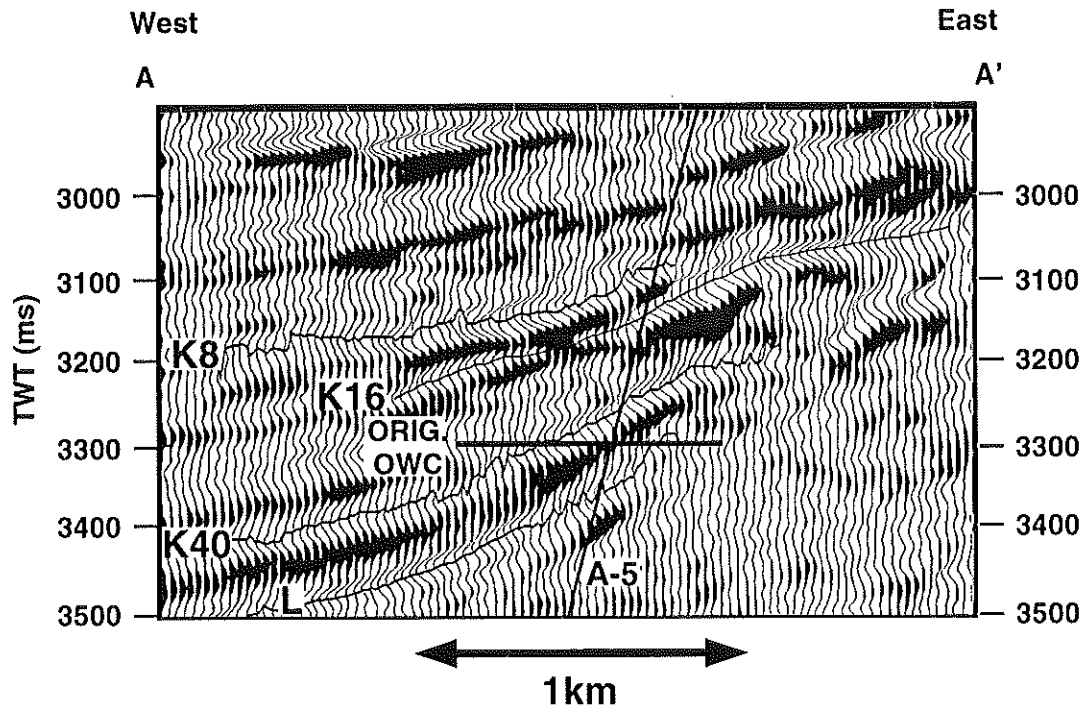
Figure 2.3. West-East seismic line (1994 survey) through the A-5 well penetration of the K40 shows the stacked turbidite pay horizons at 3.0-3.3 seconds. All horizons pinch out updip against the structural high to the east. K40 and L show good continuity, K8 and K16 do not. K8 masks the K16 signal over significant areas. The oil-water contact corresponds to a significant amplitude change in the downdip K40.
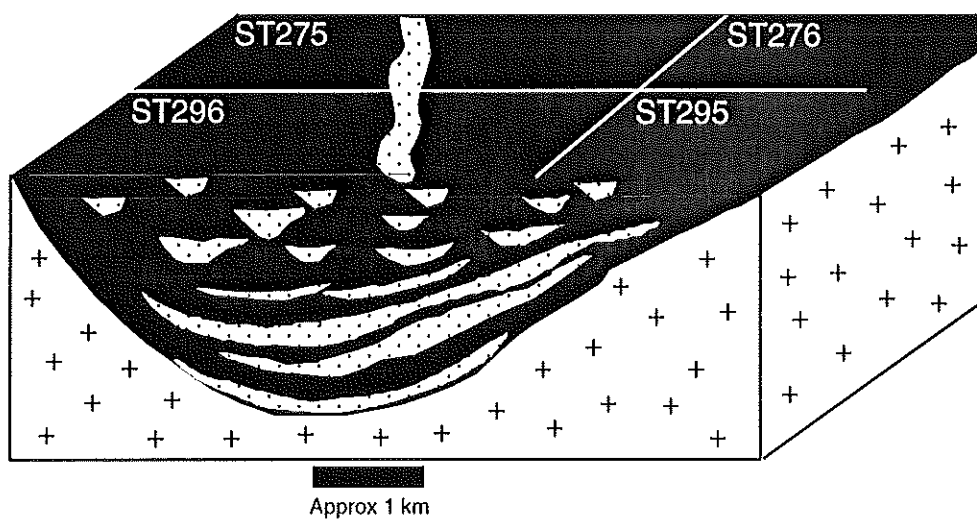
Figure 2.4. Conceptual model of L through K sand distribution in ST296 minibasin illustrating decreasing lateral continuity of sands upward in the section.
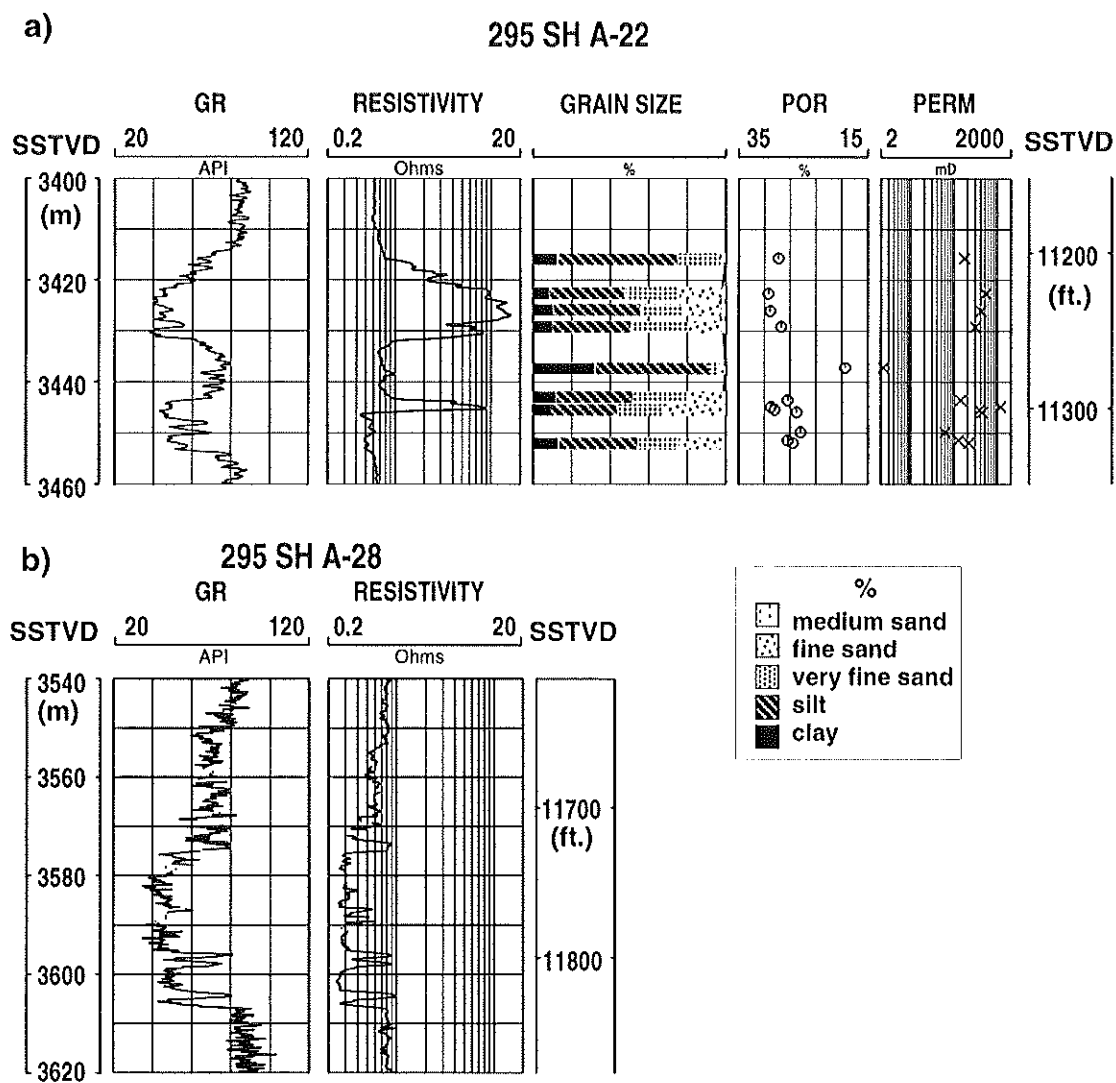
Figure 2.5. a) Log response and grainsize analysis of the K40 sand in the A-22 well. Proportions of sand, silt, and clay size fractions from sidewall core are depicted with bars. Porosity was measured from a total fluids analysis of sidewall core and permeability estimated from a relationship of porosity and grainsize distribution. The oil-water contact evident from the resistivity log reflects the position of the contact in June, 1991 after 20 months of production from the A-5 well. b) A-28 well log imaging amalgamated K40 sand downdip.
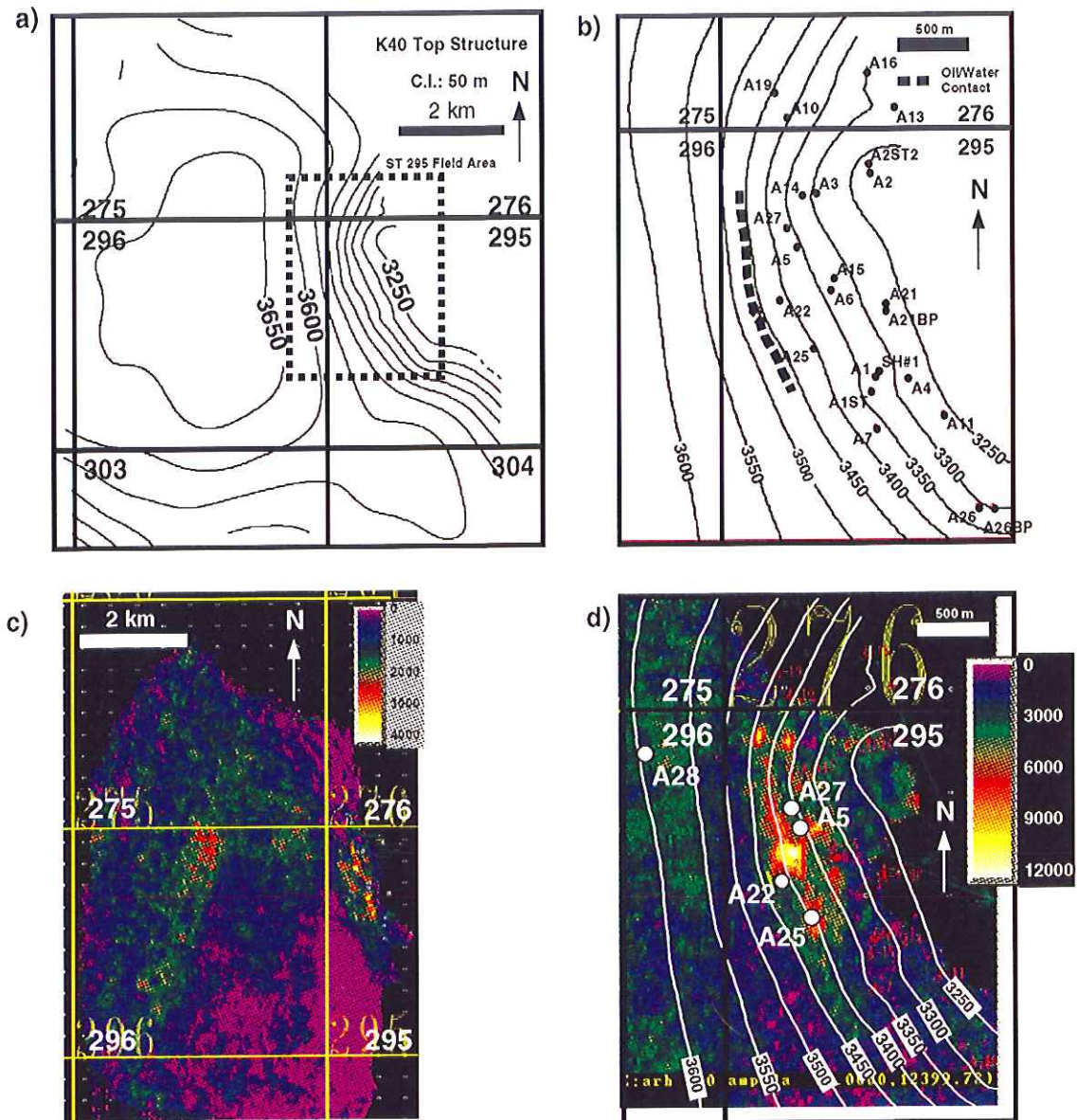
Figure 2.6. Regional (a, c) and field (b, c) structure and amplitude maps. a) Regional structure map shows minibasin centered in ST296 and vertical relief of 425 m (1400 ft.) on the K40 between basin center and top of structure to the east. This structural configuration influenced sedimentation of the K8 through L sands. b) Field structure map on top K40 shows an oil-water contact, inferred from seismic at 3468 m (11375 ft.) subsea depth. Producing wells are A-5, A-25 and A-27. Oil column height is 180 m (600 ft.). c) Regional 1994 maximum negative amplitude map of the K40 horizon shows three zones of high amplitude. The zone to the east corresponds to the field area (Figure 6d), the zones to the west appear to indicate lobes of thick amalgamated sands fanning southward from ST275. Amplitude maps from the 1994 survey define downdip amplitudes more clearly than the 1988 survey. d) Maximum negative amplitude in the field area extracted over 40ms window centered on K40 trough from pre-production (1988) survey.
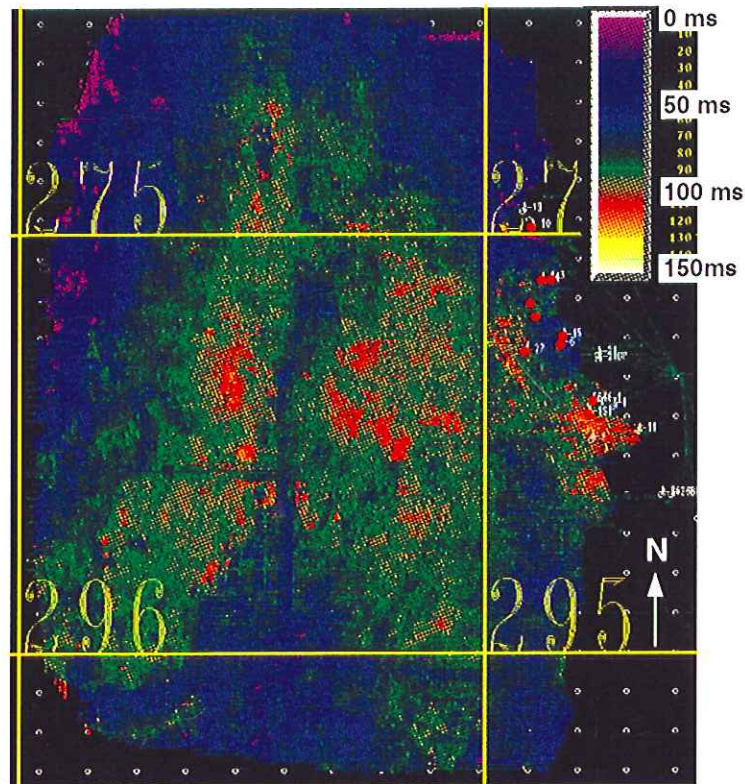
Figure 2.7. Isochron from 1994 survey of L-K40 interval shows thick intervals (90-120ms - approx. 120 m) in the structural lows of ST296. Isochron is the travel time difference between the L sand structure (in ms) and the K40 sand structure. Thick zones correspond to high amplitude regions (Figure 6c), suggesting deposition responded to local topography on the L horizon at the time of K40 deposition.
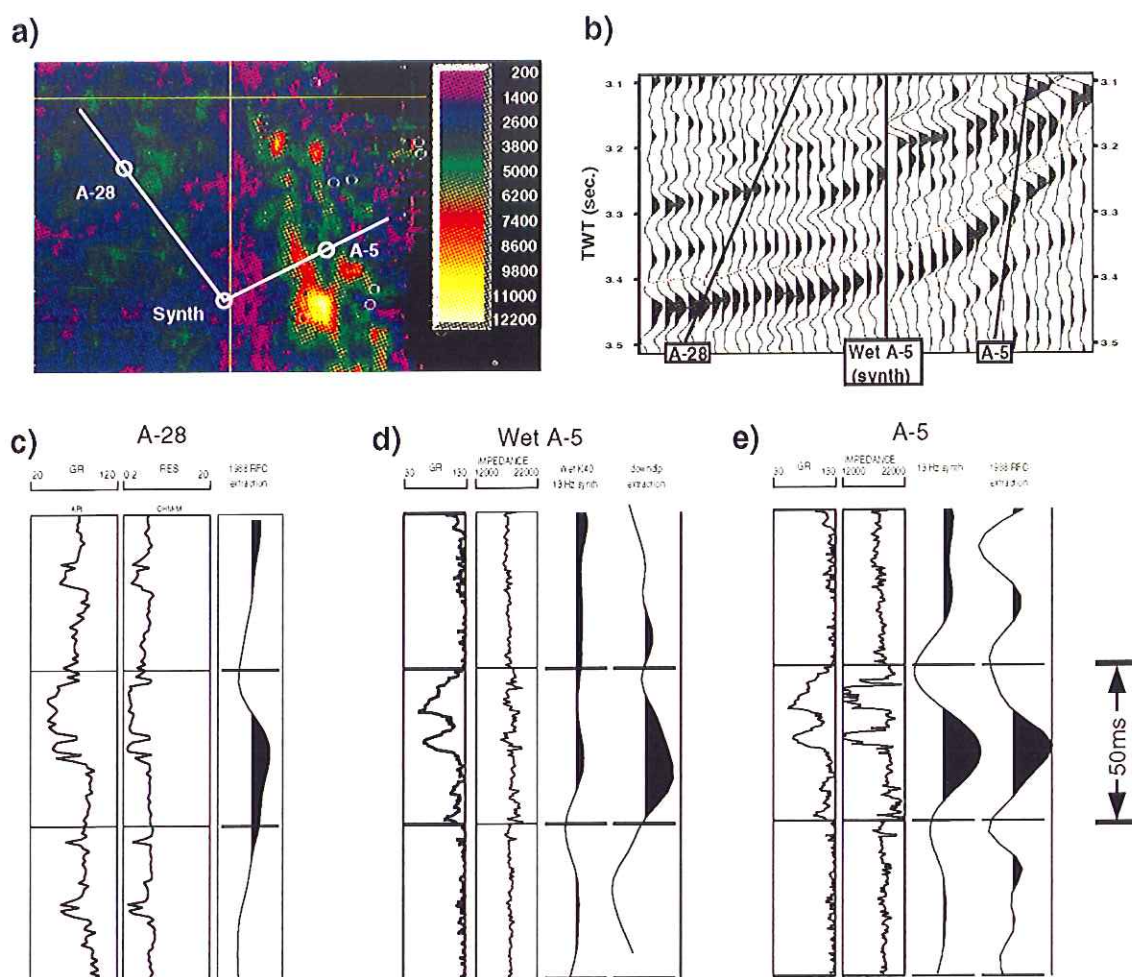
Figure 2.8. Correlation of amplitude response to sand thickness. a) Maximum absolute amplitude extracted over 40ms window centered on K40 trough (1988 survey) shows high amplitude in oil-saturated regions (A-5 well), very low amplitude along the ST295-296 lease line, and moderate amplitude downdip to the west (A-28). b) Seismic line through A-28 and A-5 wells shows amplitude variation along the dip profile. Mapped horizon is K40 trough. c) Gamma ray and resistivity logs from A-28 well drilled through K40 water leg. RFC trace (1988) extracted at this location shows moderate amplitude. d) Gamma ray and modeled impedance from the A-5 well assuming 100% water saturation. The weak impedance contrast is consistent with low amplitudes observed along the lease line. 13 Hz zero phase synthetic shows no trough at wet K40 top, extracted seismic trace has very weak negative amplitude at the K40 top. e) A-5 well with original impedance (oil saturated) and high seismic amplitude. Synthetic seismic trace (13 Hz, zero phase ricker wavelet) and extracted trace (1988) show strong negative amplitude correlating to K40 top.
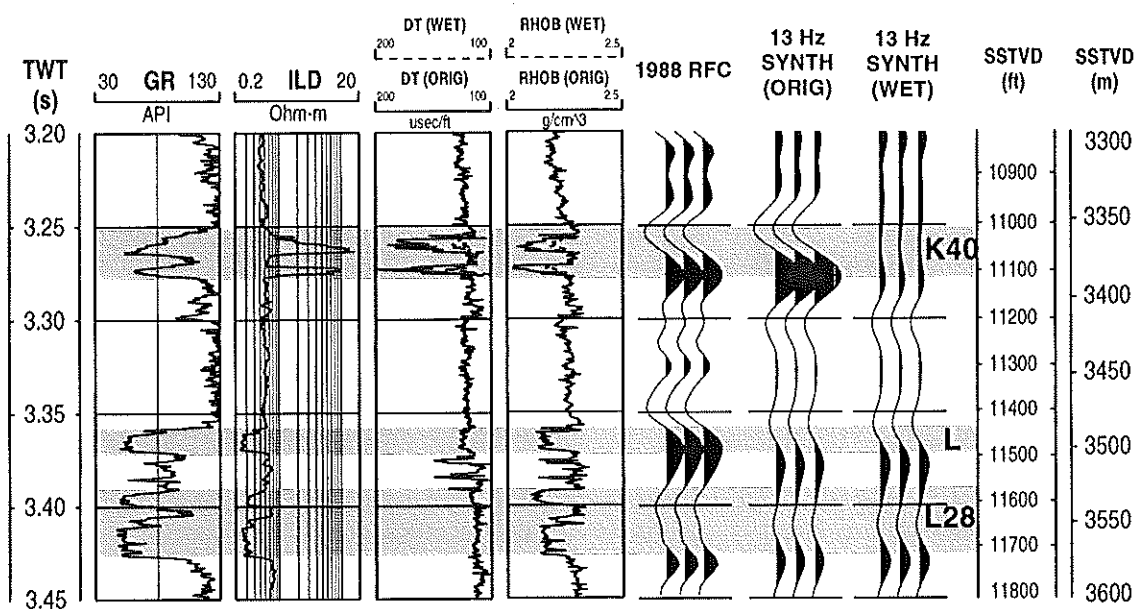
Figure 2.9. Results of fluid substitution in A-5 well simulating wet K40 seismic response. Original open hole logs (from left to right) are: gamma ray, deep induction, sonic, and density. Recalculated sonic and density logs assuming 100% water saturation are displayed as dotted lines. Seismic traces are the 1988 RFC seismic data extracted along the well path, the synthetic generated from original open hole logs, and the synthetic assuming 100% water saturation in the K40. Note the lack of significant amplitude associated with the wet K40 sand. Compare these results to the thick, wet, blocky L and L28 sands underlying the K40.
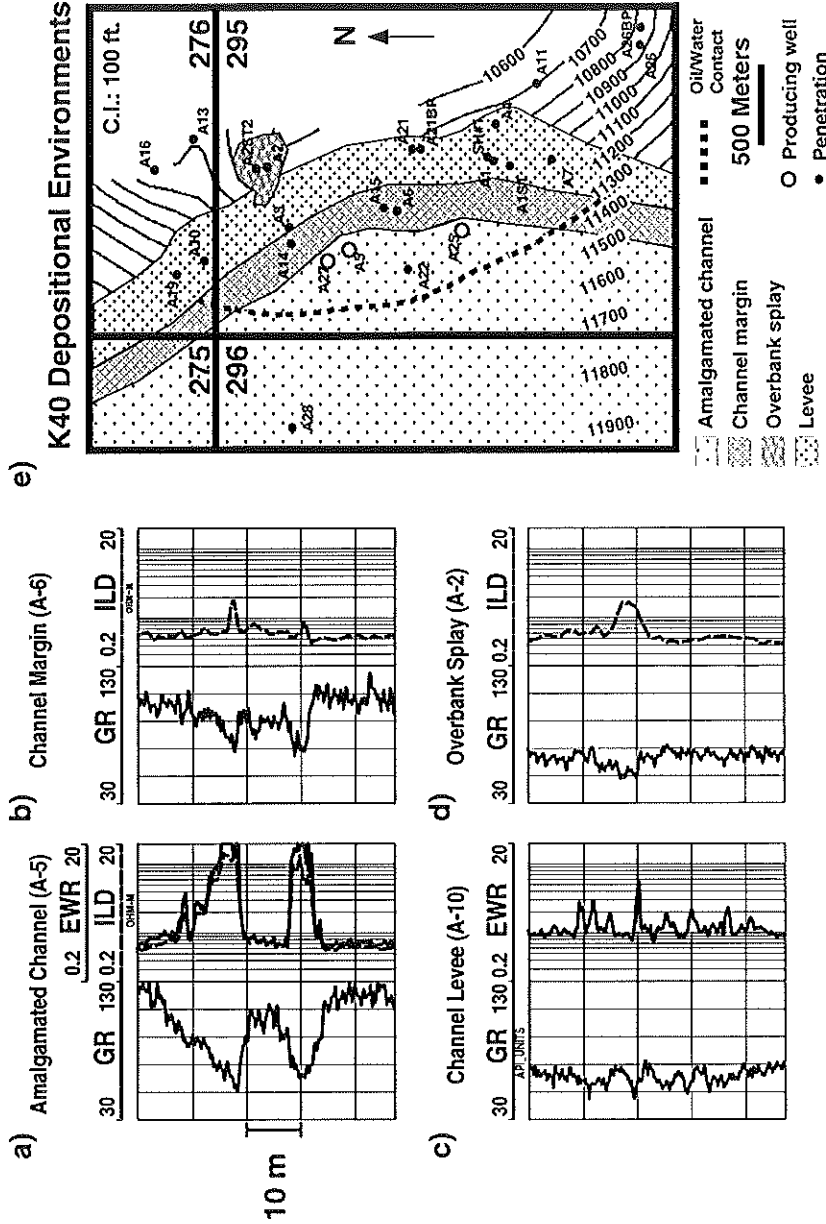
Figure 2.10. Facies type logs (gamma ray (GR), deep induction (ILD), and electromagnetic wave resistivity (EWR) - a logging-while-drilling tool) show interpreted subfacies of the submarine channel environments: a) amalgamated channel, b) channel margin, c) channel levee, and d) overbank splay. Amalgamated channel facies has thick sands with sharp bases, high net-to-gross (>50%), high porosity (30%), and low water saturations (<20%). Sidewall core permeability averages 500 mD. The channel margin subfacies has thinner (10-20 ft.) sands with higher shale content (net-gross <50%), 20-25% porosity, and lower permeability. The shale-dominated levee subfacies contain numerous thin interbedded silty sands with 20-25% porosity, and 50% water saturation. Overbank splay sand is a thin (<10ft.) lobe of silty sand deposited updip of the channel levee. e) Facies distribution map shows progression of environments based on well log interpretation. There is a trend of
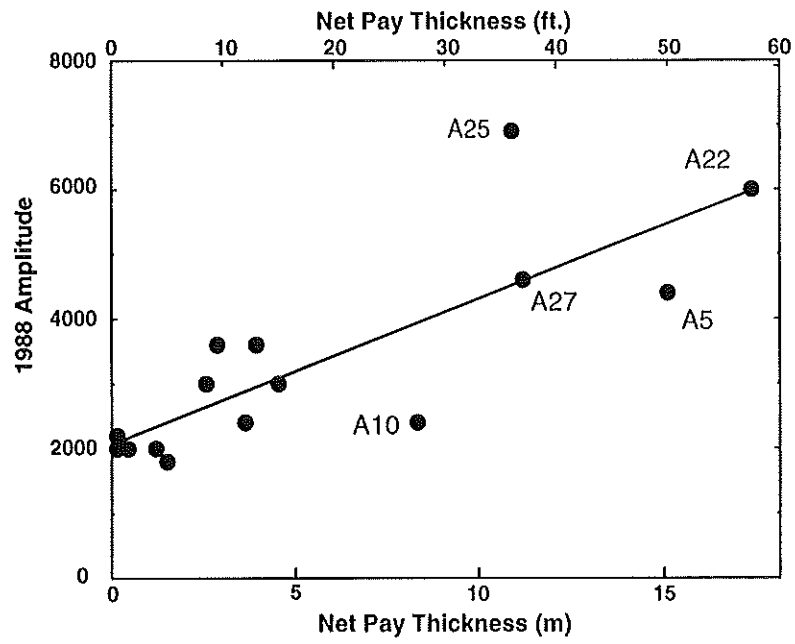
Figure 2.11. Crossplot of 1988 amplitude values and net pay at 15 well locations. A linear regression yielded a correlation coefficient of 0.815. Linear increase in amplitude with net pay is thought to be due to constructive interference of seismic data.
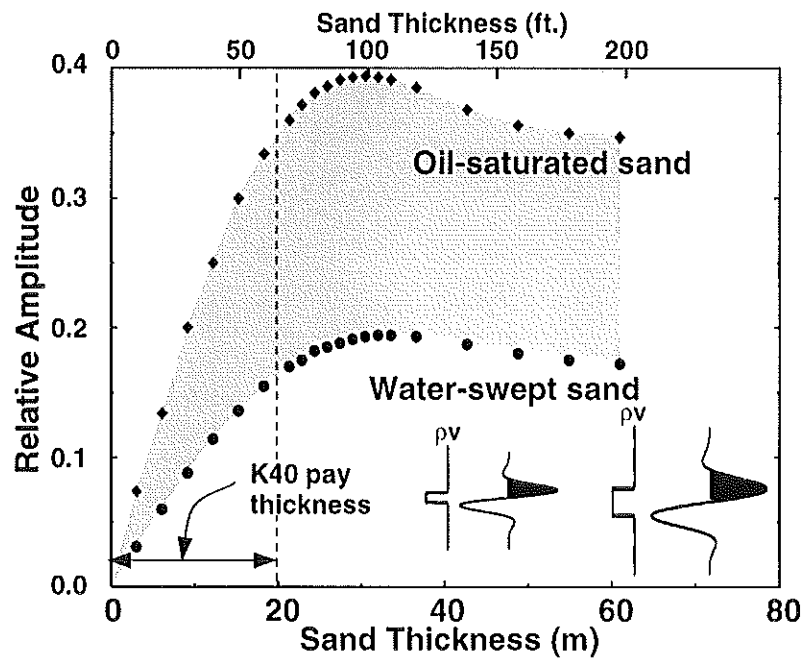
Figure 2.12. Plot of synthetic amplitudes derived from block sand model of oil and water-saturated sands between 0 and 60 meters thick. All K40 pay thicknesses are between 0 and 20 meters, the zone of near linear increase in seismic response. Simulated values assume sonic travel times of 135 μsec/ft. for oil sands, 122 μsec/ft. for wet sands, and 120 μsec/ft. for shale. Oil sand, wet sand and shale densities are 2.07, 2.10, and 2.30 g/cc, respectively. Values were obtained from clean sand intervals of the A-22 well that contains an oil-water contact (Figure 2.5a). The shaded region is shown in Figure 2.18.
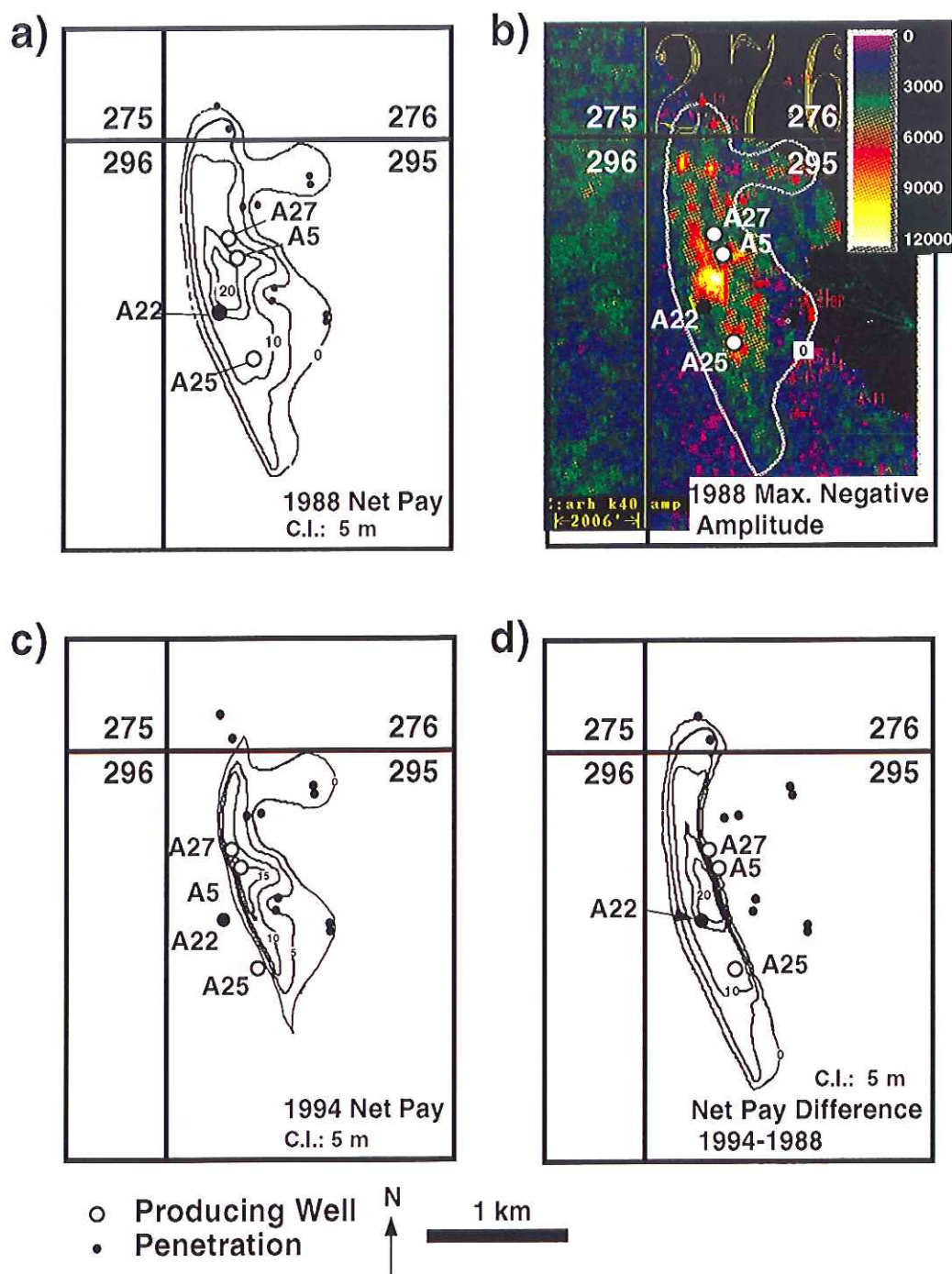
Figure 2.13 a) Net pay map derived from well logs and a linear regression of 1988 seismic amplitude shows net pay ranging from 0 to 20 meters. Net pay values were constrained by thickness at wells. b) 1988 amplitude map with limit of net pay outlined in gray. c) 1994 net pay map constrained by the breakthrough of water at the A-5 and A-27 wells (base of sand - 11108 ft., mid-perf - 11085 ft.) and assuming a flat oil-water contact. d) Net pay difference map (1994-1988) contours the decrease in net pay predicted from upward movement of an oil-water contact assumed to be horizontal.
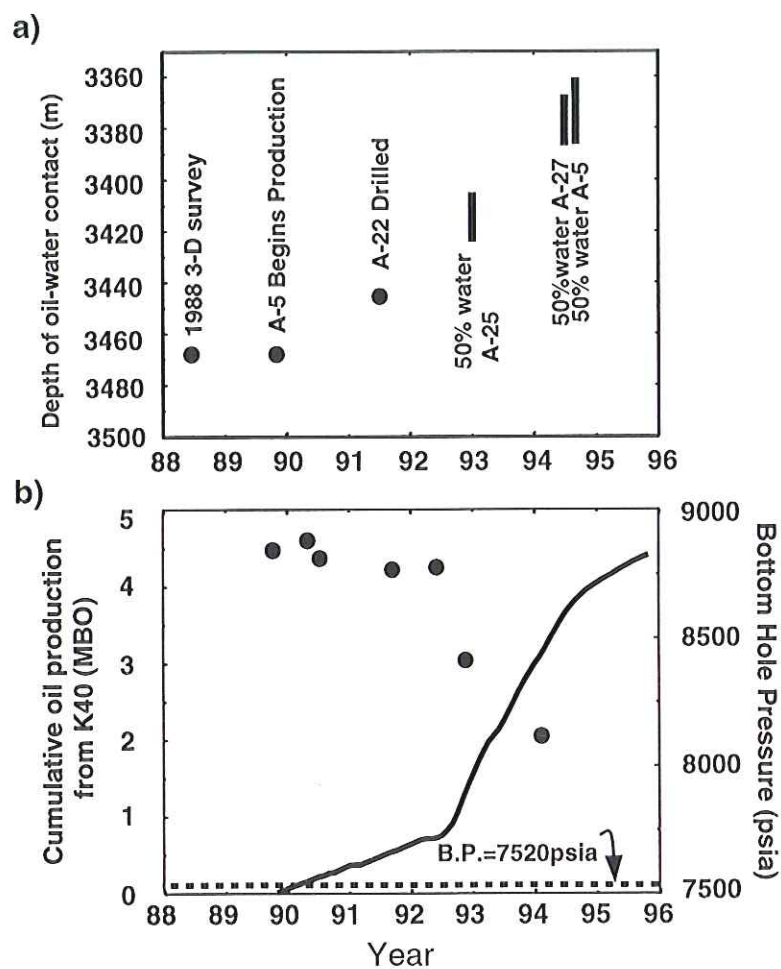
Figure 2.14. a) Plot showing vertical movement of the oil-water contact through time based on depth imaged in the A-22 well, water production data from producing wells, and the original level based on the K40 seismic amplitude. Bars on producing wells represent tops and bases of perforations in wells. b) Bottom hole pressures (dots) and cumulative production (solid line) data for K40 sand; pressure had not dropped below bubble point (B.P. - dotted line) by 1994.
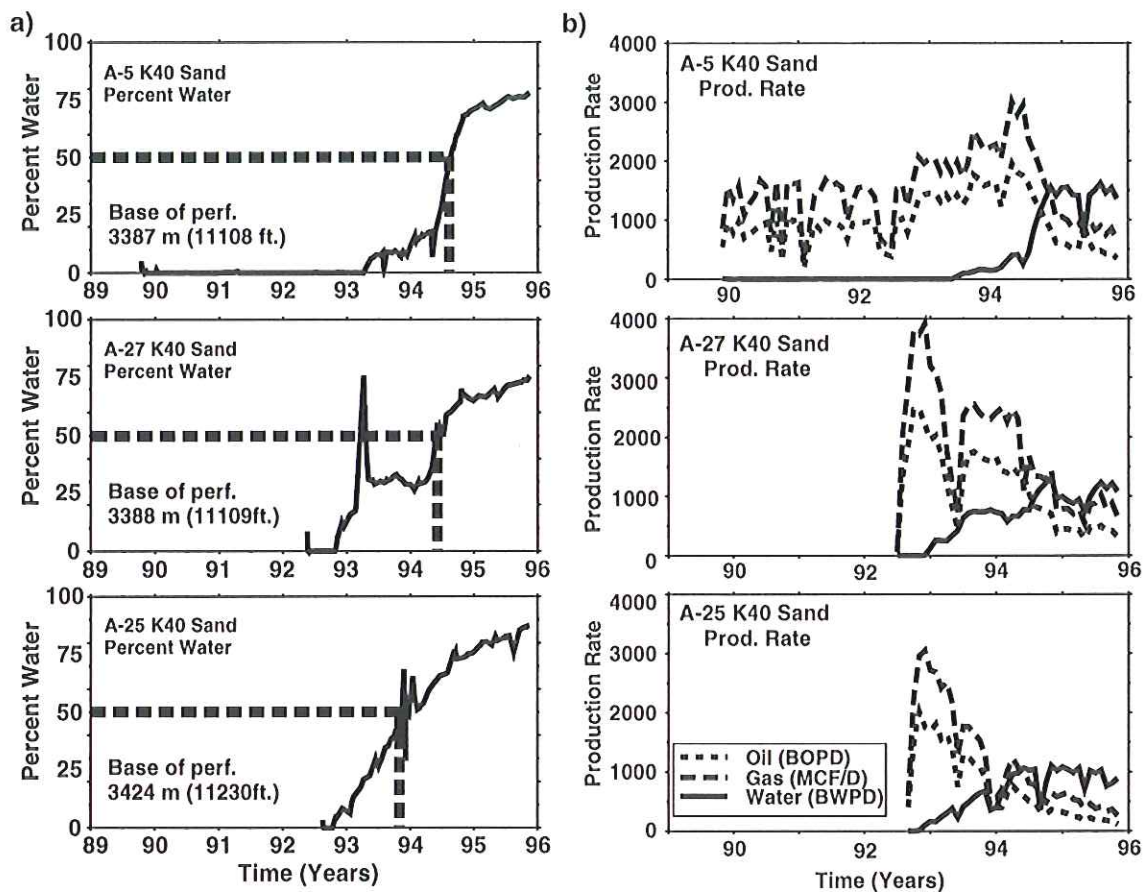
Figure 2.15. a) Water production (percent water) from A-5, A-27, and A-25 wells. The base of the K40 at A-5 and A-27 is at nearly the same depth. **b)** Daily oil, gas, and water production rates from three producing wells.
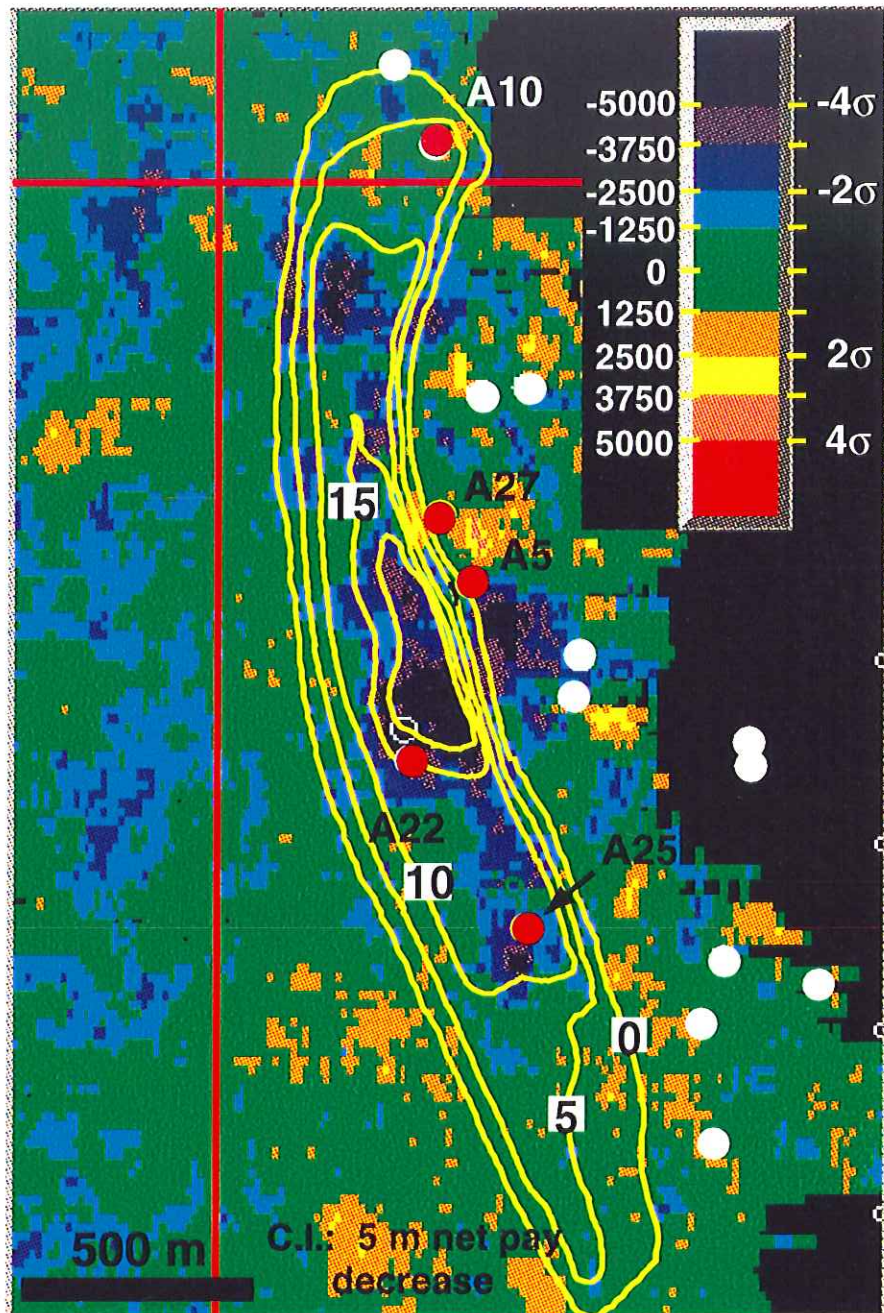
Figure 2.16. Seismic amplitude differences (1994-1988). Color scale is amplitude change from mean difference (mean=0) and steps by standard deviations (sigma=1256). Producing wells and A-22 are red, yellow contours are the decrease in net pay between 1988 and 1994 (Figure 2.13d). Areas of strongest dimming correlate to the thickest portions of the drained reservoir.
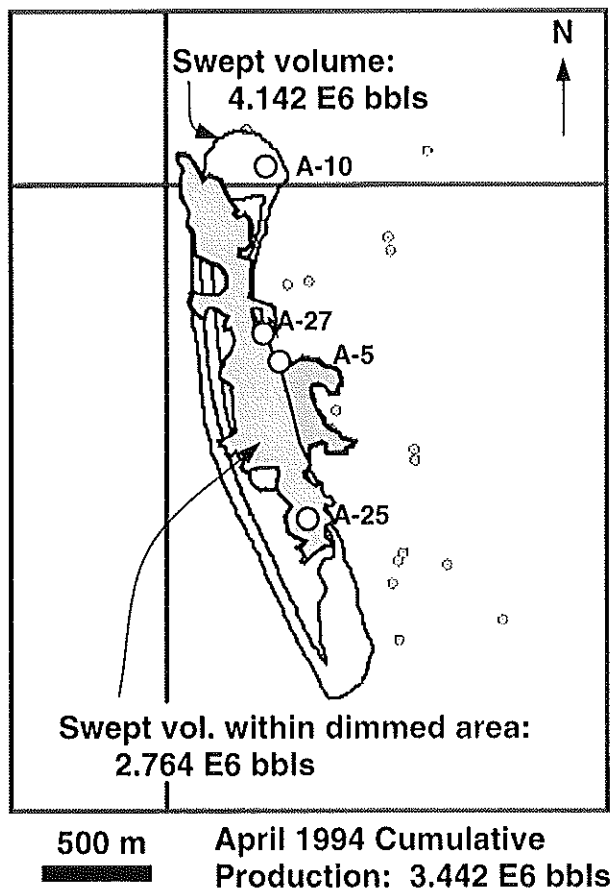
Figure 2.17. Comparison of volumetric calculations for the drained regions which yield values within 24% of the actual cumulative May 1994 production. The outline of significant dimming is light gray downdip of producing wells and darker gray updip of producing wells. Shaded area encompasses dimming equivalent to 2 or more standard deviations from the mean difference.
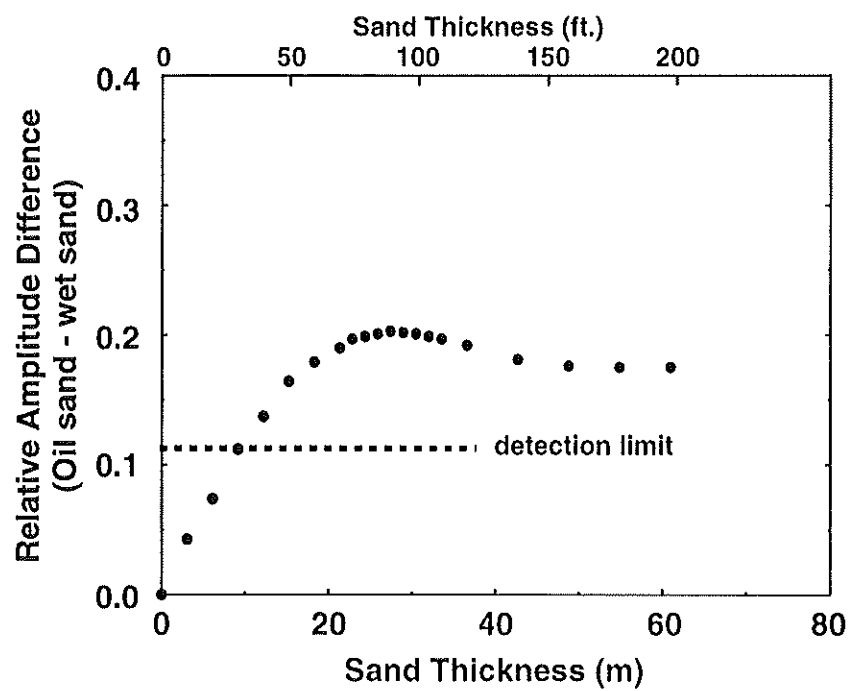
Figure 2.18. Amplitude difference (Oil sand - wet sand) vs. sand thickness. Plot of the difference between oil-saturated and water swept data points of Figure 2.12 shows small amplitude difference below the inferred level of noise in K40 difference data for sands thinner than 10 m. This threshold of detection potentially masks drainage signals in thin sands.
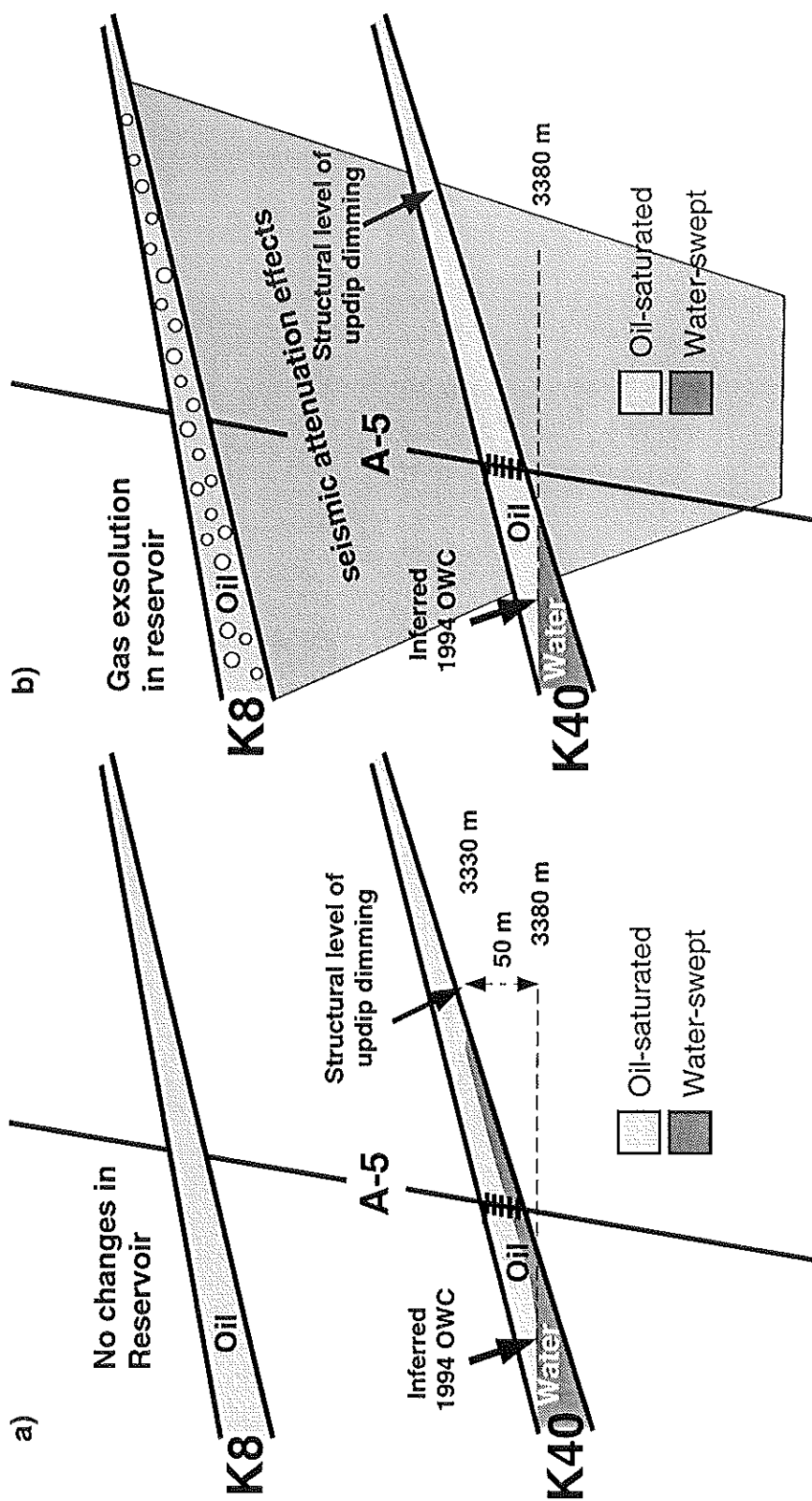
Figure 2.19. Cartoon depicts two possible explanations for observed dimming updip of inferred oil-water contact. a) Pull-up of water 50 m (vertical distance) updip of producing A-5 well. We do not consider this explanation plausible. b) Seismic attenuation of K40 signal due to observed amplitude increases, inferred to represent gas exsolution in K8 reservoir between 1988 and 1994.

a)

No changes in Reservoir

K8   Oil

A-5

Structural level of updip dimming

3330 m

50 m

3380 m

Inferred 1994 OWC

Oil

K40   Water

Oil-saturated

Water-swept

b)

Gas exsolution in reservoir

K8   Oil   Oil

Seismic attenuation effects

Structural level of updip dimming

A-5

Inferred 1994 OWC

Oil

3380 m

K40   Water

Oil-saturated

Water-swept

45

Table 2.1. Recovery factor calculation parameters

Facies	Recovery Factor (bbls/acre-ft.)	Assumed Porosity	Assumed S_w Change (recovery)	Formation Volume Factor (RB/STB)
Channel	740	0.32	0.53	1.77
Clean Channel	842	0.32	0.60	1.77
Other Channel	657	0.30	0.50	1.77

Table 2.2. Comparison of estimated volume to actual produced

Drainage Scenario	Calculated Volume (MMbbls)	% Difference from Actual
1) Entire volume, single recovery factor	4.142	+20%
2) Preferential drainage from channel facies	3.437	-0.1%
3) Drainage in region of seismic dimming	2.764	-20%
Actual production through April, 1994	3.442	-----

Chapter 3

DEVELOPMENT OF A TURBIDITE CHANNEL COMPLEX, SALT FLAT BENCH, BRUSHY CANYON FORMATION, GUADALUPE MOUNTAINS, TEXAS, AS AN OUTCROP ANLOGUE FOR SOUTH TIMBALIER 295 TURBIDITE SANDS

Abstract

A turbidite channel complex of the uppermost Brushy Canyon Formation has macro-scale geometry similar to Gulf of Mexico turbidite sands observed through subsurface data. This outcrop analogue provides insight into finer-scale variation not imaged with geophysical data. Channel elements include erosional surfaces, silt drapes, and initial and subsequent fill. Sands thicken and coarsen toward the axis of the channel complex where they are very thickly bedded and medium-grained with large rip-ups. Channel margins preserve silts and medium-to-very fine sands displaying complete Bouma sequences. Topography on a slump scar controlled the distribution of sands and steered channels toward the axis of the depositional low where coarser amalgamated sands accumulated. Flanks of the depositional low preserved less energetic events and were less prone to amalgamation by subsequent turbidite events. Subsurface observations of the K40 turbidite sand (South Timbalier 295, offshore Louisiana) deposited in a salt-withdrawal minibasin reveal

thicker, amalgamated sands downdip and thinner sands with interbedded shales preserved on the flank of the minibasin.

Introduction

To complement our investigation of the K40 turbidite sand of the South Timbalier 295 (ST295) field located offshore Louisiana (Hoover et al., 1997), we studied an outcrop analogue to gain insights into the facies architecture of deep water gravity-flow deposits. An outcrop analogue allows observation at a scale not resolved by subsurface wireline and seismic data. There are many subsurface Gulf of Mexico turbidite studies (for example, Mahaffie, 1994; Holman and Robertson, 1994; and Galloway and McGilvery, 1995) that rely on cores, geophysical logs, and seismic data to characterize reservoir sands. Use of an outcrop analog promotes understanding of lateral variations of the K40 sand and other analogous Gulf of Mexico reservoirs that are poorly resolved by geophysical data.

The Brushy Canyon Formation (middle Permian, lower Guadalupian), exposed in the Guadalupe and Delaware Mountains of west Texas, is a 0 - 1000 ft. thick sequence of deep-water siltstone and sandstone deposited in the Delaware Basin by gravity-driven flows (Harms, 1988; Harms and Williamson, 1988; Rossen and Sarg, 1988; Zelt and Rossen, 1995) (Figures 3.1 and 3.2). This large volume of siliciclastic sediment onlaps the carbonate ramp to the north.

The primary goals of this study are to observe and characterize lateral variability in channelized turbidites and to compare and contrast these observations with those from ST295. This is not intended to be a comprehensive study of Brushy Canyon deposition. Rather, we focus on a single outcrop to characterize deep water sands and infer depositional processes. We then return to our observations from the Gulf of Mexico and draw potential parallels.

Geologic Setting

The study locality, Salt Flat Bench, is located 1.5 km south of El Capitan peak at the western margin of the Delaware basin and the southern limit of the Guadalupe Mountains, (Figure 3.3). The top of this prominent bench, viewed from US route 62/180, marks the upper contact of the Brushy Canyon Formation with the overlying Cherry Canyon Formation.

The development of the Delaware Basin was controlled by faults in the Proterozoic basement of the region (Oriel et al., 1967; Hills, 1984). Bounded to the west by the Diablo platform, to the east by the Central Basin platform, and to the north by the Northwestern shelf, the Delaware basin remained low throughout the Permian (Figure 3.1) (Hills, 1984).

The Delaware Mountain Group, composed of the Brushy Canyon, Cherry Canyon, and Bell Canyon Formations (Figure 3.2), varies from 0 to 3000 feet in thickness in the Delaware Basin and is well-exposed at the southern limit of the Guadalupe Mountains, along

the western escarpment, and throughout the Delaware Mountains southeast of the study area. Prominent ledges, largely composed of thickly-bedded massive sandstone, are interpreted by King (1948) to be channels and channel complexes. Recessive intervals are composed of thinly-bedded very fine sands and silts.

Siliciclastic sediments of the Delaware Mountain Group (Permian; Guadalupian) unconformably overlie the Leonardian Bone Spring and Cutoff limestones (Figure 3.2). King (1942, 1948) published the first comprehensive field studies that established relationships between shelf, ramp, and basin sediments. Brushy Canyon sands are interpreted to have been transported to the basin across unconformities within the San Andres Formation (Kerans et al., 1993; Fitchen, 1993; Sonnenfeld, 1993; and Sarg and Lehman, 1986). Wilde (1986) and Kirkby (1988) demonstrate the erosional base of the Brushy Canyon that tops the Cutoff and Victorio Peak Formations basinward of the San Andres Formation.

The geologic setting of the Permian Basin is very different from the Gulf of Mexico, yet in both basins, gravity-driven flows delivered sands to deeper water. The Brushy Canyon Formation is generally accepted as a deep-marine sandstone, though the depositional mechanism has been debated (Harms, 1974; Harms and Williamson, 1988; Rossen and Sarg, 1988, Berg, 1979; Bozanich, 1979). Proponents of a thermohaline density current interpretation note siltstone drapes and a scarcity of classic Bouma sequences (Harms, 1974). Rossen and Sarg (1988) propose point-sourcing of siliciclastics, regional correlation to a paleoshelf disconformity, and normal-marine shallow waters on paleoslopes as

evidence against the thermohaline density current interpretation. The distinction between turbidity current and debris flow deposits is also a difficult issue to resolve. Discussion (Hiscott et al., 1997) and reply (Shanmugam et al., 1997), centered on the interpretation of North Sea basin-floor fans, demonstrates the ongoing development of process interpretations of gravity-flow deposits.

Regardless of whether the sandstones of Salt Flat Bench represent turbidity current, thermohaline density flow, or debris flow deposits, they provide a unique perspective on a turbidite channel complex. Numerous channel exposures in the Delaware basin region can be observed in outcrop (photos in Harms and Williamson, 1988), and channels have been inferred from closely-spaced well penetrations of the Brushy Canyon and overlying Cherry Canyon Formations (Harms and Williamson, 1988). The outcrop face described in this study trends perpendicular to flow orientations discussed below and allows us to observe lithofacies variation along an axis-to-margin channel profile.

Field Observations

The sandstones that form Salt Flat Bench are well exposed on its eastern, western, and southern faces. Location A (Figure 3.3) is the western face of Salt Flat Bench with 1600 feet (lateral distance) of exposure that was measured and described in detail at seventeen measured sections (Figures 3.4 and 3.5). From a distance, this outcrop shows sandstones which thin significantly to the north. These cliff-forming sands terminate northward, incising and truncating thinly-bedded very fine sands and silts. To the east, the southern

cliff face (location B on Figure 3.2) thick, massive sands up to 120 feet thick (Figure 3.6).
Measured sections demonstrate the thickness and scale of channelized sands on this face.

We distinguished five facies based on textures, structures, bedforms, and lateral relation-
ships of the quartz sandstones and siltstones at Salt Flat Bench. We describe each facies,
present type sections (composites from multiple measured sections), and interpret a
genetic origin for each. The facies are: A) organic-rich siltstone, A') gray sandy siltstone,
B) thinly-bedded very fine sandstone and siltstone, C) tabular graded sandstone beds, D)
massive sandstone. These descriptions are based on outcrop observations; no sieving or
petrography was performed. The only fossils observed were fusilinid foraminifera (possi-
bly late Early Permian *Polydiexodina*) within the lower unit of facies D.

Facies A - Organic-rich siltstone (Figure 3.7): This is a black, fissile siltstone with rare,
thinly bedded, interbedded, fine-to-very fine sandstones (Figure 3.7). The thickness of
facies A varies from 0.5 to 3 feet with the upper portion grading upward into the gray
sandy siltstone facies, described below. Two persistent oxidized iron-rich surfaces are
present in this unit. The basal surface of this facies is in places marked by angular discor-
dance between the organic-rich silts and underlying interbedded very fine sandstone and
siltstone.

We interpret facies A as a condensed interval that accumulated as a hemipelagic drape
prior to significant input from sand-rich bottom currents. The high-organic content of this
facies suggests high pelagic input relative to terrigenous siliciclastics. Preservation of

organic material and the lack of bioturbation in facies A suggest that anaerobic bottom

conditions prevailed at this location within the Delaware Basin. Hemipelagites described

by Reading (1996) are organic-rich, fissile, and clay-rich where deposited in restricted

basins with anaerobic bottom conditions. Hemipelagic sediments are dominant on many

continental slopes and in marginal or semi-enclosed basins (Reading, 1996). Zelt et al.

(1994) interpret similar organic-rich lithofacies containing volcanic ash layers as con-

densed sections within the Brushy Canyon.

Facies A' - Gray sandy siltstone (Figure 3.8): This facies consists of finely-laminated silt-

stone with thin (1mm) layers of fine-to-very fine sand (Figure 3.8). Facies A' is less

organic-rich than underlying facies A siltstones and contains more sand-sized grains.

Rare thin and very thin (0.5 - 5cm) beds of medium-to-very fine sandstone exhibit com-

plete Bouma sequences with sharp bases, graded beds, and plane parallel laminations

grading upward to ripple laminae and siltstone. Climbing ripple crests on a sandstone bed

top indicates flow oriented at 280 degrees. Number and thickness of sandstone beds

increase upward and southward.

We interpret facies A' to be a hemipelagic drape with rare distal turbidites and a greater

siliciclastic component. Increased siliciclastic input is evident from the increased sand

content and relative decrease in organic material. Zelt et al. (1994) recognize this lithofa-

cies as a hemipelagic drape deposited slowly from suspension and distinguish it from con-

densed sections (facies A).

Facies B - Interbedded sandstone and siltstone (Figure 3.9): Interbedded thinly-to-very thinly-bedded, very fine sandstones and siltstones display plane parallel laminae and ripple cross-laminae. Some graded beds show partial (base missing) T_{bcd} Bouma sequences, and erosional surfaces are rare. Thinly-bedded sandstones have sharp bases; bed tops are sharp and gradational. Sandstone beds gradually thin northward, and overall this facies grades northward into gray sandy-siltstone and southward to the tabular graded sandstone beds of facies C.

We interpret the interbedded thin sandstones and siltstones of facies B as hemipelagic siltstone punctuated by distal flank turbidites; it marks a transition between siltstones and channelized massive sandstones. The distal classification of Walker (1967) and is used here to distinguish thinly-bedded sandstones of facies B from very thickly-bedded massive sandstones of facies D. Distal turbidites are thin, fine-grained, individual sandstone beds that lack channels and scours and have well-developed mudstone layers between sandstones and common laminations and ripples. Because the clay component of the entire Brushy Canyon Formation is very small, siltstone layers rather than mudstones are interbedded with thin sandstone beds of facies B.

Facies C - Tabular graded sandstone beds (Figure 3.10): Repetitive layers of normally-graded, medium-to-very fine sandstones have erosive bases and commonly contain climbing ripples, plane-parallel laminae, and rare scours and groove casts (Figure 3.10). Siltstone interbeds are rare; most beds fine upward through very fine sand sizes to the base of

the overlying graded bed. Though most bedding surfaces are planar, rare low amplitude sinusoidal bedtops with crude internal laminae are present . Two discrete bedsets occur in outcrop separated by a facies B interbedded sandstones and siltstones. The lower bedset is characterized by increasing bed thickness upward while the upper bedset shows no vertical bed thickness trend. Individual beds have planar tops and bases (excepting rare hummocky bed tops) but these planar beds demonstrate demonstrates systematic thinning from south to north over a distance of 200 feet (Figure 3.11).

The tabular graded sandstones of facies C represent a transition between interbedded thin turbidite sandstones and very thickly-bedded, erosive, massive sands. Unlike facies B, facies C lacks siltstone interbeds; in addition, numerous ripple laminae and normal grading distinguish it from facies D. Graded beds exhibit T_{abc} and T_{bc} sequences of Bouma divisions (Bouma, 1962). We interpret sinusoidal bed tops of facies C to represent anti-dune forms within the Bouma C division. Although anti-dunes occur at a flow regime associated with the Bouma A division (Walker, 1967), Hand (1972) examines antidune formation in density currents and suggests they may form within any turbidite division. The lack of silts and very fine sands, along with the presence of medium sand sizes at bases of graded beds, suggest flows at this location (sections 8 through 10) were strong enough to winnow silts preserved at northern locations (sections 1 through 7) (Figure 3.5).

Facies D - Massive sandstone (Figure 3.12): This unit is subdivided into upper and lower units, the upper unit being continuous across the outcrop and the lower unit being

restricted to the southern portion. The upper massive unit (facies D_U) is fine-to-medium-grained, medium-to-thickly bedded sandstone with siltstone rip-ups often weathered out of the outcrop. The proportion of sandstone in the upper unit decreases northward where more siltstone interbeds are present. Most beds are massive, but interbedded silts display climbing-ripples. Trough cross-stratification and internal scour surfaces are common at the southern portion of the outcrop. Groove casts, trending north-south, are common to the north. Rare convolute bedding is present in sands and interbedded silts (Figure 3.12, photo B). Most beds are continuous across the outcrop, thinning to the north. Sandstones thicken upward then thin through the uppermost portion of the unit. White-weathering beds, restricted to the upper sands of this unit, display a mottled weathered surface suggestive of bioturbation; however, no specific traces were observed in outcrop (Figure 3.12, photo A).

The lower massive unit (facies D_L) comprises very thickly-bedded medium sandstones. Some plane parallel laminae, troughs, and discontinuous internal erosional surfaces are visible in the sands, though most beds are entirely massive. Coarse siltstone rip-ups and fusilinids occur in layers within very thick beds. Groove casts and flute casts are common with orientations indicating paleoflows directed between 95 and 145 degrees. Locally, medium-bedded medium-grained sands with interbedded siltstone and very fine sandstone are present at the base of very thick massive sands at the southern end of the outcrop.

We interpret sandstones of facies D as amalgamated high-density turbidites based on their association with Bouma sequences on channel margins and work by Arnott and Hand (1989), Hiscott and Middleton (1979), and Kneller and Branney (1995). Arnott and Hand (1989) demonstrated that rapid aggradation of fine sand (> 4.2 cm/s) can produce "massive" sedimentary structures of the Bouma A division. Hiscott and Middleton (1979) interpreted similar facies of very thickly-bedded, massive, poorly-graded sandstones with indurated rip-ups as turbidity current and submarine debris flow deposits. As a depositional mechanism for thick massive sands, Kneller and Branney (1995) proposed gradual aggradation of sand beneath steady or quasi-steady high-density turbidity currents.

Fusilinids in facies D_L were likely transported from the northwestern shelf, a distance of several miles. Layers of fusilinids oriented with long axes parallel to the main flow orientation are present only in the lower massive facies. If fusilinids were indigenous to this locality, we would expect them to be more evenly distributed between the facies.

Trough cross-stratified sandstones within the lower massive unit are not a classic sedimentary structure of turbidites and are more commonly found in fluvial and shallow shelf environments. Trough cross-strata suggest high-density flows of sufficient duration to produce migrating dune-forms. Zelt et al. (1994) detail amalgamated channel complexes of the Brushy Canyon that include cross-stratified sands associated with massive sands and siltstone rip-ups within amalgamated channel complexes. Harms and Williamson (1988) document trough cross-stratification and trough-filled scours within Delaware Mountain

Group sandstones and interpret them as channel deposits from long duration high-density underflows.

Facies Architecture

At the outcrop scale, we synthesize channel orientation, bounding surfaces, and facies relationships that allow us to interpret the development of the channel complex at Salt Flat Bench. Facies have distinct lateral and vertical relationships, either gradational or abrupt, related to the bounding surfaces and channel orientation (Figures 3.13 and 3.14).

We interpret accommodation space at the outcrop to have been formed by a slump. Evidence for slumping includes: 1) a sharp surface at the base of facies A which truncates underlying strata and 2) rotated siltstone beds that underlie the interpreted slump surface (Figure 3.15). Gardner (1997, pers. comm.) and Zelt (1997, pers. comm.) also interpret slumping to be the mechanism that created accommodation space at this locality. Although the sandstone body is eroded beyond the outcrop promontory, we envision an elliptical depression, approximately 2-3 km in diameter and trending NW-SE, as the initial accommodation space filled by the slump. Admittedly, we do not see slump deposits preserved in the basin, and the accommodation space could have been created by subaqueous erosion with bed rotation caused by shear forces during emplacement of the overlying sands.

Outcrop and Paleoflow Orientations

The Salt Flat Bench exposure is oriented NNE-SSW, essentially perpendicular to the dominant set of flow indicators (Figure 3.13B). Flow indicators were measured from 27 gutter casts, tool marks, and flute casts present at bases of beds throughout the upper and lower massive facies. One measurement is from climbing ripple crests oriented at 280 degrees within facies A'. Most measurements are from the lower massive facies, and show a dominant orientation of 100-110 degrees. Flow indicators within the upper massive facies are dominantly oriented southward, although fewer measurements were made from these sands.

Using flow indicators as a proxy for channel orientation, we interpret the exposed sequence as an axis-to-margin transect of a turbidite channel complex (Figure 3.14). Channel axis (thick sandstones) through channel flank (siltstones, interbedded sands) deposits exposed along this transect display increased sand content, coarser sands, and thicker beds southward. These observations are consistent with increasing energy and accommodation space at the axis of the slump. We are unable to confidently locate the position of the axis of this channel complex because no thinner sands representing deposits of the opposite channel flank are preserved. These were eroded back to the thick sands that form the cliff face of Salt Flat Bench. We place the channel axis south of the Salt Flat Bench outcrop because channel sands continue to thicken in this direction (Figures 3.13, 3.14).

Bounding Surfaces

Three significant bounding surfaces are present: the base of facies A, the base of facies D, and the top of facies D (Figure 3.13). These surfaces are interpreted to reflect paleoenvironmental changes during development of the channel complex at Salt Flat Bench. The base of facies A is marked by a change from silty sands (facies B) to organic-rich silts (facies A). This surface is interpreted to represent the base of a slump that created the original accommodation space for the Salt Flat Bench channel complex. Unpublished research detailing the architecture of Salt Flat Bench identifies this basal surface as a slump scar (M. Gardner, pers. comm.). This interpretation is supported by observations of rotated siltstone beds (Figure 3.15), and 120 feet of relief on the base facies A.

The base of facies D has 110 feet of relief and has different morphology from the slump scar at the base of Facies A (Figure 3.13). Truncation of silts, sands, and tabular beds of facies B and C by the base of facies D demonstrates the erosive nature of the gravity-driven flows depositing facies D sands. The erosional surface is best expressed between sections 10 and 12 where the surface truncates facies B and C and shows 40 feet of relief (Figure 3.13).

The upper surface of facies D is the top of Salt Flat Bench and marks the boundary between the Brushy Canyon Formation and the overlying Cherry Canyon (Figure 3.13). At Salt Flat Bench, this surface corresponds to an abrupt change from medium sandstone to interbedded thin sandstones and siltstone. A unit of laterally-continuous thinning-

upward sandstone beds with some signs of burrowing is the uppermost portion of facies D and directly underlies this surface that corresponds to a regional change from a sand-rich to a sand-poor interval.

Lateral and Vertical Facies Relationships

Organic-rich siltstones (facies A) mark the base of the channel complex and demonstrate little lateral variation across the outcrop. The siltstones of facies A form a 0.5-3 ft. drape on the abrupt basal contact that overlies and truncates interbedded siltstone and thinly-bedded sandstone. The upper contact of facies A is truncated by massive sands in the southernmost portion of the outcrop and grades upward to sandy silts (facies A') in the north. Facies A' has gradational contacts upward and southward to facies B interbedded sandstones and siltstones. At sections 1 and 2, facies A' siltstones grade directly upward to the upper unit of facies D with increasing number and thickness of interbedded sand-stones.

Vertical changes in facies B are gradational, downward to silt-dominated facies A', and upward to medium-bedded upper massive sands (facies D_U) at sections 4 through 7 (Figure 3.13). Southward toward the channel axis (sections 8 through 10), facies B is incised by sands of the upper massive unit and rare preserved units of facies B within massive sands have limited lateral extent.

Tabular graded beds (facies C) demonstrate a transition between higher-energy southern facies and lower-energy northern facies. Laterally, facies C is truncated to the south but thins gradually to the north (Figure 3.11), away from the inferred channel axis. Northward thinning is consistent with the overall model of decreasing energy and accommodation space northward.

The lower massive facies (facies D_L) shows little lateral variation within the unit, but its distribution is limited to measured sections 11-17 (Figure 3.13). Rare units of facies B occur within the massive sandstone unit and are truncated laterally over distances less than 10 feet. Southward thickening is accompanied by increased evidence of erosion that reflects higher energy near the axis of the channel complex. A continuous bedding plane separates facies D_L from the upper massive unit (facies D_U) (Figure 3.13).

The upper massive facies has fewer erosional features than the lower massive facies, though scours, ripups, and groove casts are present. At the southern extent of the outcrop (Figure 3.5, measured sections 14-17), the unit is 100% sand, but it thins and grades later-ally to a unit of massive and laminated medium sands interbedded with silts and very fine sand. Individual beds thin northward, as does the unit as a whole, and trough cross-beds are not present in the interbedded northern sands. The uppermost beds of the unit are recessive and thin upward to a sharp contact with overlying silts.

Depositional Processes and Paleogeographic Evolution

Measured sections and facies architecture suggest that deposition at Salt Flat Bench was strongly influenced by local accommodation space. Topography created by the slump controlled subsequent gravity-driven flows and focused high energy events along the axis of the slump scar. We relate depositional processes to distance from the slump axis and propose four stages of development for the Salt Flat Bench channel complex.

Thick massive sands of facies D are the amalgamated channel deposits of high energy gravity-driven flows and represent sedimentation from the highest-energy regime of turbidite deposition, equivalent to the Bouma A division (Bouma, 1962). Repeated events focused along the slump axis winnowed fines, produced numerous scours and amalgamation surfaces, and removed evidence of Bouma sequences. Lower-energy units were either not deposited or were eroded in subsequent events.

Climbing ripple crests in silty sands of Facies A' near measured section 2 (Figure 3.5) indicate flow oriented at 280 degrees, perpendicular to flow indicators of the upper massive sandstone facies (approximately 180 degrees). This suggests laterally-expanding flows deposited sediments on the margin of the slump, while incised channels were restricted to the channel axis. This is consistent with turbidity currents on slopes in which the head of the flow travels at a lower velocity than the body (Simpson, 1987). In this mud-poor system, a lack of channel levees likely allowed a large lateral flow component during turbidite events. Thin sands and silts deposited on slump margins by lateral flows

were preserved because the higher-energy down-slope component of flow was constrained to the slump axis.

The four stages in the development of the Salt Flat Bench channel complex are based on outcrop observations and a conceptual model of point-sourced gravity-driven flow events. Stages are: 1) initial slump and pelagic/hemipelagic sedimentation, 2) distal gravity-flow deposits, 3) proximal gravity-flow deposits, 4) filling and development of a flooding sur- face (Figure 3.16). The terms "distal" and "proximal" are not intended to place sands in the context of a particular depositional model. Rather, the "distal" or "proximal" character of the facies reflect proximity to the axis of main channel flows.

Following slumping, organic-rich silts began to fill the newly created space on the slope. The abundance of organic material indicates that siliciclastic input was low during this stage. Organic-rich silts grade upward to sandy silts and thinly-to-medium bedded sands. This trend suggests a gradual increase in siliciclastic input. Medium-bedded sands (distal gravity-flow deposits) were deposited near the axis of the depositional low as the locus of turbidite deposition approached the Salt Flat Bench position. These sands mark the begin- ning of sand deposition at this location, but may represent a lower flow regime than over- lying very thickly-bedded sands with ripups and numerous scours. An alternate interpretation is that these are laterally equivalent to channel sandstones deposited south of Salt Flat Bench and not preserved.

The third stage, marked by proximal gravity-flows, marks the time at which high-energy gravity flows were focused at the Salt Flat Bench locality. These gravity flows were steered into the axis of the depositional low created by the slump. Erosion and subsequent channel fill deposited amalgamated medium sands. Scours, flute casts, groove casts, incised channel forms, and siltstone rip-ups are evidence of erosive flows. Thinner sands deposited on the margin of the depositional low are likely associated with larger events that were later amalgamated closer to the channel axis. Though truncated by subsequent events, the thinner, normally-graded beds with complete Bouma sequences are preserved on the slump margins and likely represent laterally projected turbidites from the main flows focused at the channel axis.

Filling of accommodation space produced by slumping represents the final stage of channel complex evolution at Salt Flat Bench. Generally, sands preserved on the slump margin thicken upward then thin through the upper 3 feet of exposure. Flow indicators within the laterally continuous upper massive unit are oriented in a southerly direction, implying that flow orientation changed as accommodation space filled (Figure 3.13B). The majority of accommodation space was filled by this time, and channelized high-energy gravity flows were being directed elsewhere on the slope. Burrows in these deep marine sands suggest that they were exposed at the sea floor significantly longer than deeper sands which were rapidly buried. The "flooding surface," marked by the abrupt change from sands to silt, records abandonment and sediment starvation rather than an actual change in bathymetry.

Parallels with K40 Sand, South Timbalier 295

As an example of a submarine channel complex that filled available accommodation space, Salt Flat Bench serves as a good analogue for turbidites of the South Timbalier block 295 field (Figure 3.17). Salt withdrawal due to sediment loading created the Pliocene minibasin of ST295 that provided accommodation space for gravity-flow deposition. This mechanism is different from slumping that is interpreted to have created accommodation space at Salt Flat Bench, and is the most significant factor that may affect the validity of the field analogue. However, in both cases the magnitude and dimensions of local accommodation space are similar, and this depositional topography resulted in lateral variation of turbidites observed in the outcrop and subsurface.

Observations of the K40 sand in ST295 demonstrate the effect of local accommodation space on lateral variation in the K40 sand. Subsurface K40 data from wells and seismic in ST295 show thick sands (108 ft. in A-28 well) in downdip positions. Sands thin and become shalier updip before pinching out against the structural high to the east (Figure 3.18). This onlapping relationship is due to depositional topography. The A-5 well updip of the A-28 has two sand lobes (50 ft. net sand) separated by 25 feet of shale. Updip of the A-5, the gross interval and net sand of the K40 thin further and sands become highly interbedded with shale. Sands and shales of the A-6 and A-21BP wells are channel margin and levee deposits preserved on the updip flank of the salt withdrawal minibasin. We interpret this trend as lateral facies change due to downdip channel amalgamation and updip preservation of lower-energy facies.

Noting these parallels between the Salt Flat Bench outcrop exposure and ST295 subsurface data allows us to make more confident predictions about reservoir and aquifer connectivity, downdip sand quality, and updip reservoir quality. We expect that thick amalgamated sands downdip will promote even water sweep in the strong water-drive K40 reservoir. The updip interbedded sands and have poorer reservoir quality and may promote uneven water sweep dependent on producing well locations.

Although no sidewall cores for grainsize sampling were recovered from the downdip A-28 well, we use the outcrop analogue to predict basinward coarsening in the K40 and extrapolate this trend westward to the center of the minibasin in ST296. Other fine-scale outcrop features not fully resolved by well logs include finely-interbedded siltstone and sand and tabular graded beds. However, by putting log observations in the context of a depositional model, we may interpret ambiguous well log responses as interbedded or shaley sands (A-21BP in Figure 3.18).

Conclusions

The Salt Flat Bench outcrop of the Brushy Canyon Formation provides a good field analogue for lateral variation of Plio-Pleistocene turbidites deposited in Gulf of Mexico salt withdrawal minibasins. Coarser thickly-bedded, massive, amalgamated sandstones mark the channel axis and truncate medium and thinly-bedded sands and interbedded silts deposited on channel margins. Deposition was controlled by local accommodation space. Turbidity currents were focused down the axis of the slump scar while lower-energy

deposits were preserved on slump margins. These lateral relationships are consistent with

observations from the subsurface Gulf of Mexico South Timbalier block 295 field. Sand

thickens and becomes amalgamated toward the axis of a salt-withdrawal minibasin, with

thinner sands and interbedded shales, channel margin and levee deposits, are preserved on

the flank of the minibasin.

References

Arnott, R.W.C., and B.M. Hand, 1989, Bedforms, primary structures and grain fabric in
the presence of suspended sediment rain: Journal of Sedimentary Petrology, v. 59,
p. 1062-1069.

Berg, R.R., 1979, Reservoir sandstones of the Delaware Mountain Group, southeast New
Mexico, in N.M. Sullivan, ed., Guadalupian Delaware Mountain Group of west
Texas and southeast New Mexico: Permian Basin Section SEPM Publication 79-
18, p. 75-95.

Bouma, A.H., 1962, Sedimentology of some flysch deposits: Elsevier, New York, 168 p.

Bozanich, R.G., 1979, The Bell Canyon and Cherry Canyon formations, eastern Delaware
basin, Texas: Lithology, environments and mechanisms of deposition, in N.M.
Sullivan, ed., Guadalupian Delaware Mountain Group of west Texas and southeast
New Mexico: Permian Basin Section SEPM Publication 79-18, p. 121-141.

Fitchen, W.M., 1993, Sequence stratigraphic framework of the Upper San Andres Forma-
tion and equivalent basinal strata in the Brokeoff Mountains, Otero County, New
Mexico, in D.W. Love et al., eds., Carlsbad region, New Mexico and west Texas:
New Mexico Geological Society guidebook, 44th field conference, p. 185-194.

Galloway, W.E. and T.A. McGilvery, 1995, Facies of a submarine canyon fill reservoir
complex, lower Wilcox Group (Paleocene), central Texas coastal plain, in R.D.
Winn and J.M. Armentrout, eds., Turbidites and associated deep-water facies:
SEPM Core Workshop No. 20, p. 1-23.

Hand, B.M., 1974, Supercritical flow in turbidity currents: Journal of Sedimentary Petrol-
ogy, v. 44, p. 637-648.

Harms, J.C., 1974, Brushy Canyon Formation, Texas: A deep-water density current deposit: GSA Bulletin, v. 85, p. 1763-1784.

Harms, J.C. and C.R. Williamson, 1988, Deep-water density current deposits of Delaware Mountain Group (Permian), Delaware basin, Texas and New Mexico: AAPG Bulletin, v. 72, p. 299-317.

Hills, J.M., 1984, Sedimentation, tectonism, and hydrocarbon generation in Delaware basin, west Texas and southeastern New Mexico: AAPG Bulletin, v. 68, p. 250-567.

Hiscott, R.N. and G.V. Middleton, 1979, Depositional mechanics of thick-bedded sandstones at the base of a submarine slope, Tourelle Formation (Lower Ordovician), Quebec, Canada, in L.J. Doyle and O.H. Pilkey, eds., Geology of continental slopes: SEPM Special Publication 27, p. 307-326.

Hiscott, R.N., K.T. Pickering, A.H. Bouma, B.M. Hand, B.C. Kneller, G. Postma, and W. Soh, 1997, Basin-floor fans in the North Sea: sequence stratigraphic models vs. sedimentary facies: discussion, AAPG Bulletin, v. 81, p. 662-665.

Holman,W.E. and S.S. Robertson, 1994, Field development, depositional model, and production performance of the turbiditic "J" sands at prospect Bullwinkle, Green Canyon 65 field, outer-shelf Gulf of Mexico, in P. Weimer, A.H. Bouma, and B.F. Perkins, eds., Submarine Fans and Turbidite Systems: GCSSEPM Foundation 15th annual research conference, p. 233-244.

Hoover, A.R., T. Burkhart, and P.B. Flemings, 1997, Reservoir and production analysis of the K40 sand, South Timbalier 295, offshore Louisiana, with comparison to time-lapse (4-D) seismic results, to be presented at the 67th annual international meeting of the Society of Exploration Geophysicists.

Kerans, C., W.M Fitchen, M.H. Gardner, and B.R. Wardlaw, 1993, A contribution to the evolving stratigraphic framework of Middle Permian strata of the Delaware basin, Texas and New Mexico, in D.W. Love, et al., eds., Carlsbad region, New Mexico and west Texas: New Mexico Geological Society guidebook, 44th field conference, p. 175-184.

Kirkby, K.C., 1988, Deposition and Permian erosion of the upper Victorio Peak Formation (Leonardian), western escarpment, Guadalupe Mountains, west Texas, in S.T. Reid, Bass, R.O., and Welch, P., eds., Guadalupe Mountains revisited: West Texas Geological Society Publication 88-84, p. 127-132.

King, P.B., 1942, Permian of west Texas and southeastern New Mexico: AAPG Bulletin, v. 26, p. 535-763.

King, P.B., 1948, Geology of the southern Guadalupe Mountains, Texas: USGS Prof. Paper 215, 183 p.

Kneller, B.C. and M.J. Branney, 1995, Sustained high-density turbidity currents and the deposition of thick massive sands: Sedimentology, v. 42, p. 607-616.

Mahaffie, M.J., 1994, Reservoir classification for turbidite intervals at the Mars discovery, Mississippi Canyon 807, Gulf of Mexico, *in* P. Weimer, A.H. Bouma, and B.F. Perkins, eds., Submarine Fans and Turbidite Systems: GCSSEPM Foundation 15th annual research conference, p. 233-244.

Oriel, S.S., D.A. Myers, and E.J. Crosby, 1967, West Texas Permian basin region, *in* Palotectonic investigations of the Permian System in the United States: USGS Prof. Paper 515C, p. C17-C60.

Reading, H.G., 1996, Sedimentary Environments: Blackwell Science Ltd., 688 p.

Rossen, C. and J.F. Sarg, 1988, Sedimentology and regional correlation of a basinally restricted deep-water siliciclastic wedge: Brushy Canyon Formation Cherry Canyon Tongue (Lower Guadalupian), Delaware Basin, *in* S.T. Reid, Bass, R.O., and Welch, P., eds., Guadalupe Mountains revisited: West Texas Geological Society Publication 88-84, p. 127-132.

Sarg, J.F. and P.J. Lehmann, 1986, Lower-middle Guadalupian facies and stratigraphy San Andres/Grayburg Formations, Permian Basin, Guadalupe Mountains, New Mexico, in G.E. Moore and G.L. Wilde, eds., Lower and middle Guadalupian facies, stratigraphy, and reservoir geometries, San Andres/Grayburg Formations, Guadalupe Mountains, New Mexico and Texas: Permian Basin Section SEPM, p. 1-35.

Shanmugam, G., R.B. Bloch, J.E. Damuth, and R.J. Hodgkinson, 1997, Basin-floor fans in the North Sea: sequence stratigraphic models vs. sedimentary facies: reply, AAPG Bulletin, v. 81, p. 666-672.

Silver, B.A. and R.G. Todd, 1969, Permian cyclic strata, northern Midland and Delaware basins, west Texas and southeastern New Mexico: AAPG Bulletin, v. 53, p. 2223-2251.

Simpson, J.E., 1987, Gravity currents in the environment and the laboratory: Ellis Horwood, Chichester, 244 p.

Sonnenfeld, M.D., 1993, Anatomy of offlap: upper San Andres Formation (Permian, Guadalupian), Last Chance Canyon, Guadalupe Mountains, New Mexico, *in* D.W. Love et al., eds., New Mexico Geological Society guidebook, 44th field conference, Carlsbad region, New Mexico and west Texas, p. 195-204.

Walker, R.G., 1967, Turbidite sedimentary structures and their relationship to proximal and distal depositional environments: Journal of Sedimentary Petrology, v. 37, p. 25-43.

Wilde, G.L., 1986, Stratigraphic relationship of the San Andres and Cutoff formations, northern Guadalupe Mountains, New Mexico and Texas; in G.E. Moore and G.L. Wilde eds., San Andres and Grayburg Formations, Guadalupe Mountains, New Mexico and Texas: Permian Basin Section SEPM Publication 86-25, p. 1-36, 83-94.

Williamson, C.R., 1979, Deep-sea sedimentation and stratigraphic traps, Bell Canyon Formation (Permian), Delaware basin, *in* N.M. Sullivan, ed., Guadalupian Delaware Mountain Group of west Texas and southeast New Mexico: Permian Basin Section SEPM Publication 79-18, pl. 39-74.

Zelt, F.B. and C. Rossen, 1995, Geometry and continuity of deep-water sandstones and siltstones, Brushy Canyon Formation (Permian) Delaware Mountains, Texas, in K.T. Pickering et al., eds., Atlas of Deep Water Environments: Architectural style in turbidite systems: Chapman & Hall, London, p. 167-182.

Zelt, F.B., C. Rossen, and M.B. DeVries, 1994, Deep-water depositional environments of the Brushy Canyon Formation (Permian), Texas: Recognition criteria and stratal architecture, *in* P. Weimer, A.H. Bouma, and B.F. Perkins, eds., Submarine fans and turbidite systems: GCSSEPM Foundation 15th annual research conference, p. 439-440.
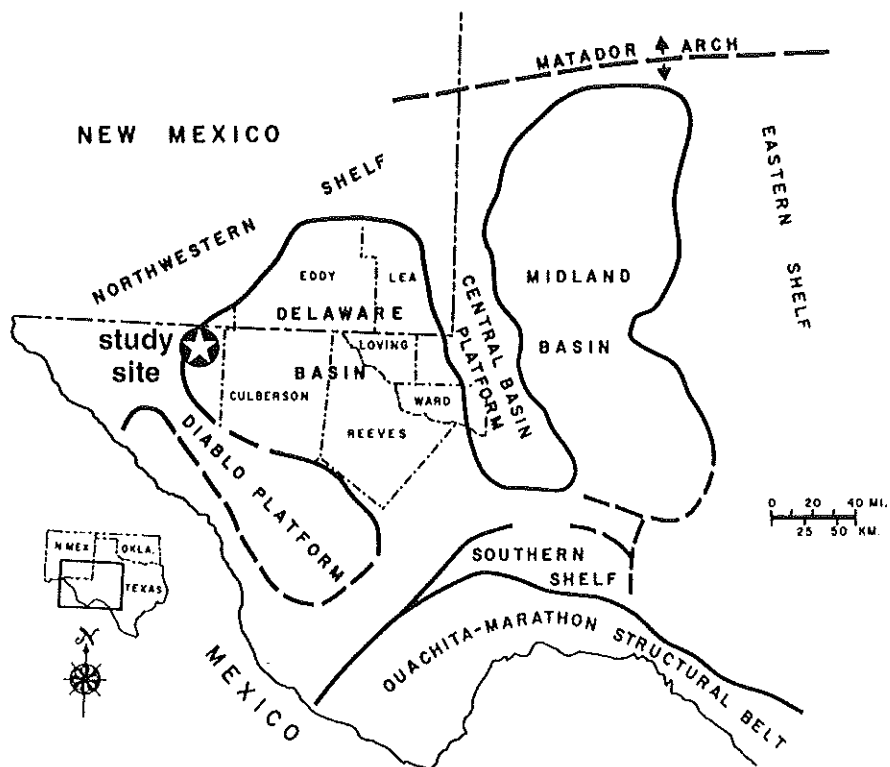
Figure 3.1. Tectonic elements and paleobathymetry of Permian basin, west Texas and southeast New Mexico. Modified from Williamson (1979); after Oriel and others (1967), Silver and Todd (1969).
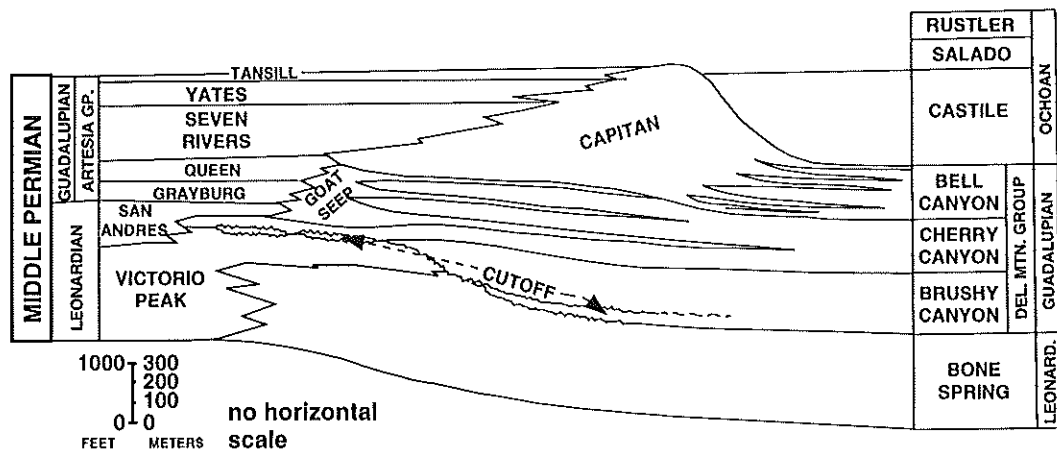
Figure 3.2. Permian stratigraphy of west Texas and southeastern New Mexico. Guadalupian Brushy Canyon strata are deposited on an unconformity and correlate to the San Andres Formation on the shelf. Note the inclined timelines from left to right. Modified from Williamson (1979).
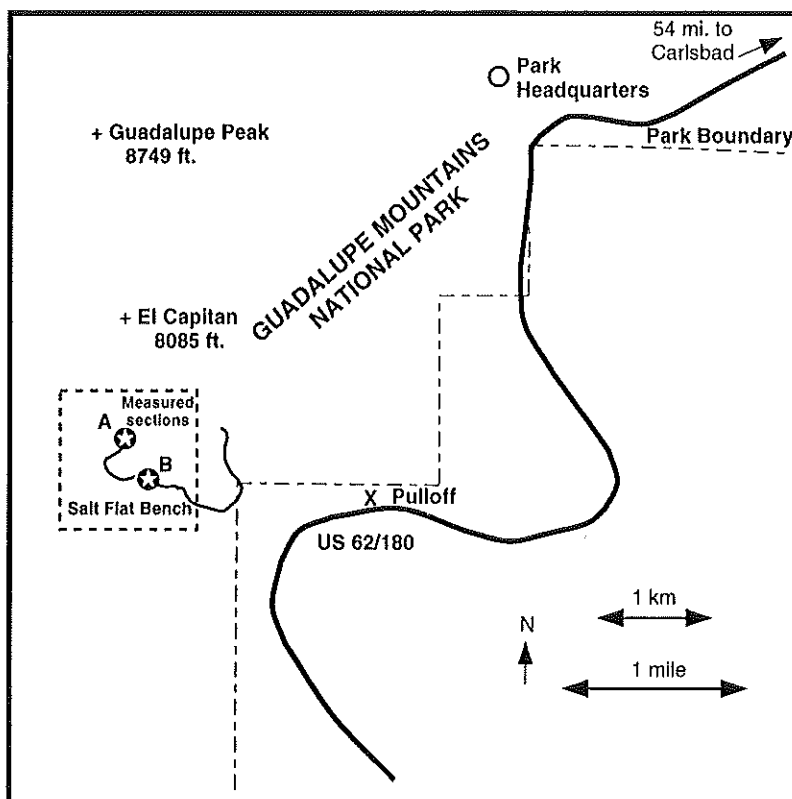
Figure 3.3. Orientation map of Salt Flat Bench study area located at the southern tip of the Guadalupe Mountains within the national park limits. Access to the outcrop is from a pull-off from US62/180 (marked with X on map) that was the old highway.
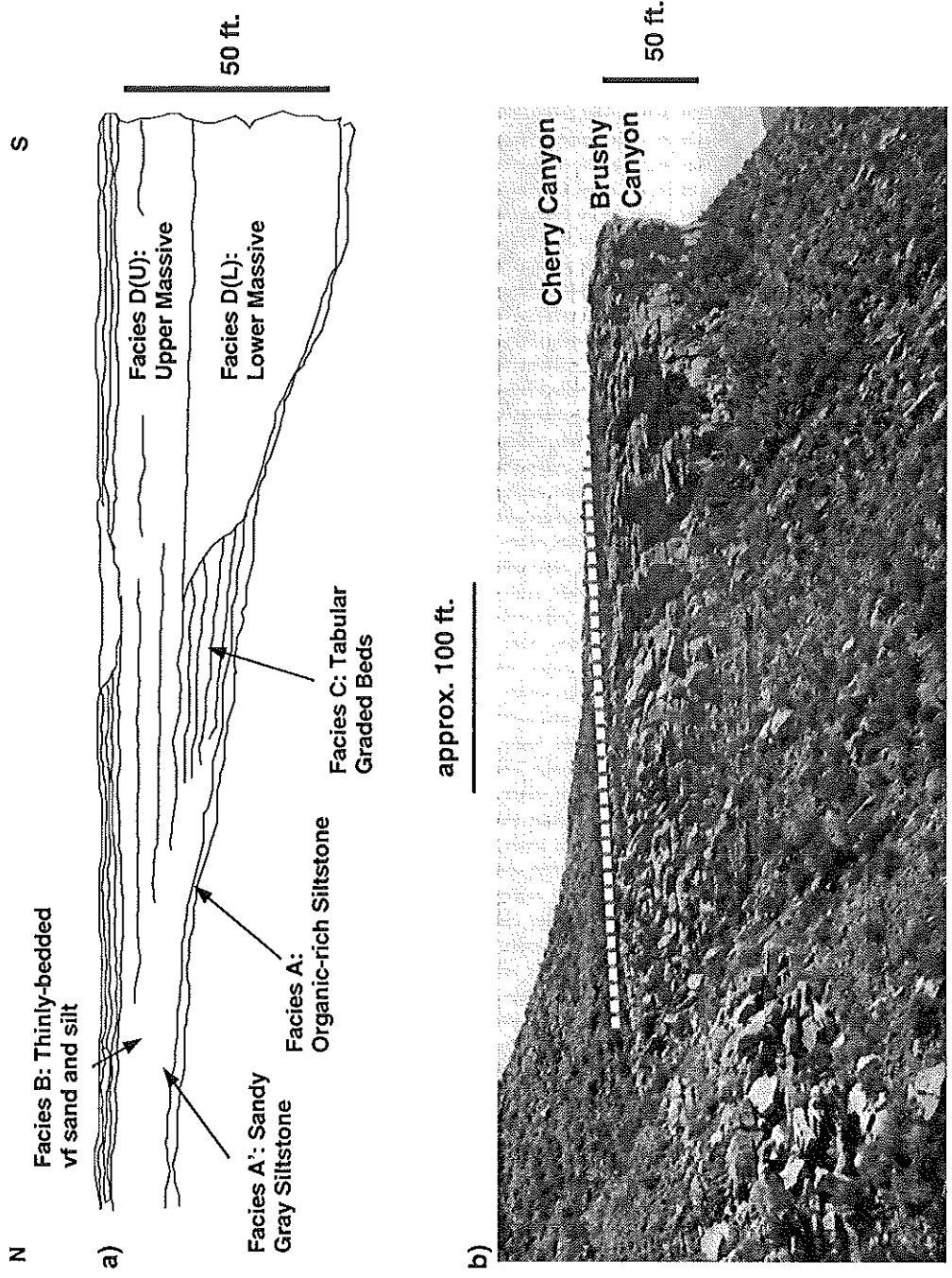
Figure 3.4. Salt Flat Bench outcrop sketch (A) and photo (B). Measured sections 1 through 17 from north to south were described along this face. Sketch includes architecture of facies with thickening sands to the south and abundant siltstone to the north.
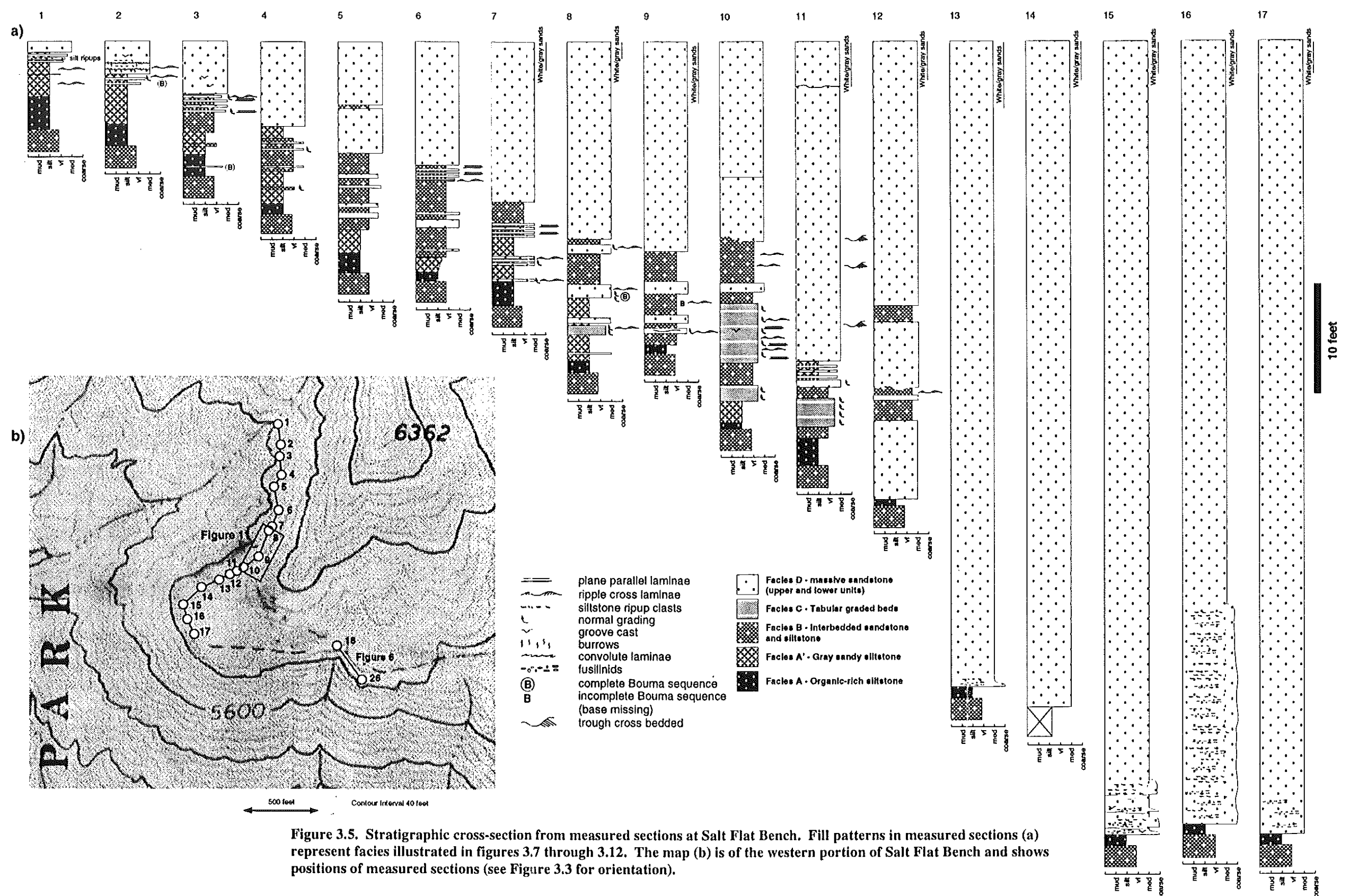
Figure 3.5. Stratigraphic cross-section from measured sections at Salt Flat Bench. Fill patterns in measured sections (a) represent facies illustrated in figures 3.7 through 3.12. The map (b) is of the western portion of Salt Flat Bench and shows positions of measured sections (see Figure 3.3 for orientation).
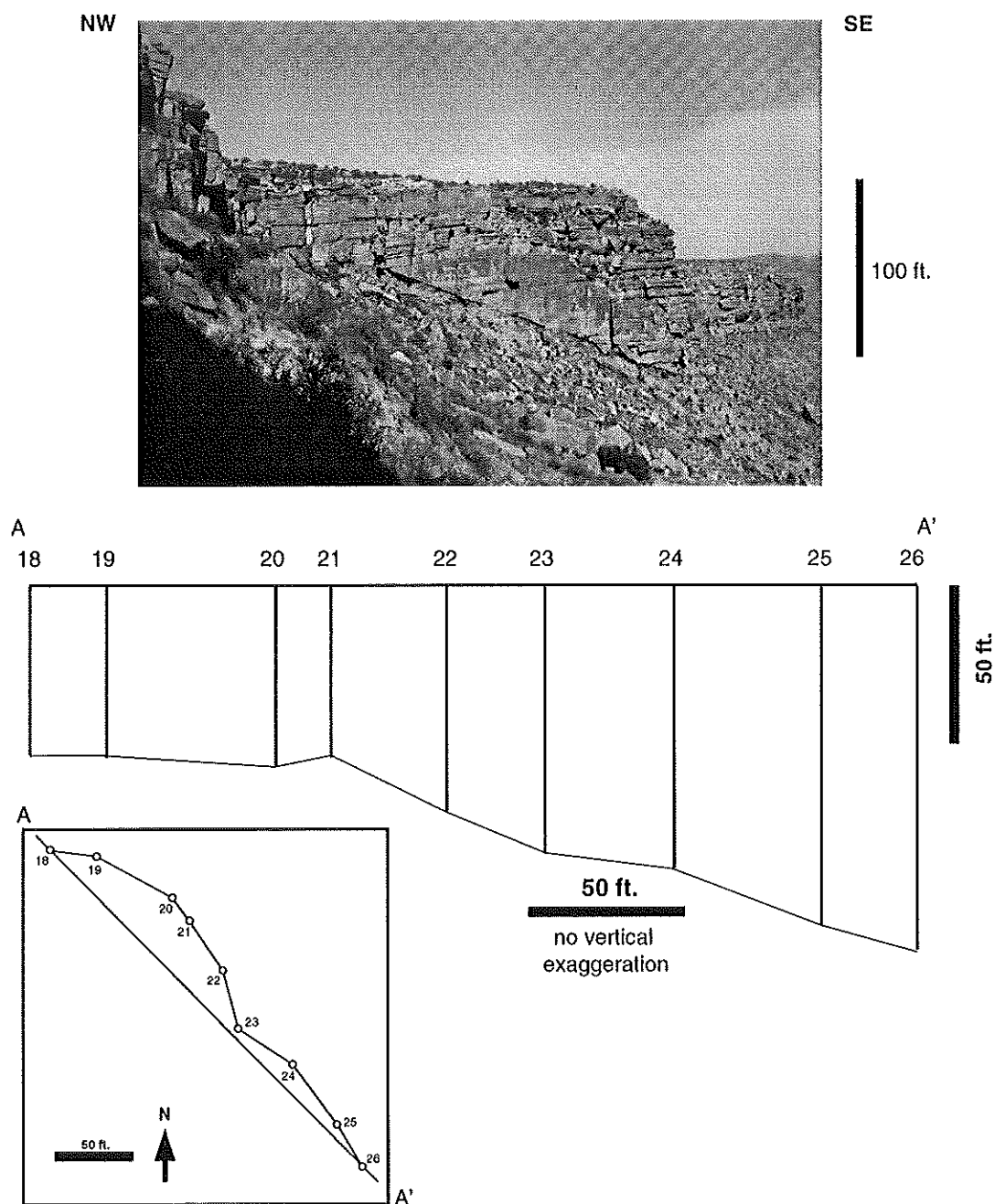
Figure 3.6. Incised channel at southern end of Salt Flat Bench. Flat-lying sandstones onlap steeply-dipping erosional surface to the north. Sections 18 through 26 show the thickness of massive sandstone from channel base through recessive sand interval at top of bench. Thickness of sands exceed 100 feet at the southern end of outcrop (right edge of photo).

Gray sandy siltstone (facies A')

Organic-rich siltstone (facies A)

Interbedded sandstone and
siltstone (facies B)

plane parallel laminae
ripple cross laminae
normal grading
complete Bouma sequence
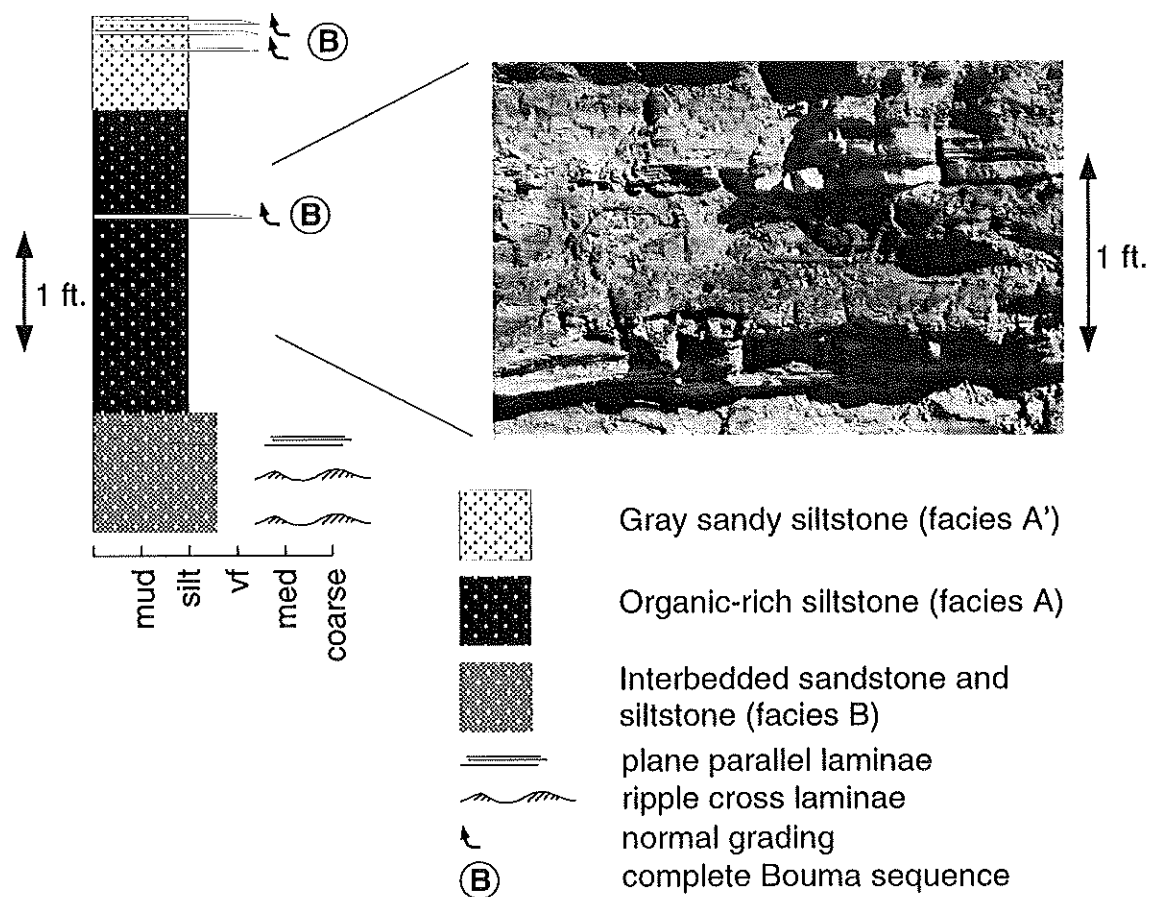
Figure 3.7. Typical section containing organic-rich siltstone, facies A, near measured section 2. Sandstone are rare in this facies, siltstone is fissile and black with some clay-sized component. Mechanical pencil for scale in center of photo.

plane parallel laminae
ripple cross laminae
normal grading
(B) complete Bouma sequence

Gray sandy siltstone (facies A')

Organic-rich siltstone (facies A)

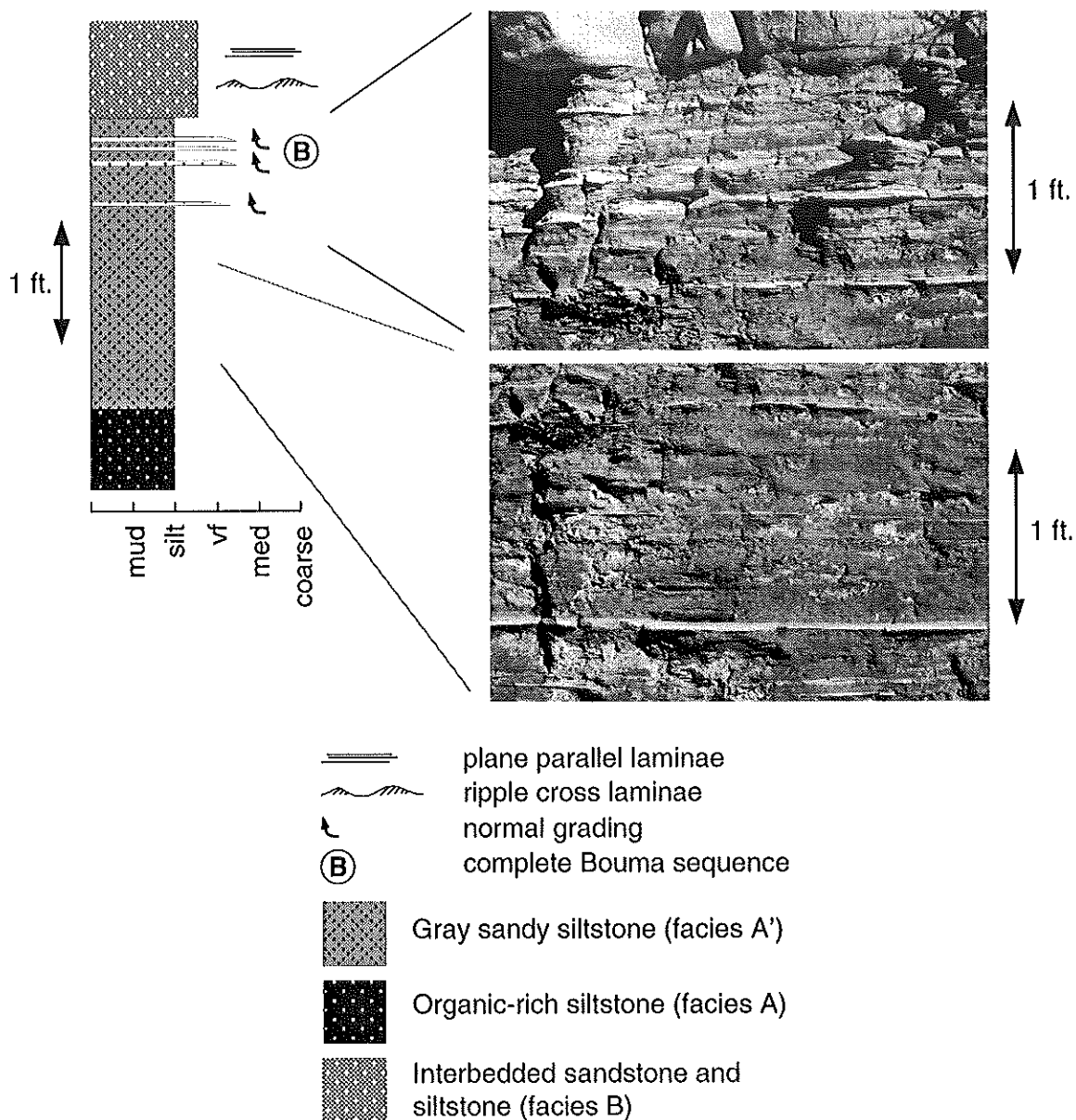Interbedded sandstone and
siltstone (facies B)

Figure 3.8. Typical section containing gray sandy siltstone, facies A', near measured sections 2 and 3. Very thin beds of very fine to medium sandstone show Bouma sequences, increasing abundance upward.

plane parallel laminae
ripple cross laminae
normal grading
groove cast
(B) complete Bouma sequence
B incomplete Bouma sequence
(base missing)
trough cross bedded

Gray sandy siltstone (facies A')

Massive sandstone (facies D)

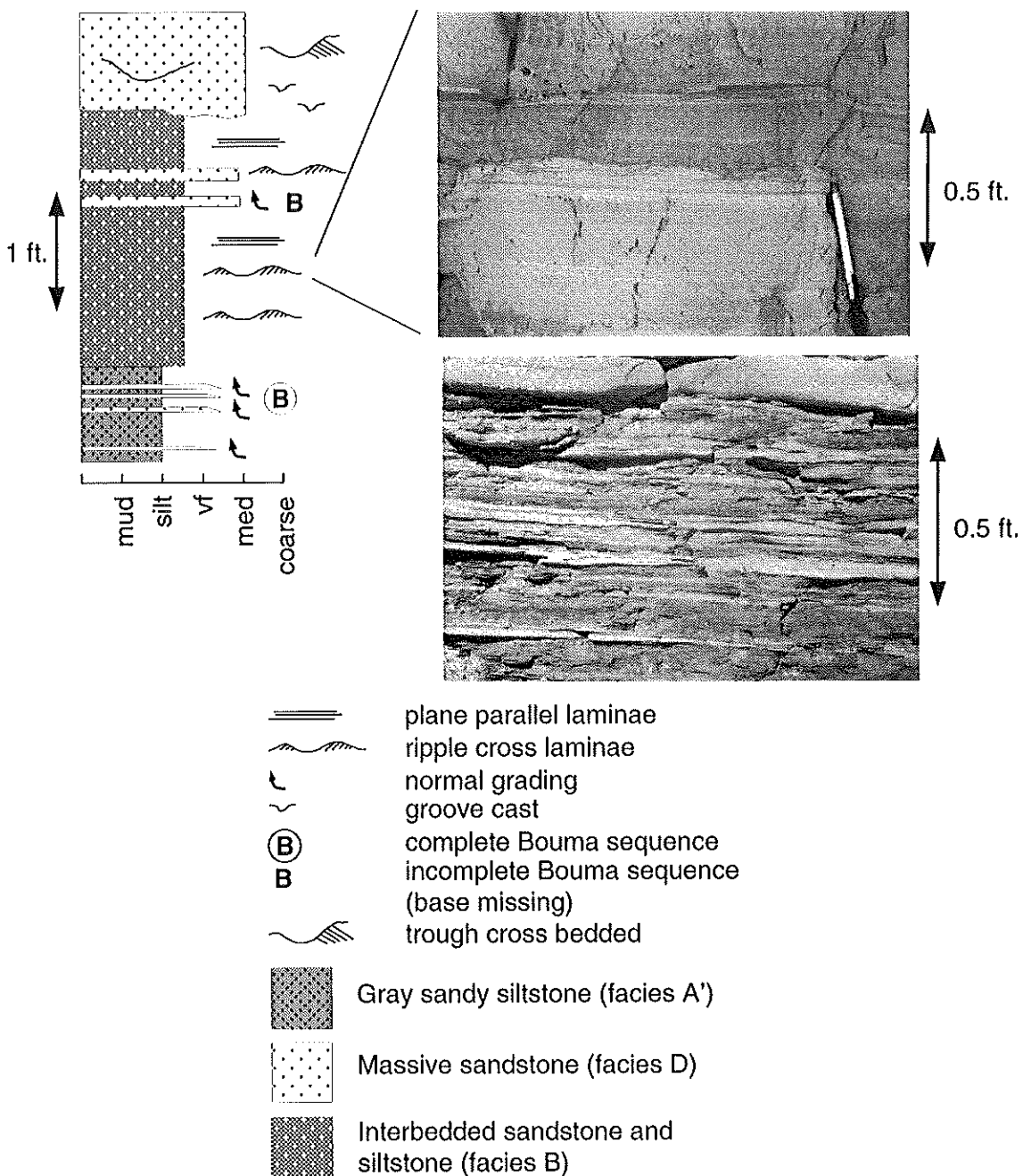Interbedded sandstone and
siltstone (facies B)

Figure 3.9. Typical section of thinly-bedded very fine sandstone and siltstone, facies B, near measured section 4. Upper photo shows example of ripple cross-laminated sandstone. Lower photo shows sheared siltone layer below massive sand at top of photo. See inclined surfaces dipping to the left.

mud silt vf med coarse

plane parallel laminae
ripple cross laminae
normal grading
groove cast

Tabular graded beds (facies C)

Interbedded sandstone and
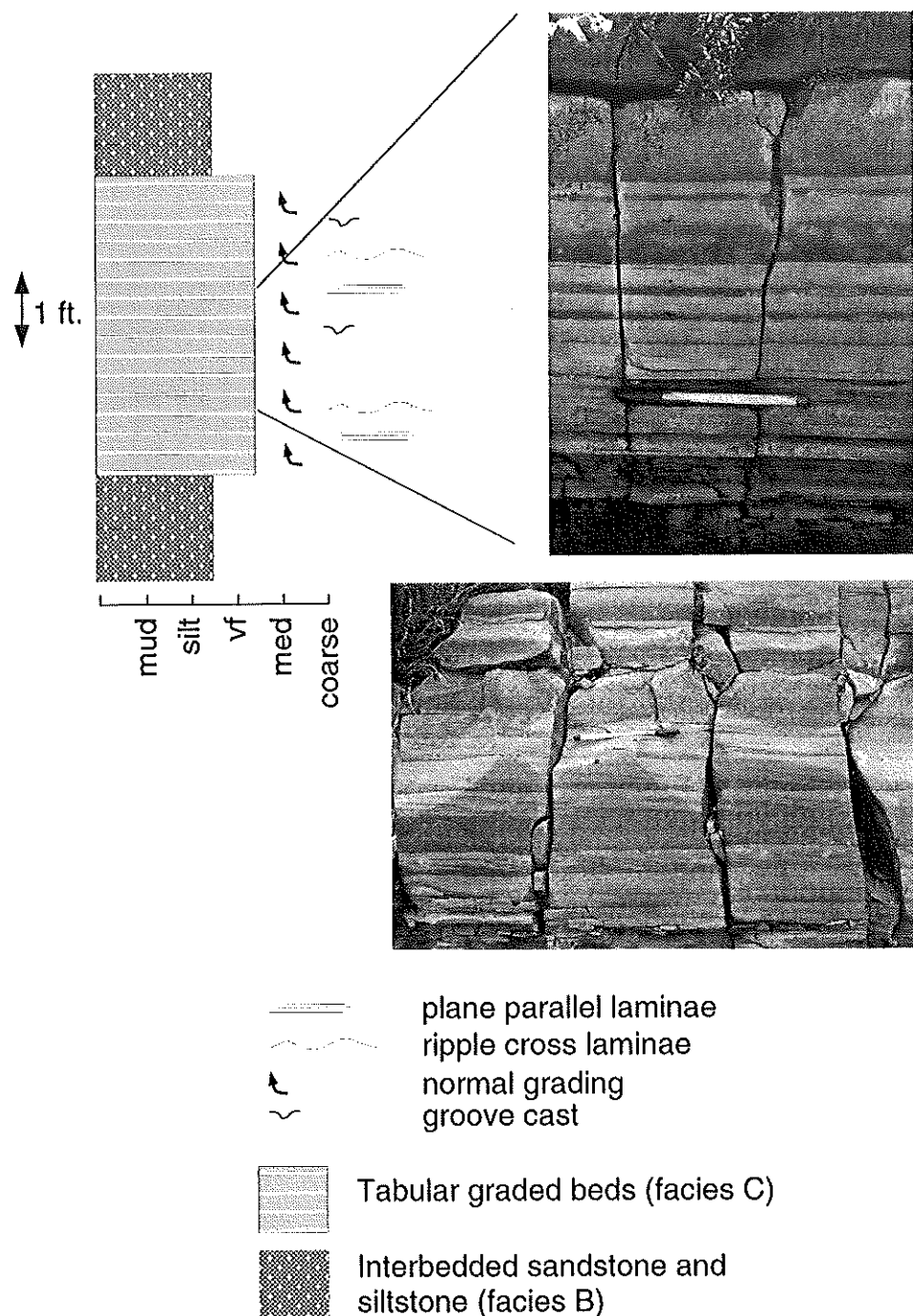siltstone (facies B)

Figure 3.10. Typical section of tabular graded sandstone beds, facies C, located near measured section 10. Upper photo is of lower unit of tabular graded beds which thicken upward (pen for scale). Dark layers (medium grains) grade upward to lighter layers (fine and very fine grains). Lower photo shows tabular graded beds with rippled tops and no vertical bed thickness trend.

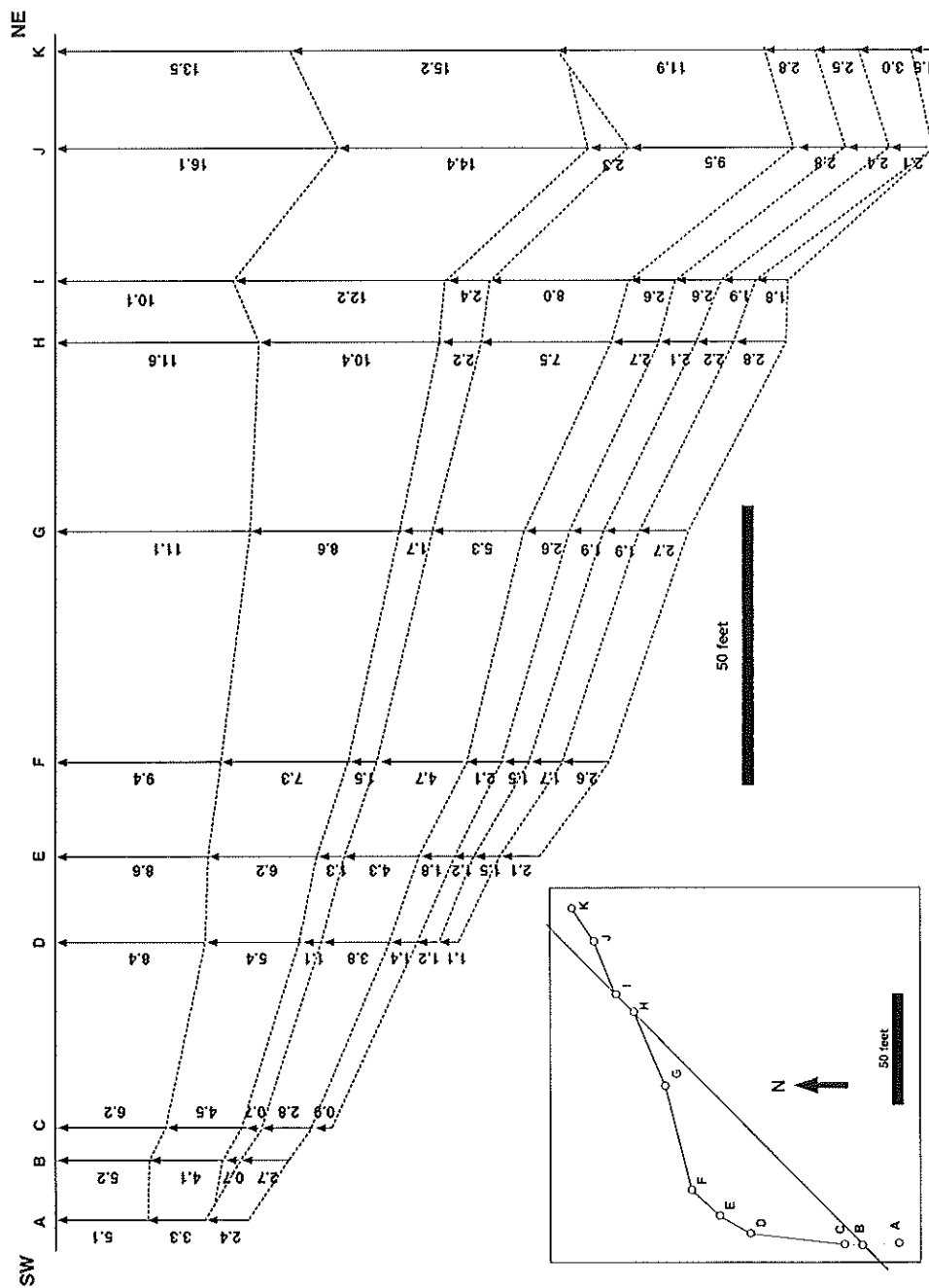Figure 3.11. Thinning tabular graded beds. Southward thickening of tabular graded beds is illustrated with numbers representing bed thickness in inches. Note that this figure is a subset of Figure 3.5, displaying lateral variation in a single facies (tabular graded beds) from 11 sections projected orthogonally onto a 230 ft SW-NE profile. Map at lower left shows relative positions of measurements.
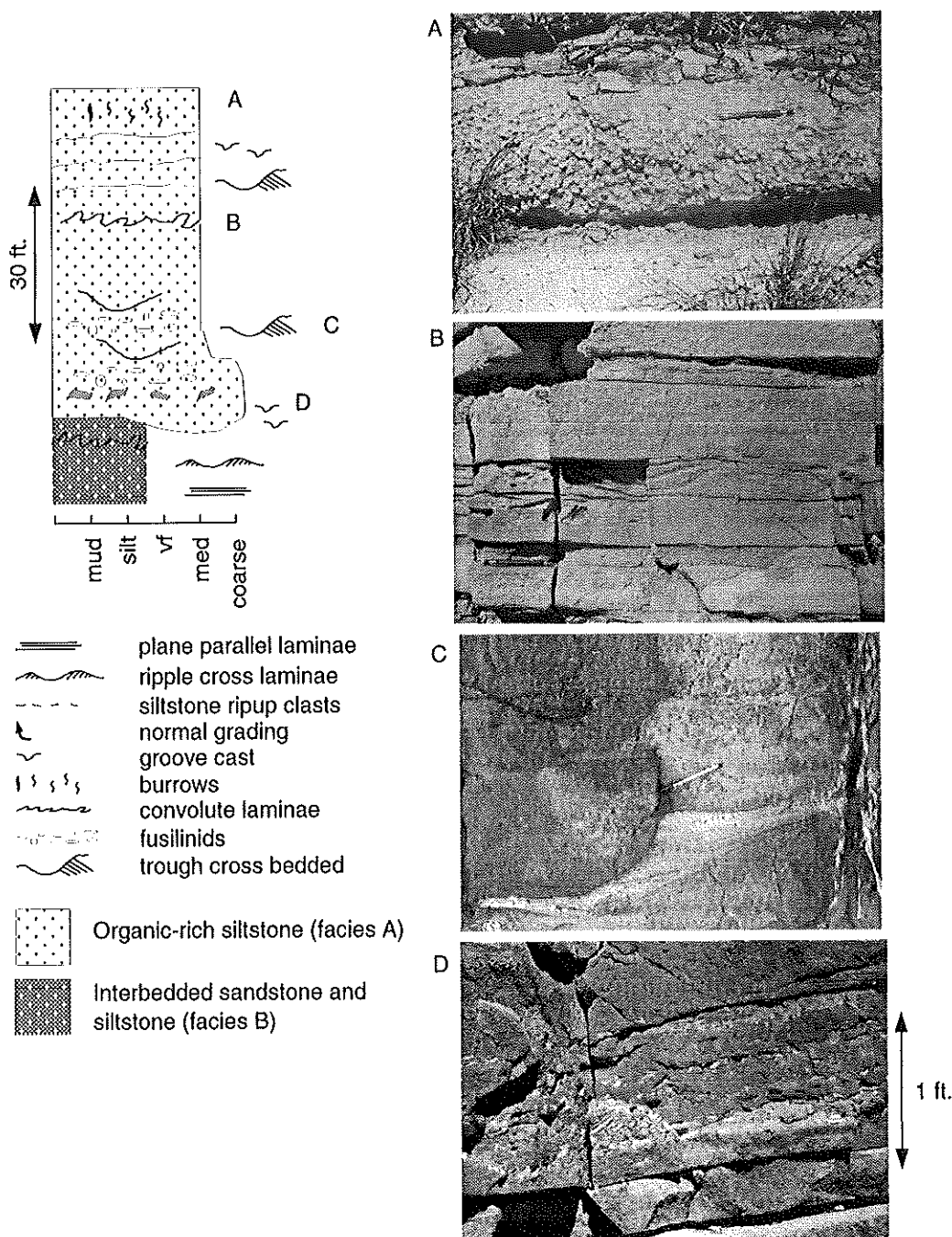
Figure 3.12. Idealized section of thickly-bedded massive sandstones, facies D_L and D_U located near measured sections 14-16. Upper massive unit contains some trough cross-stratification, some burrow-mottled sandstones at the top of the unit, and lacks ripups and fusilinids. The lower massive unit contains fusilinids, siltstone ripups, numerous scours and some trough cross-stratification. Photo A displays burrow-mottled sandstone bed near measured section 8. Photo B shows convolute bedding with eroded siltstone ripups bounded by massive sands at measured section 2 (mechanical pencil at lower left for scale). Photo C shows trough cross-stratification of the lower massive unit near measured section 15 (pen for scale at center of photo), and photo D shows numerous siltstone ripups at the base of the section 23 of Figure 3.6.
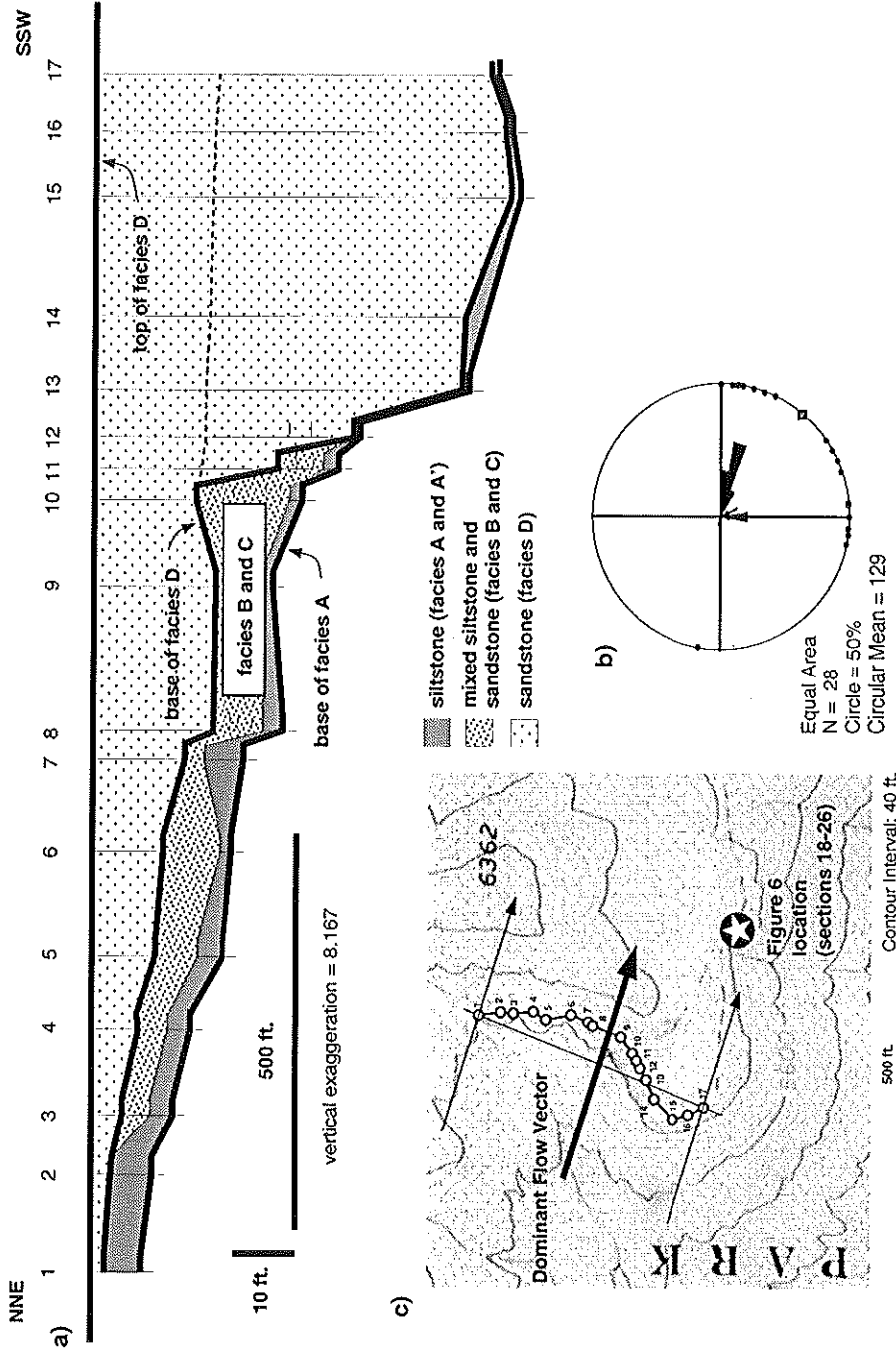
Figure 3.13. (a) Orthogonal projection of measured sections onto north-south profile perpendicular to dominant orientation of flow indicators. These sections show significant thickening of sandstones and truncation of low-energy facies to the south. (b) Flow orientations from tool marks, gutter casts, and flute casts at bases of massive sandstone beds are displayed on rose diagram indicating a distribution of 28 azimuths directed southward and eastward with a mean orientation of 129 degrees. Map (c) shows locations of measured sections, the orthogonal line of section and dominant azimuth of paleoflow indicators.
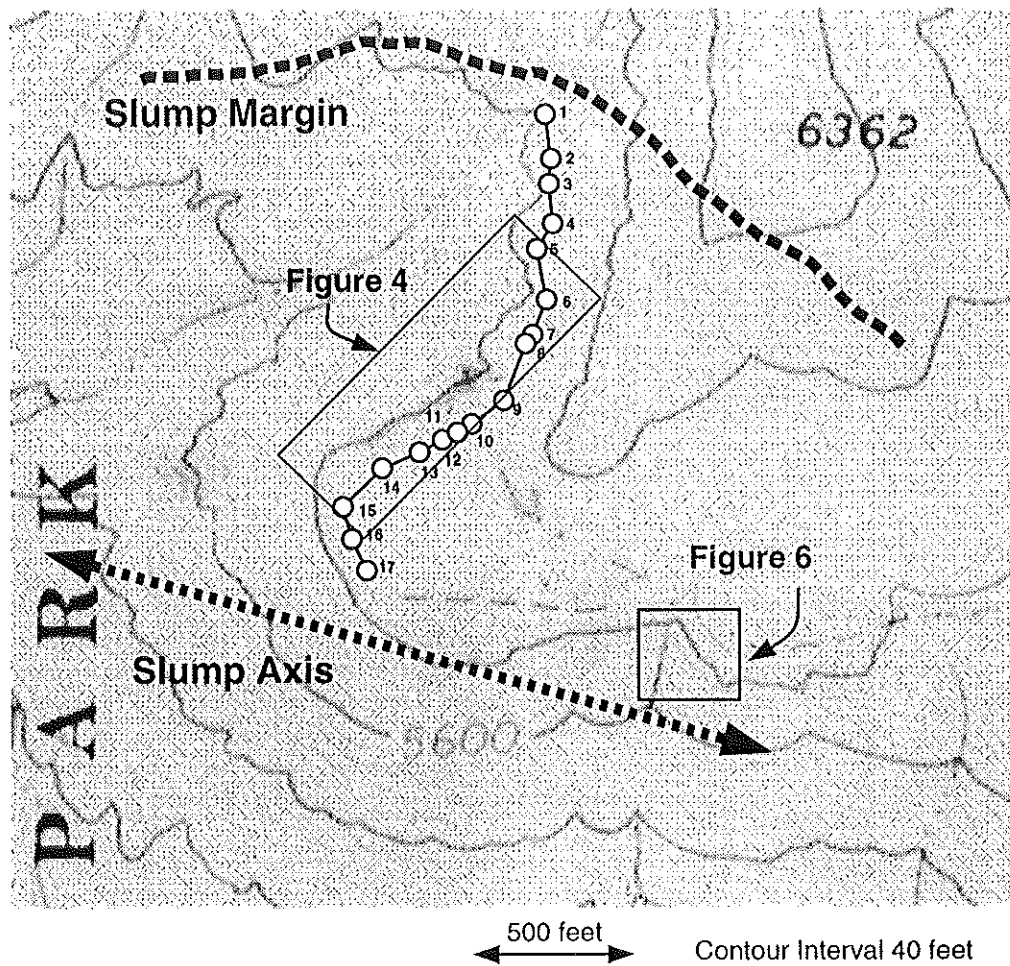
Figure 3.14. Inferred slump orientation in map view, as interpreted from measured sections. Axis of slump is unknown because bench is eroded to south, but orientation is interpreted to parallel dominant flow orientation measured from massive sands in facies D_I. For reference, locations of Figures 3.4 and 3.6 (photos of southward-thickening sandstones are outlined.

N   S
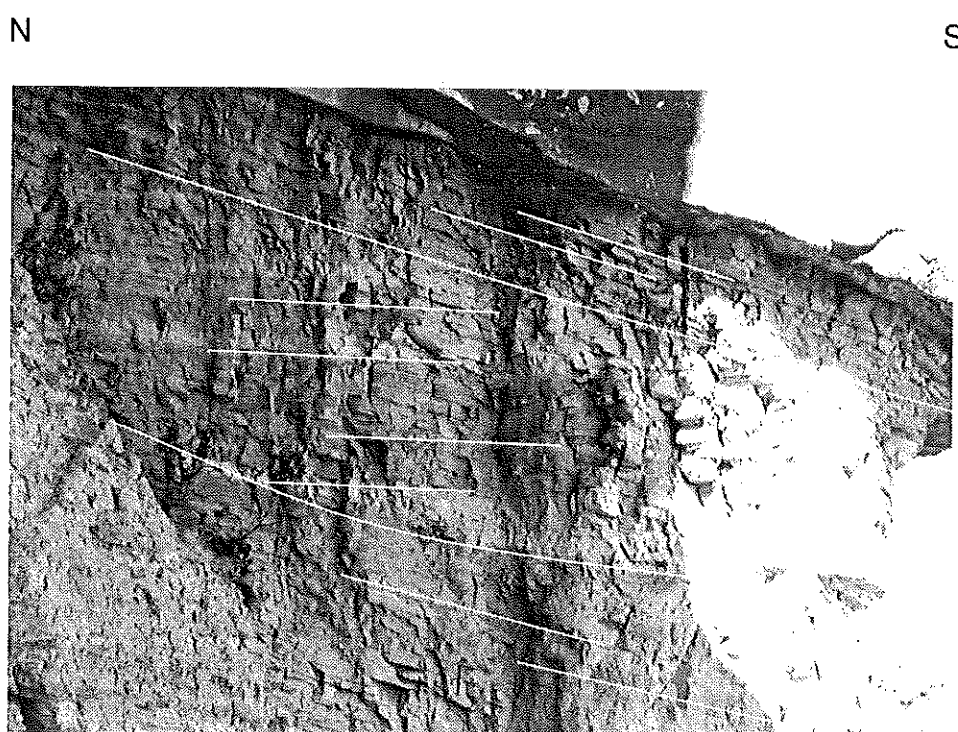
Figure 3.15. Discordant beds in very fine sandstones and siltstones underlying massive channel sandstone. View from west shows two surfaces that truncate underlying beds and suggest slumping and subsequent fill. The lower was filled by similar very fine sandstone and siltstone, the upper slump was filled by a siltstone drape and subsequently by thick massive sands of the channel complex exposed at Salt Flat Bench.

a) Initial slump and hemipelagic sedimentation

b) Distal gravity flow deposition

c) Proximal gravity flow deposition

d) Filling and flooding surface development

Outcrop

interbedded
siltstone and sandstone (facies A)

organic rich siltstone
and gray sandy siltstone (facies B, B')

tabular graded
beds (facies D)

initial channel fill, medium
bedded sandstone (facies C)

massive sandstone
(facies C)
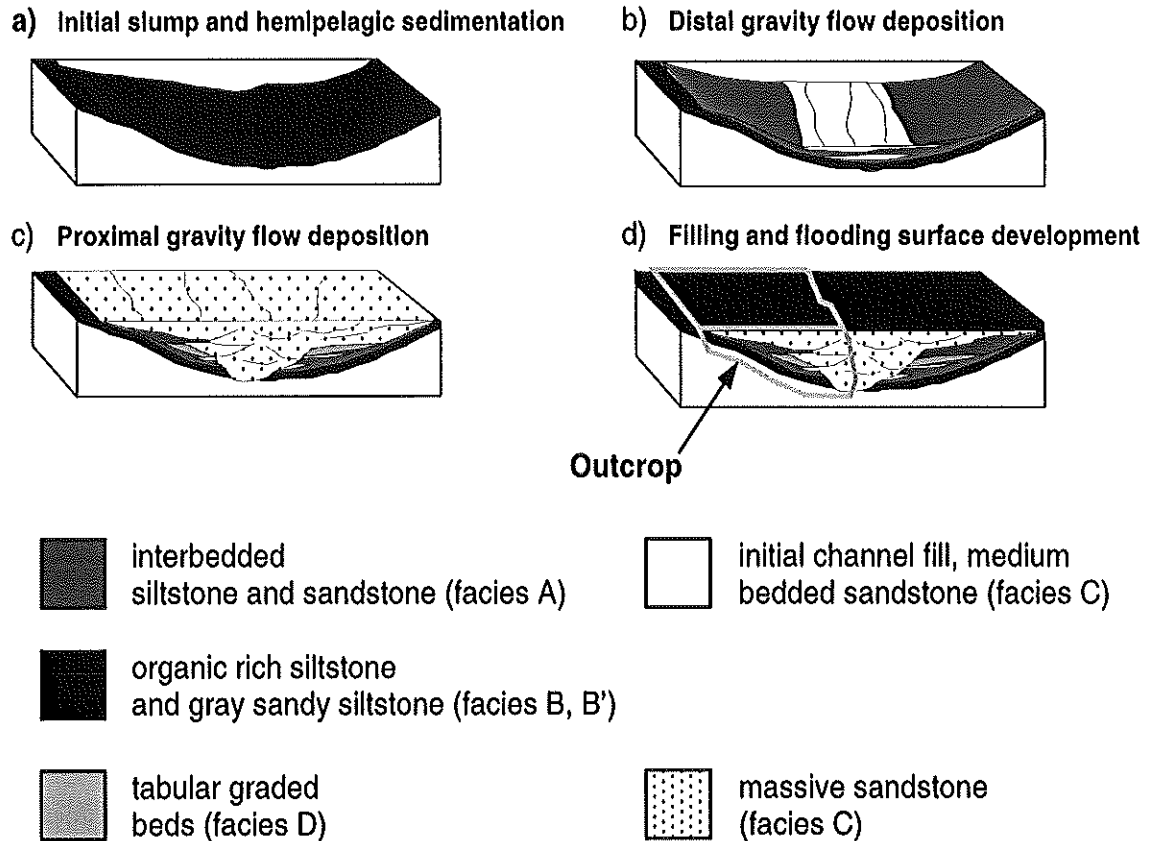
Figure 3.16. Interpreted stages of development of channel complex exposed at Salt Flat Bench. a) Initial slumping (creates accommodation space) and siltstone drape of slump scar; b) Secondary gravity-driven flows; c) Main debris flow channels directed down axis of slump scar; d) Complete filling of accommodation space, flooding surface development.
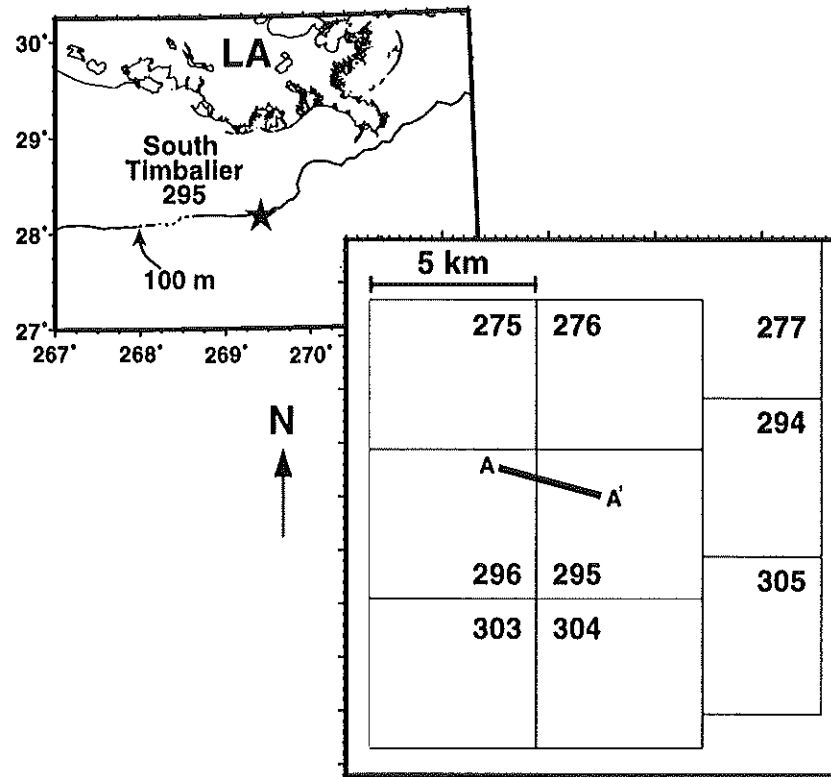
Figure 3.17. South Timbalier 295 basemap. The field is located 120 miles south of New Orleans in 290 feet of water. Traverse A-A' is wireline cross-section in Figure 18. Blocks are 5 km (3 mi.) square.

Figure 3.18. Wireline cross-section (A) and structure map (B) of Pliocene K40 sand, South Timbalier 295 field off-shore Louisiana. The thinning of sands to the east is caused by onlap onto a structural high that controlled deposition. This lateral variation is analogous to that observed at Salt Flat Bench

Appendix

RESERVOIR AND PRODUCTION ANALYSIS OF THE K8 SAND WITH COMPARISON TO TIME-LAPSE (4-D) SEISMIC RESULTS (SOUTH TIMBALIER 295, OFFSHORE LOUISIANA)

Abstract

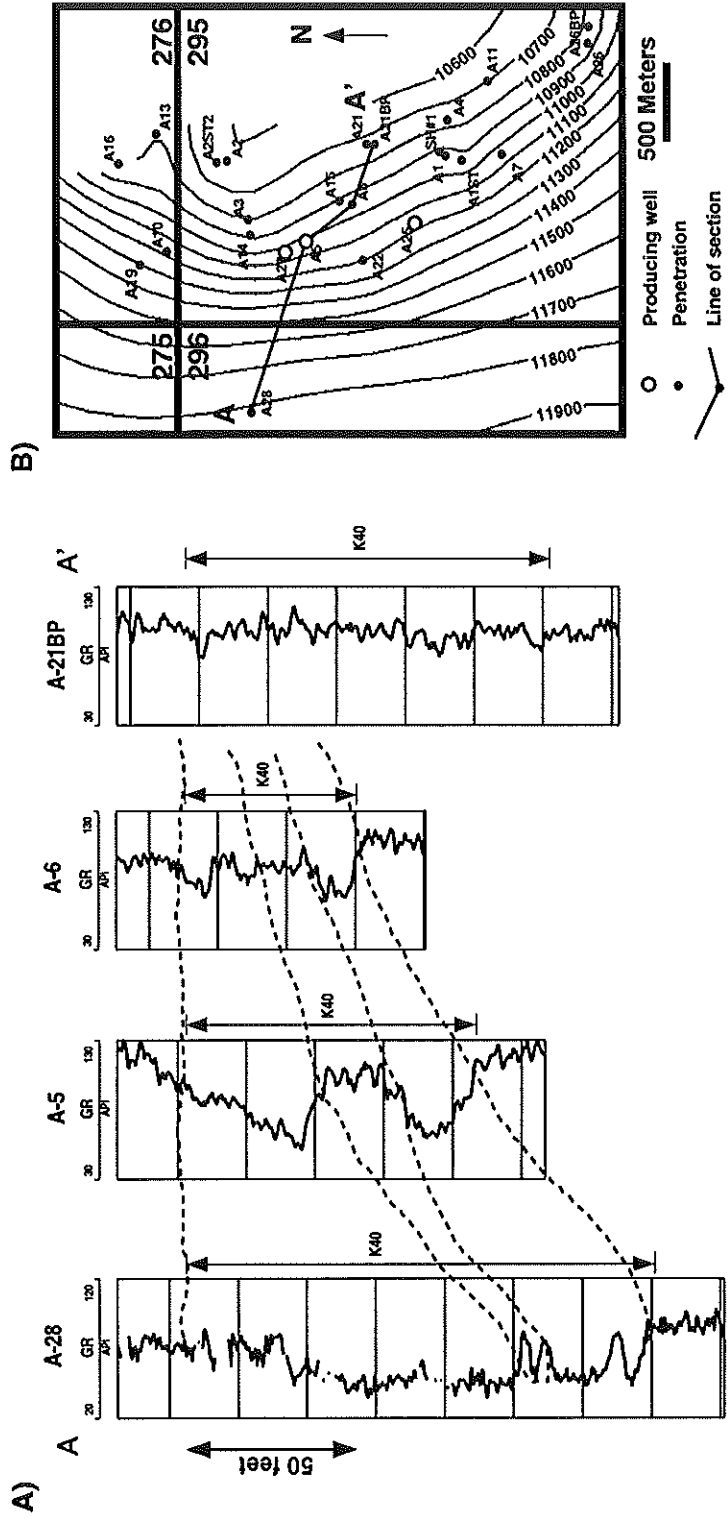Two proposed models describe the K8 sand (South Timbalier 295, offshore Louisiana) as a reservoir comprising three discrete hydrocarbon compartments or as a gas cap reservoir. We present supporting evidence for these hydrocarbon distributions and interpret seismic differences in the context of each proposed model. Seismic differences between surveys acquired before production (1988) and during production (1994) suggest that gas exsolution is significant in the northern portion of the reservoir while compaction may be acting to the south.

Introduction

This appendix is part of a case study that interprets and evaluates seismic difference results from the South Timbalier Block 295 (ST295) field in the Gulf of Mexico (Figure A.1). Background on the field and the study of seismic differences is provided in Hoover

et al. (1997). The goal of this study is to characterize the K8 sand and to relate a geologic model to observed time-lapse seismic differences.

The K8 sand is the stratigraphically highest major reservoir of the ST295 field (Figure A.2). Stacked Pliocene turbidite sands were deposited in a salt-withdrawal slope miniba-sin onlapping a structural high to the east. Other major reservoirs are the K16 and the K40 sands (Figure A.2). The K16 is the largest reservoir in the field and comprises several hydrocarbon compartments (T. Stellman, pers. comm.). K16 compartments are imaged seismically and bottom-hole pressure data confirms poor communication. The K40 is a laterally continuous sand with a large downdip aquifer and strong water drive (Hoover et al., 1997; Mason, 1992).

We investigate the K8 as a compartmentalized solution-drive reservoir (geologic model I) or gas cap oil reservoir (geologic model II). Neither geologic model is conclusively supported by available data. Nonetheless, we integrate log, seismic, and production data to develop these geologic models and relate them to observed seismic differences. Structure maps and net pay maps interpreted from seismic data and wireline logs delineate reservoir extent. Both proposed geologic models may account for observed seismic differences.

K8 Sand

The K8 sand top ties to a strong negative amplitude in seismic data (Figure A.2). The K8 has restricted lateral extent as is demonstrated by seismic data and well penetrations. Seis-

mic section A-A' shows the abrupt decrease in amplitude that marks the downdip limit of the reservoir (Figure A.3). The structure map derived from time-depth conversion of the K8 trough shows 150 m (500 ft.) of relief in the field area (Figure A.4).

The K8 is a fine-grained silty sand with interbedded shale (Figure A.5). Sidewall cores show highly-variable grainsize ranging from mud to medium sand in several samples. Shale content of the interval varies laterally, and gamma ray logs display variable blocky, fining-upward, and serrated character over the interval (Figure A.6). Variable log character makes stratigraphic correlation between wells difficult; however, four downdip wells penetrate the K8 along a NW-SE trend and have the highest K8 net pay values in the field (A-28, A-12, A-22, and A-25) (Figure A.6). Despite abundant shale and the wide range of grainsizes, good reservoir properties (32% porosity, 30% Sw, 500mD perm) characterize the K8 (Mason, 1992).

Wells penetrate both oil and gas pay intervals at the K8 level. Downdip oil pay, penetrated by the A-12, A-22, A-25, A-28, A-5, and A-27 wells is the main portion of the reservoir produced by the A-12 and A-22 wells (Figure A.4). Updip gas pay (unproduced to date) is penetrated by the A-1, A-1ST, SH#1, A-7, A-6, and A-15 wells. Below we characterize the reservoir and its production history, and present two possible geologic models.

Seismic Response

Extractions from the 1988 survey in the downdip oil zone reveal sinuous southeast-trending high-amplitude regions that correlate to net oil pay thickness at five well locations (Figures A.7a and A.8). Gas penetrations were excluded from this analysis. Maximum negative seismic amplitude correlates to oil net pay thickness of the five penetrations with a correlation coefficient of 0.98 when the A-12 outlier is dropped out (Figure A.8). Using the regression without the A-12, we calculated net pay thickness which ranges between 0 and 25 meters over short distances (100 m). Recontouring the map to fit the data at well locations results in the pay distribution in Figure A.9.

Comparison of oil and gas sand amplitude response reveals high amplitudes associated with thinner gas sands (Figure A.7). Regions of high amplitude response in the 1988 survey correspond to updip gas-saturated compartments (Figure A.7b), likely due to high reflectivity associated with gas. Thick oil sands of the downdip oil zone (A-25, 50 ft. net pay) produce amplitudes near 9000 in 1988 seismic data, while thinner gas sands (A-1, 25 ft. net pay) produce the same response (Figures A.6, A.7, and A.10).

Production Analysis

Available K8 production data is limited to the A-12 and A-22 oil wells. No gas wells produce from the K8. Oil production at the A-12 well began in September, 1989. A-22 production began in July, 1992. Through April, 1994, the time the second survey was

acquired, cumulative production was 2.3 MMbbls oil and 5.7 BCF gas. Accompanying this production was a pressure drop from an initial reservoir pressure of 8360 psia in September, 1989 to 6700 psi in June, 1994 (Figure A.11a).

According to PVT analysis from the A-12 well, K8 oil is initially undersaturated with a bubble point of 7495 psia. This implies that updip gas is not in equilibrium with oil of the A-12 and is thus in a different reservoir compartment. Yet, as we discuss below the production data suggests this may not be the case.

Production data from the K8 reservoir reveal a complex GOR history (Figure A.11b). The A-12 began production in 1989 with GOR of 900 scf/stb, plateaued near 1350 scf/stb in early 1991 and rose to 2500 scf/stb by late 1993. A second significant increase to 4000 scf/stb occurred before GOR declined through 1995 (Figure A.11.b). The A-22 began production in 1992 with an initial GOR of 1400 scf/stb rising rapidly to 4500 scf/stb by late 1993. The A-22 sanded up in 1994 and was shut in.

The differences between A-12 and A-22 GOR histories cannot be attributed to structural position and static pressure gradient effects on the timing of gas exsolution. The structural position of K8 tops in the A-12 and A-22 are 3238 m and 3224 m (10622 and 10576 ft.), respectively. For a pressure gradient of 0.3 psi/ft., the resulting pressure differential between the A-12 and A-22 is only 14 psi. This small pressure difference and the rapid rate of pressure decline between 1992 and 1994 (about 420 psi/year) suggest that the dif-

ference in GOR history for the two producing wells is due to specific conditions at those wells.

Local pressure drawdown near producing wells likely accelerated gas exsolution at the A-12 and A-22 locations before reservoir pressures reached the bubble point in early 1993. Although pressures and PVT analysis indicate the K8 reservoir dropped below the bubble point in early 1993, rising GOR's between September 1989 and December 1990 suggest the oil was already saturated.

There are two ways to interpret these data: 1) we can discount PVT data and interpret rising GOR to reflect initially saturated oil (gas cap model), or 2) assume PVT is correct, oil is initially undersaturated, and GOR data reflect changing wellbore conditions (compartment model). Below we present evidence for the two geologic models.

Geologic Model I: Compartmentalized Oil and Gas

This first of two proposed geologic models describes the K8 as a complex reservoir with three hydrocarbon-saturated compartments. This interpretation is supported by PVT analysis, well penetrations, and suggested by seismic data. We divide the reservoir into: A) a large oil compartment downdip, B) an small updip gas compartment, and C) a small gas compartment to the south (Figure A.10).

The large oil compartment (A) that contains the majority of K8 hydrocarbon reserves and is the only compartment with production. The A-12 and A-22 wells produced over 3 million barrels of oil from Compartment A between 1989 (onset of production) and the end of 1995. Six wells penetrate the compartment: A-5, A-12, A-22, A-25, A-27, and A-28. In seismic profiles, the compartment can be distinguished by subtle discontinuities in seismic reflectors. Figure A.10 delineates compartments in map view and in seismic profiles.

The interpretation of two gas-saturated compartments is supported by log data, seismic data, and the presence of oil at a higher structural level than gas. Compartments B and C contain gas based on interpretation of density-neutron crossover similar to the response from the A-1 well (Figure A.12). The A-6, A-15, and A-21BP wells penetrate Compartment B, and the Shell #1, A-1, A-1ST, and A-7 wells penetrate Compartment C (Figures A.10, A.12). No well produces from either gas compartment. Within these wells, there is no evidence of a gas/oil contact, though this may be difficult to distinguish in neutron-density logs.

The three compartments were defined from 1994 seismic data which has better resolution than the 1988 (pre-production) survey. The subtle discontinuities in seismic reflectors tie to low amplitude response on the amplitude extraction and suggest compartment boundaries in seismic profiles. The updip limit of Compartment A approximates structural contours, and in the gas cap model below, this is interpreted to be the gas-oil contact.

In addition to the seismic and log data supporting reservoir compartments, we note that the level of lowest known gas in the A-7, A-1, and SH#1 wells is deeper than oil in the A-5 and A-27 wells (Figure A.12). This implies that gas from these wells (Compartment C) is not in communication with oil pay sands (Compartment A). These observations are not conclusive because lateral variations in sand quality limit reliability of density-neutron crossover interpretation.

Geologic Model II: Gas Cap Reservoir

The second possible K8 reservoir model consists of a gas cap that expands as pressure declines due to A-12 and A-22 production. This model assumes that oil is initially saturated, although PVT reports describe oil as undersaturated with a bubble point 865 psi below initial reservoir pressures. This contradiction may be due to poor sampling of reservoir fluids, although PVT analyses for K8 and K40 oil yield similar bubble point pressures. In this model, we note that the change in seismic character at the updip boundary of the oil compartment closely follows structural contours and may in fact record the gas-oil contact.

Well penetrations do not clearly identify an oil-water contact. No sidewall cores sample the interval in updip gas penetrations, and density-neutron crossover is ambiguous because of poor sand quality in updip wells. Sidewall cores from the A-5 well (sampled in 1986) contain oil at a level equivalent to gas condensate sampled in A-27 sidewall cores (sampled in March, 1992). The A-1 ST well penetrates the K8 at a structural level (3197 m -

10490 ft. subsea) equivalent to the A-5 and A-27 oil penetrations. The cleanest sand in the A-1ST exhibits strong crossover response that is structurally equivalent to A-5 oil-saturated sand (Figure A.12).

In this model, pressure decline and gas exsolution should lead to gas cap expansion. This scenario would likely be recorded by production GOR data that increase throughout the producing life of the well. Additional evidence of gas cap expansion may be condensate in A-27 sidewall cores sampled after 2.5 years of production (March 1991) (Figure A.12, A-27 well).

Seismic Differences

Significant increases and decreases in seismic amplitude across the K8 horizon occur between the 1988 (pre-production) and 1994 (syn-production) 3-D seismic surveys (Figure A.13). Increases are prominent updip of the A-12 and A-22 producing well locations as well as in the northeast corner of block 296, where the A-28 well was drilled for water-injection purposes (January 1997). Strike-parallel amplitude decreases, downdip of producing wells, contrast with the updip amplitude increases. Barring extraneous seismic acquisition or processing effects, differences between seismic amplitudes should be due to impedance changes in the reservoir. With this assumption, we predict that brightening in Figure A.13 is due to gas exsolution and migration. Dimming can result from compaction or water influx as increased K8 sand impedance reduces the impedance contrast of the sand-shale interface.

These significant changes in seismic amplitude during production between 1988 and 1994 coincide with a 1660 psi pressure drop (Figure A.11a). The 1660 psi pressure drop due to K8 production between 1989 and 1994 likely resulted in gas exsolution and reservoir compaction. Both effects produce impedance changes in the reservoir (Burkhart, 1997). These impedance changes are significant, but more work is needed to interpret the seismic response from simultaneous compaction and gas exsolution during pressure decline. Qualitatively, we predict brightening, or increased amplitude, associated with increased gas saturations. Likewise, we predict dimming associated with compaction or water influx.

Mechanisms for Seismic Differences

To address brightening updip of producing wells, we look to migration of gas, whether as gas cap expansion or secondary migration between compartments. Gas exsolution centered around producing wells likely caused 'brightening' observed at the K8 horizon after six years of production (Figure A.13). We know from high production GOR's that large volumes of gas were exsolved and produced during 1993 and 1994 (Figure A.11b). Unproduced free gas, when saturations are above irreducible, is able to migrate updip of the well, and we interpret this to have caused significant brightening updip of the producing A-12 and A-22 wells. Dimming in the southern portion of the reservoir may be due to compaction associated with the large pressure drop and potential weak water influx.

Regions where the reservoir is initially gas saturated should exhibit dimming if gas

migrates due to the combination of decreased gas saturation and compaction associated

with pressure decline. This is a potential explanation for dimming near the A-1 well (Fig-

ure A.13). We cannot confidently explain significant dimming observed south of the A-25

well, because no wells penetrate this area and it is unclear whether that portion of the res-

ervoir is initially gas-saturated or oil-saturated (Figure A.13).

Seismic Differences and Proposed Geologic Models

How do seismic differences and proposed mechanisms relate to our inferred geologic

models? We observe dimming downdip of producing wells and in the southern gas com-

partment near well A-1. Significant brightening is prevalent updip of producing wells and

in the northern portion of the oil compartment. If the oil compartment is isolated from

updip gas compartments, we expect differences to be restricted to regions of amplitude

associated with oil-saturated sands.

Volumetric comparisons of produced gas with original solution gas volumes and predic-

tions of exsolved gas volumes, suggest that the majority of exsolved gas was produced.

We calculate an initial dissolved gas volume of 15.3 BSCF (billion standard cubic feet)

using PVT data and in place reserves (initial = 10.4 STB) calculated from a mass balance

equation assuming no gas cap and no water drive. In 1994, remaining oil is 8.1 STB con-

taining 9.5 BSCF of dissolved gas. Of 5.8 BSCF exsolved gas, 5.7 BSCF was produced.

Remaining free gas in the reservoir (0.1 BSCF) should produce an average saturation of

1%, a value lower than typical irreducible saturations. These calculations contradict interpretation of seismic brightening with increased gas saturation updip. This result is intriguing in that it indicates another source of produced gas may be present if geologic model I is correct. If a gas cap does exist, a new mass balance equation must be used for the reservoir, and calculated gas volumes will change.

Possible secondary gas migration between inferred oil compartments may resolve discrepancies in produced gas volumes by providing an additional source of gas to the reservoir (Figure A.14a). This would also explain dimming observed in the southern gas compartment. Producing wells are located in the oil compartment, no producers drain the gas compartments. Pressure decline would initially be restricted to the oil compartment, but as the gradient between the oil and gas compartments increases, gas potentially could migrate from Compartments B and C to the oil compartment. This would account for the dimming in the southern gas compartment. Pressure drop and accompanying compaction due to the removal of fluids would increase the reservoir impedance, reducing the impedance contrast between the sand and bounding shales. Furthermore, migrating gas would decrease reservoir impedance and cause brightening in the oil compartment.

Seismic differences observed at the K8 reservoir may also be produced in a gas cap reservoir. Because volumetric analysis and production data indicate a lack of exsolved gas in the reservoir, a downward-migrating gas-oil contact may be a plausible way of explaining brightening in the oil zone (Figures A.13b, A.14b). The brightening, however, is not evenly distributed across the reservoir, but is concentrated in the northern portion of the

field. Downdip brightening can be attributed to gas exsolution and trapping of exsolved gas by permeability barriers.

Downdip dimming in the oil zone is problematic because gas exsolution and migration may be acting simultaneously with compaction. Compaction acted on the reservoir from 1990 to 1992, prior to pressures reaching the bubble point (Figure A.11a). When gas exsolution began in 1992-1993, gas may have migrated updip to the producing wells, but irreducible gas saturation should remain in the downdip zone. Thus, barring seismic acquisition or processing effects on observed differences, we propose that the impedance increase due to compaction (2-3 porosity unit decrease) is greater than the decrease in impedance due to the irreducible gas saturation.

Potentially, weak water drive produces the narrow band of dimming on the western margin of the reservoir. The A-28 well logged approximately 5 meters of wet sand in January, 1997 which indicates a small amount of water influx after 7 years of production. Perhaps the weak water drive combined with compaction forces overcame the impedance effect of irreducible gas saturations to produce observed dimming.

Further work on this reservoir should focus on isolating the correct model for K8 hydro-carbon distributions. Careful log interpretation of oil and gas penetrations linking neu-tron-density crossover to percent sand estimates may be able to accurately identify a gas-oil contact, or its absence. Also, careful analysis of production data relating GOR to pro-duction rates and PVT data should help to identify the correct geologic model.

New data should provide significant insight on reservoir response to reservoir fluid changes. Water injection at the A-28 well could be monitored by a new 3-D survey acquired over the field. Effective water sweep could produce significant amplitude decreases east of the A-28 where the 1994 survey suggests elevated downdip gas saturations. Pressure data from updip gas-saturated intervals would help our assessment of the connectivity between downdip oil and updip gas. Furthermore, fluid composition data from updip and downdip compartments would help us to favor one model. Finally, cased hole log analysis, with new logging runs could be compared to seismic changes to better understand the saturation changes associated with brightening.

References

Anderson, R.N., A. Boulanger, W. He, Y.F. Sun, L. Xu, and B. Hart, 1996, 4-D seismic monitoring of reservoir production in the Eugene Island 330 Field, Gulf of Mexico, *in* P. Weimer and T.L. Davis, eds., Applications of 3-D seismic data to exploration and production, AAPG Studies in Geology, No. 42 and SEG Geophysical Developments Series, No. 5: AAPG/SEG, Tulsa, p. 9-20.

Burkhart, T., 1997, Time-lapse seismic monitoring of the South Timbalier block 295 field, M.S. Thesis: Pennsylvania State University.

Greaves, R.J., T.J. Fulp, 1987, Three-dimensional seismic monitoring of an enhanced oil recovery process: Geophysics, v. 52, p. 1175-1187.

Hoover, A.R., 1997, Reservoir and production characteristics of the South Timbalier 295 field, offshore Louisiana, with outcrop analogues and comparison to 4-D seismic results: M.S. Thesis, Pennsylvania State University, 115 p.

Mason, E.P., 1992, Reservoir geology and production performance of turbidite sands at South Timbalier 295 Field, offshore Louisiana, Transactions of the 42nd annual GCAGS convention, Jackson, MS, v. 42, p. 267-278.
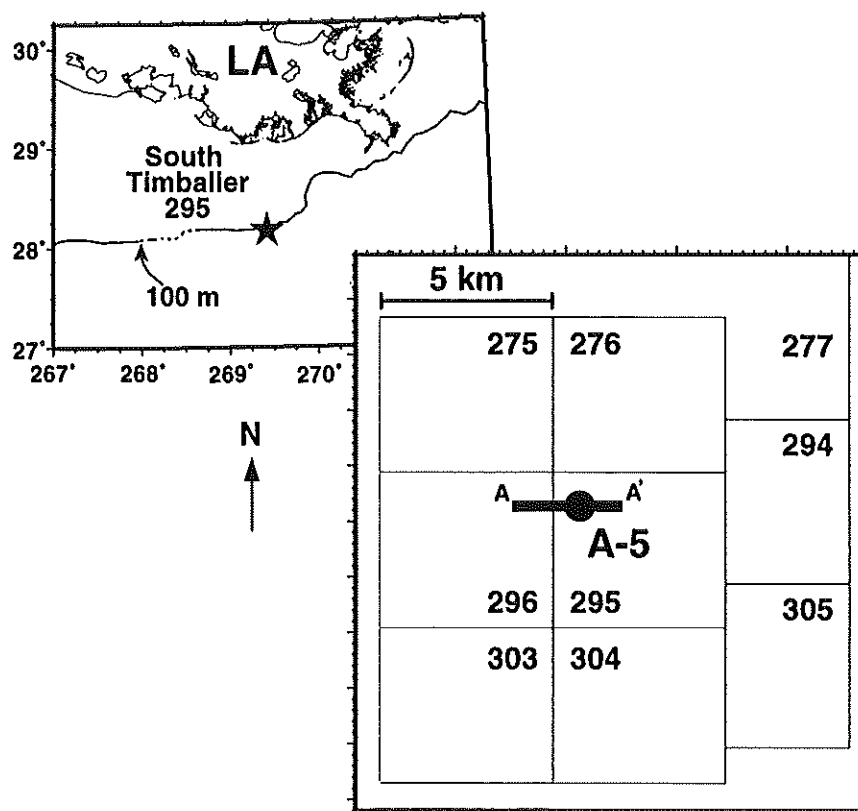
Figure A.1. South Timbalier 295 basemap. The field is located 120 miles south of New Orleans in 290 feet of water. Traverse A-A' is seismic line in Figure A.3. Blocks are 5 km (3 mi.) square.
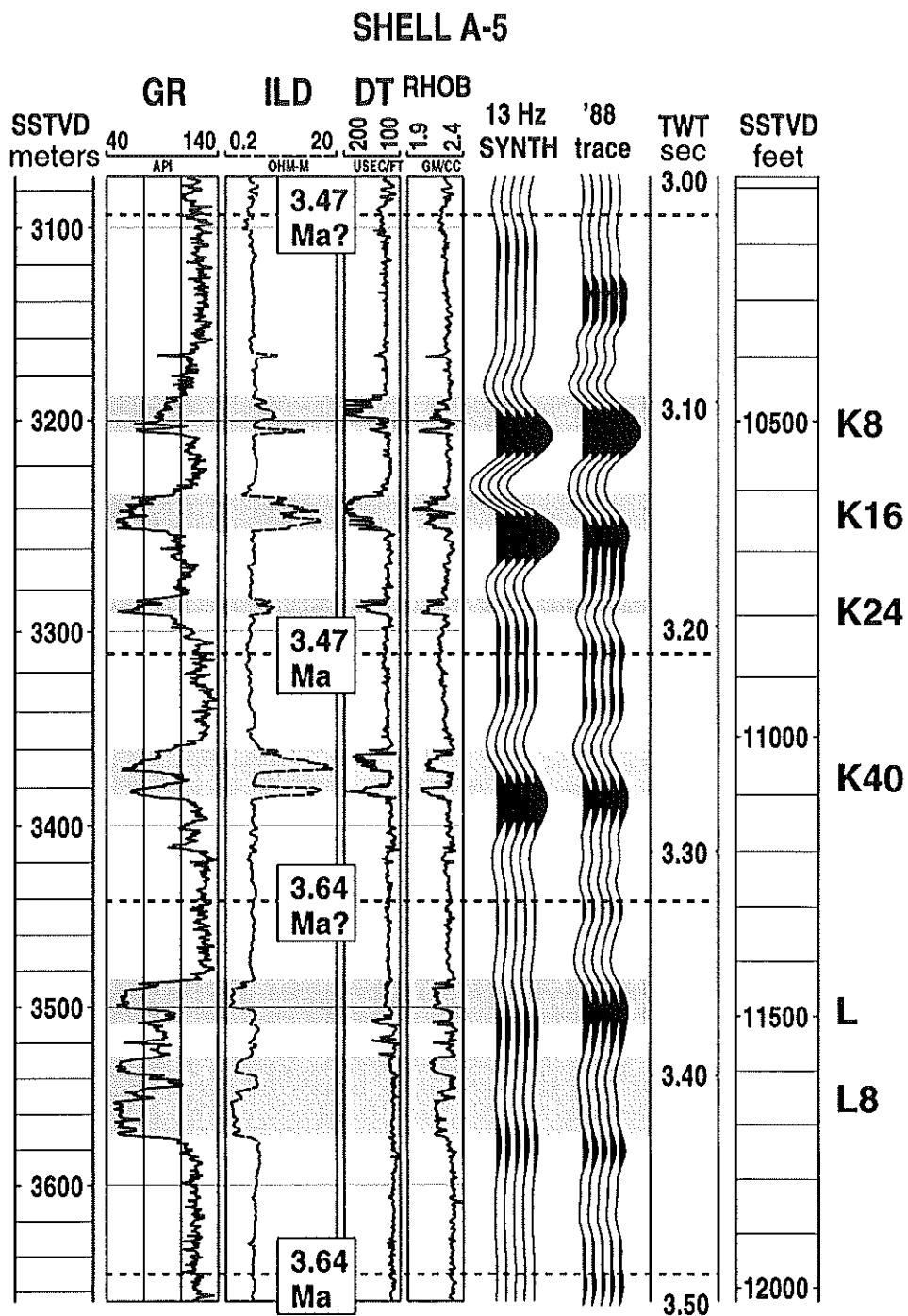
SHELL A-5

Figure A.2. Type log with synthetic tie: gamma ray, deep induction (resistivity), sonic, and density logs from the Shell A-5 well are tied to a 13 Hz zero phase synthetic seismogram and a seismic trace extracted along the A-5 well path. K and L sands are late Pliocene age with biostratigraphic age dates of near 3.5 million years. Seismic troughs in synthetic and extracted trace tie to sand tops. Oil-saturated K sands have lower impedance (product of density and velocity) than shales and wet L sands.
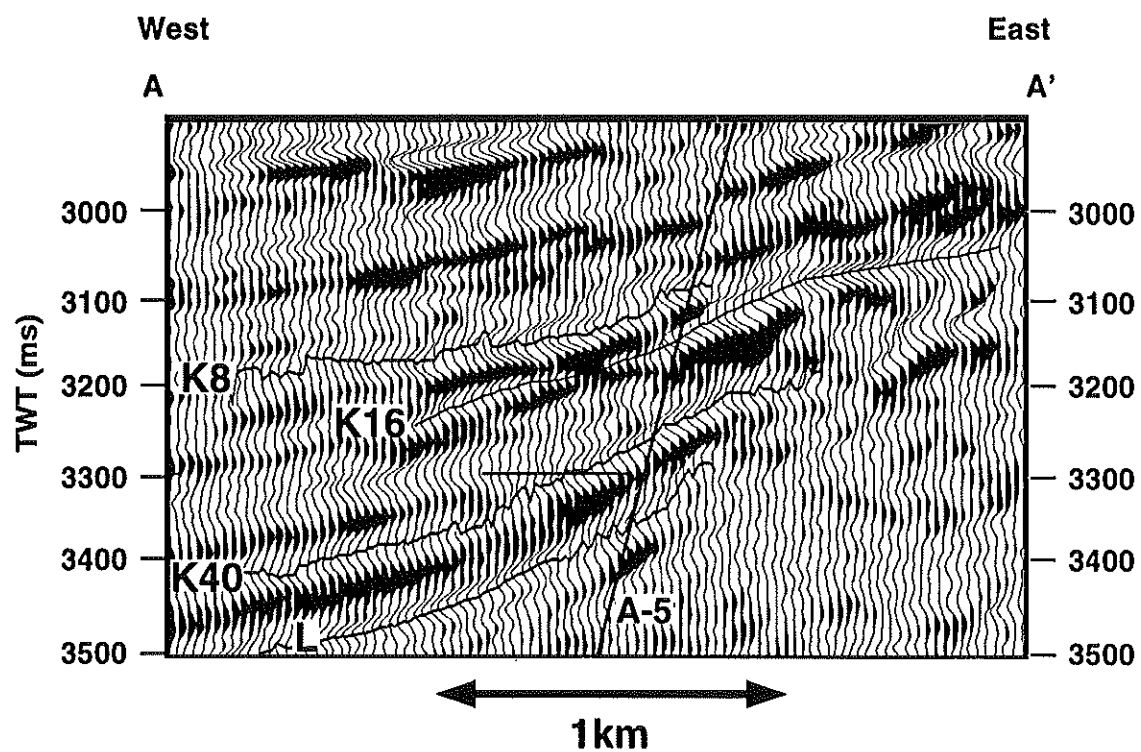
Figure A.3. West-east seismic line through the A-5 well penetration shows the stacked turbidite pay horizons at 3.0-3.3 seconds. All horizons pinch out updip against the structural high to the east. K40 and L show good continuity, K8 and K16 do not. K8 masks the K16 signal over significant areas.
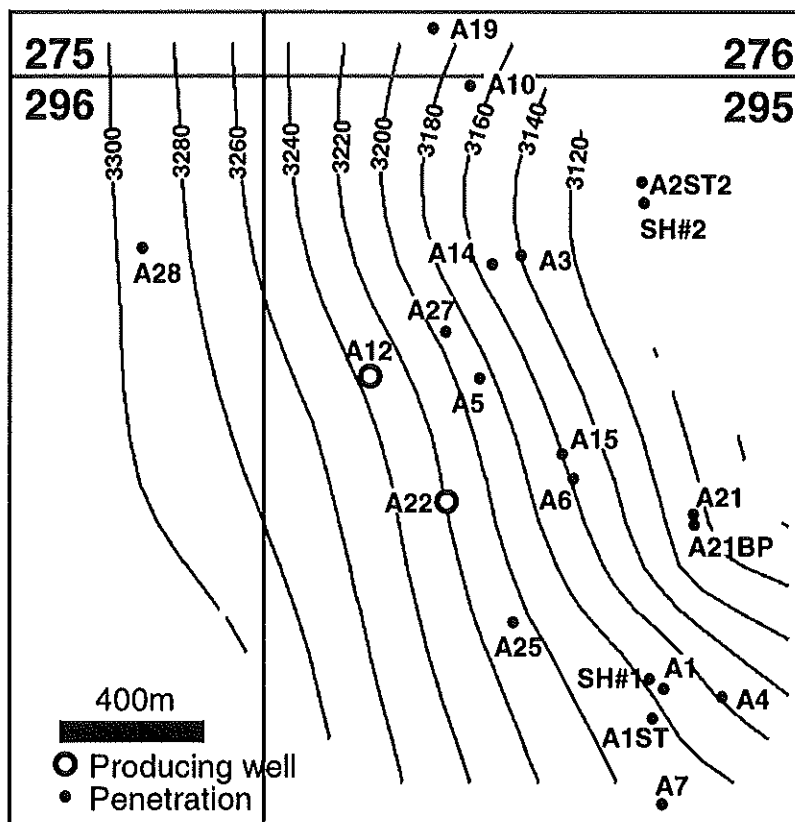
Figure A.4. Structure map of the K8 sand top. Structural relief is 200 m (980 ft.) from western extent of the reservoir to the pinchout against structure to the east. Structure contours are derived from seismic travel times and tied to penetration depths at well locations. Contour interval is 20 m, producing well locations displayed as open circles.

295 Shell A-25
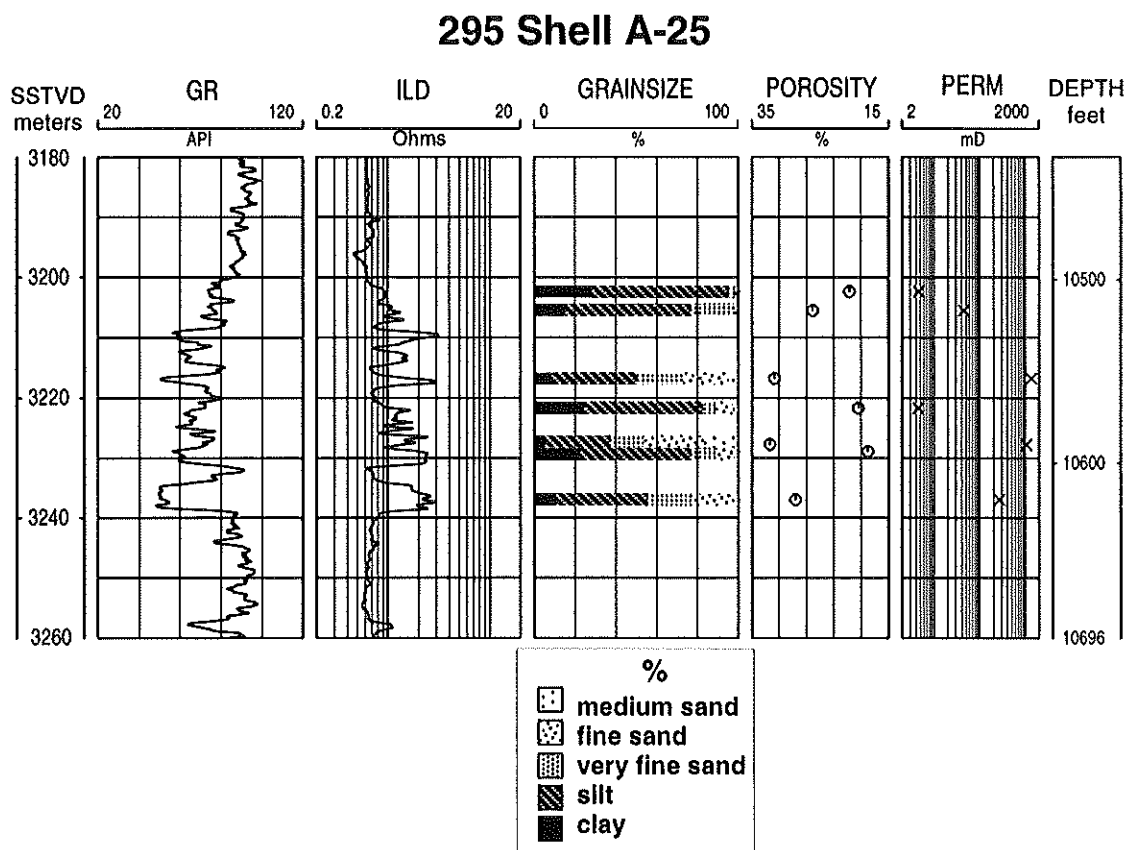
Figure A.5. Plot of K8 log character and grainsize distribution in A-25 well. Well location plotted in Figure A.4. Gamma ray (GR) and deep induction (ILD) logs show interbedded, fining-upward log character. Grainsize abundance plotted with bar scales indicate percentage of sample within grain-size range. Grainsize, porosity, and permeability data obtained from sidewall cores.
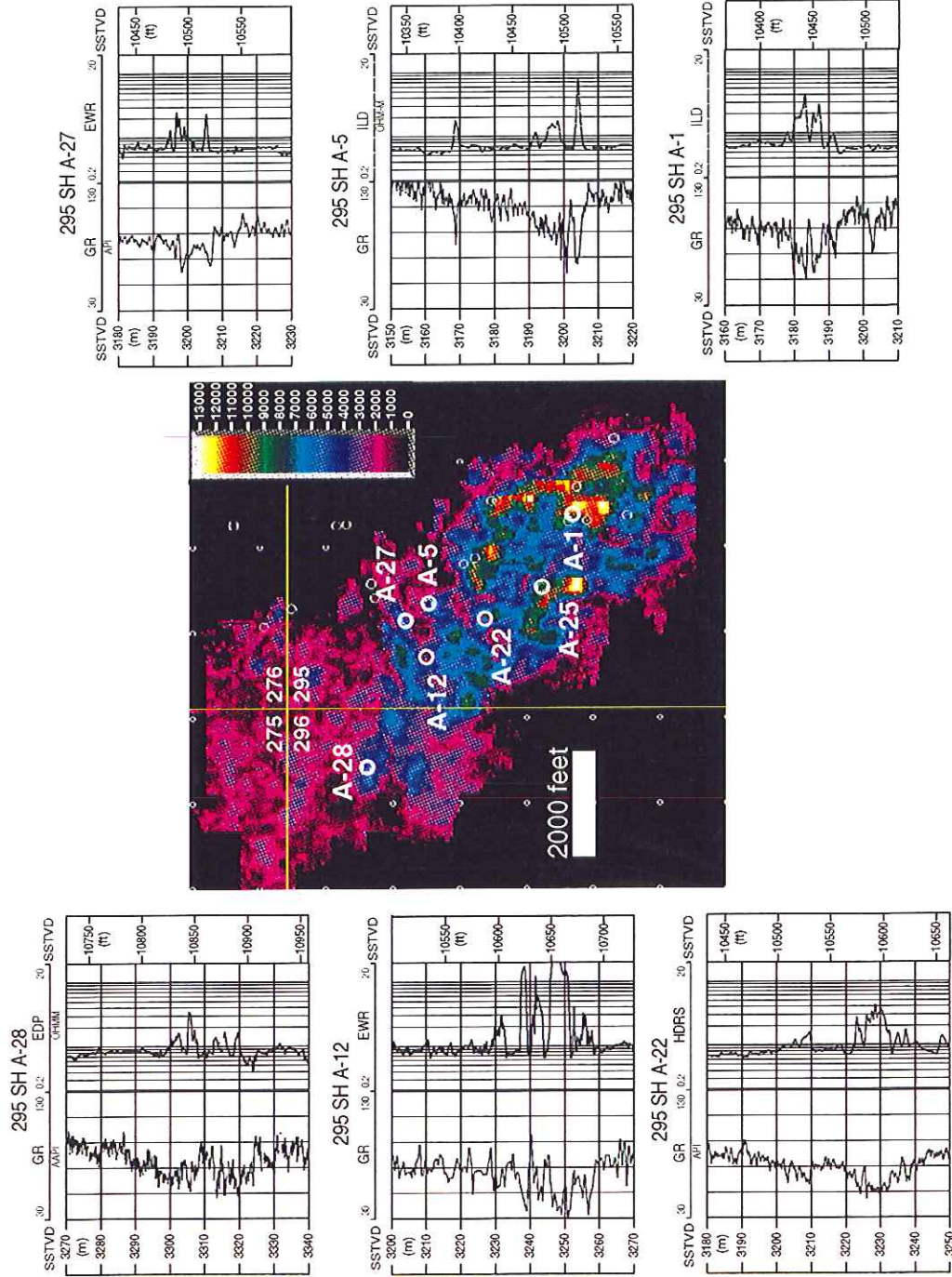
Figure A.6. Well log signatures and 1988 amplitude map: Gamma ray and resistivity logs from six wells in ST295 and ST296 show log character related to seismic amplitude. Greater net sand correlates to higher amplitude except for thinner gas sands in A-1 well that produce the greatest seismic amplitude response.
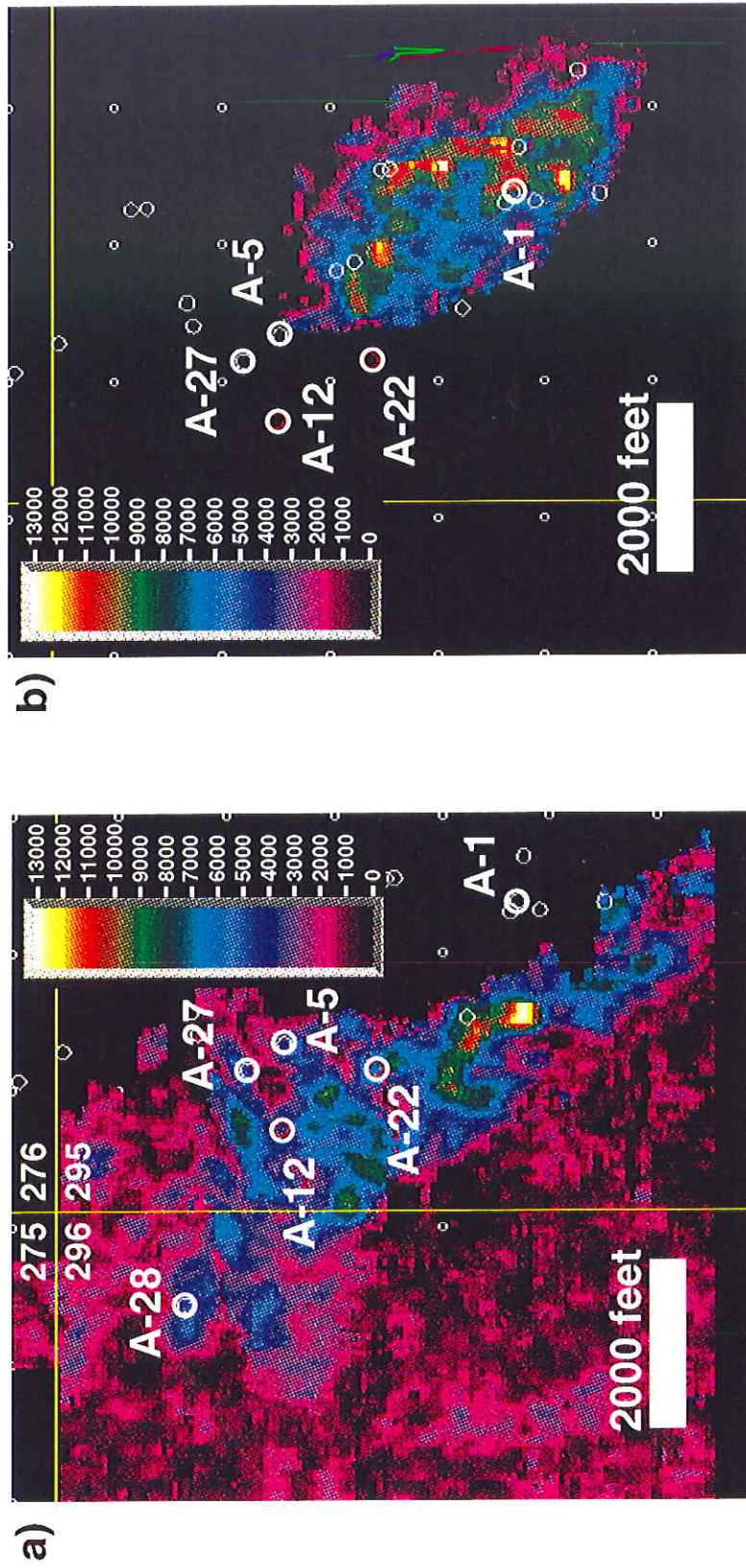
Figure A.7. a) 1988 maximum negative amplitude from 10ms window extracted from top of oil compartment (mapped on seismic trough) with locations of wells from Figure A.4. b) 1988 maximum negative amplitude extracted from 10ms window at top of gas compartment (mapped on seismic trough). Color scale is identical for both maps.
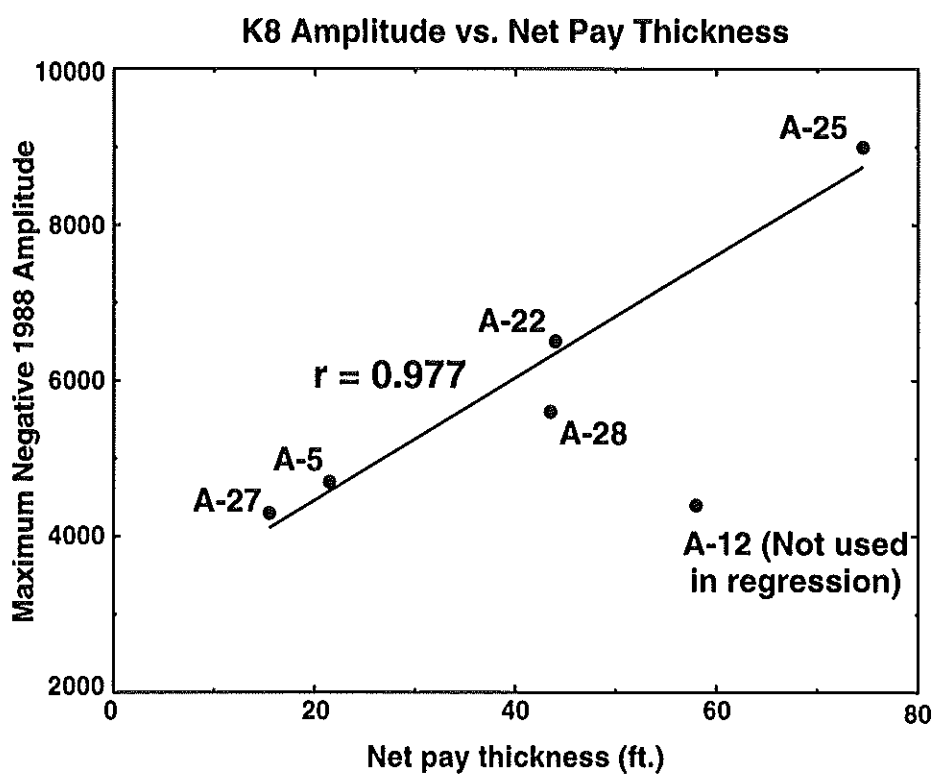
K8 Amplitude vs. Net Pay Thickness

Figure A.8. Net Pay vs. Amplitude crossplot: Six penetrations of K8 oil compartment (compartment A) used to crossplot net pay thickness and maximum negative amplitude. The regression line with correlation coefficient 0.977 was derived from only 5 points, the sixth (A-12) was not used. We use this correlation to map net pay thickness over the field area (Figure A.9).
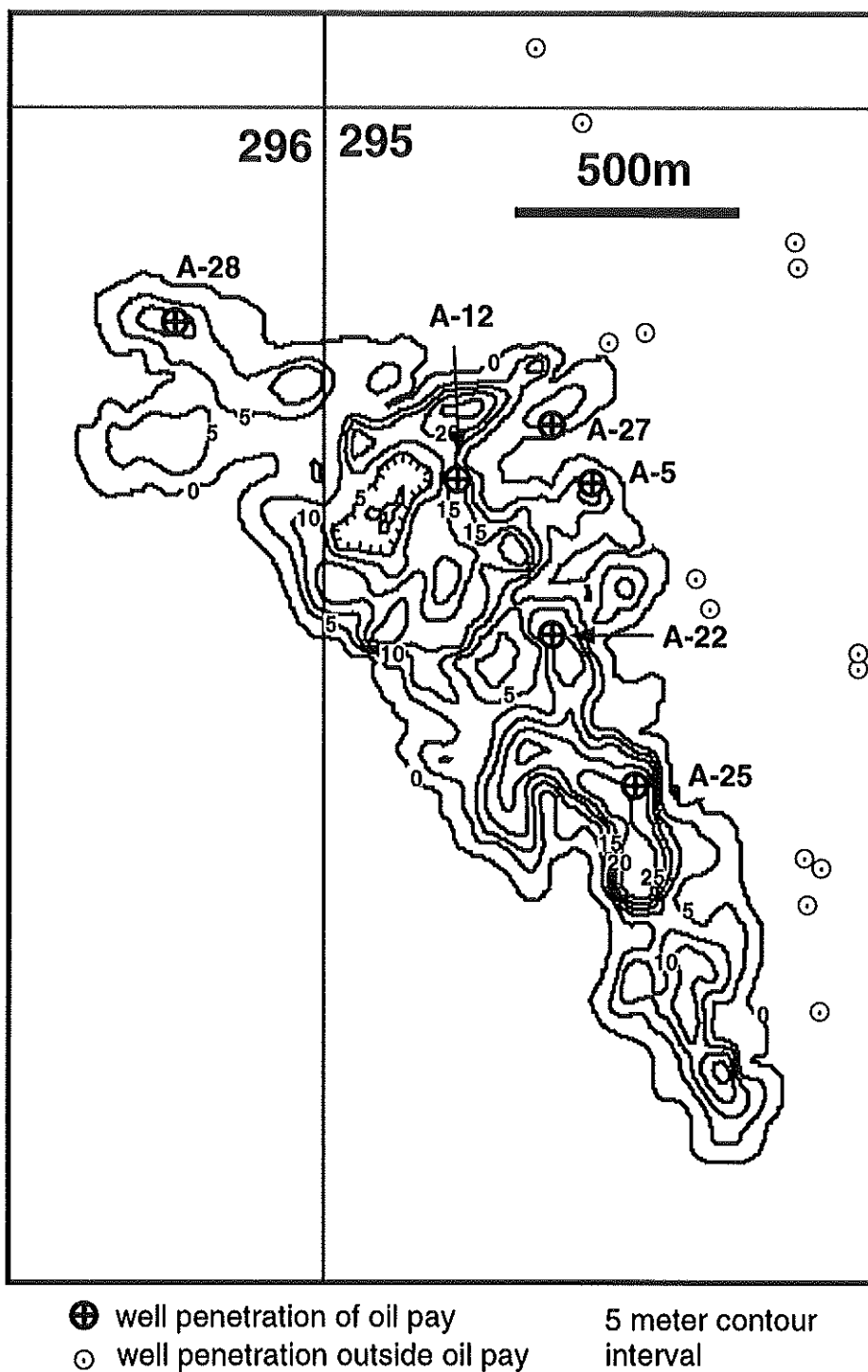
Figure A.9. Net pay thickness map of downdip oil zone derived from net pay vs. 1988 seismic amplitude correlation of Figure A.8. Map was recontoured to fit known net pay thickness at all six well penetrations of the oil zone.
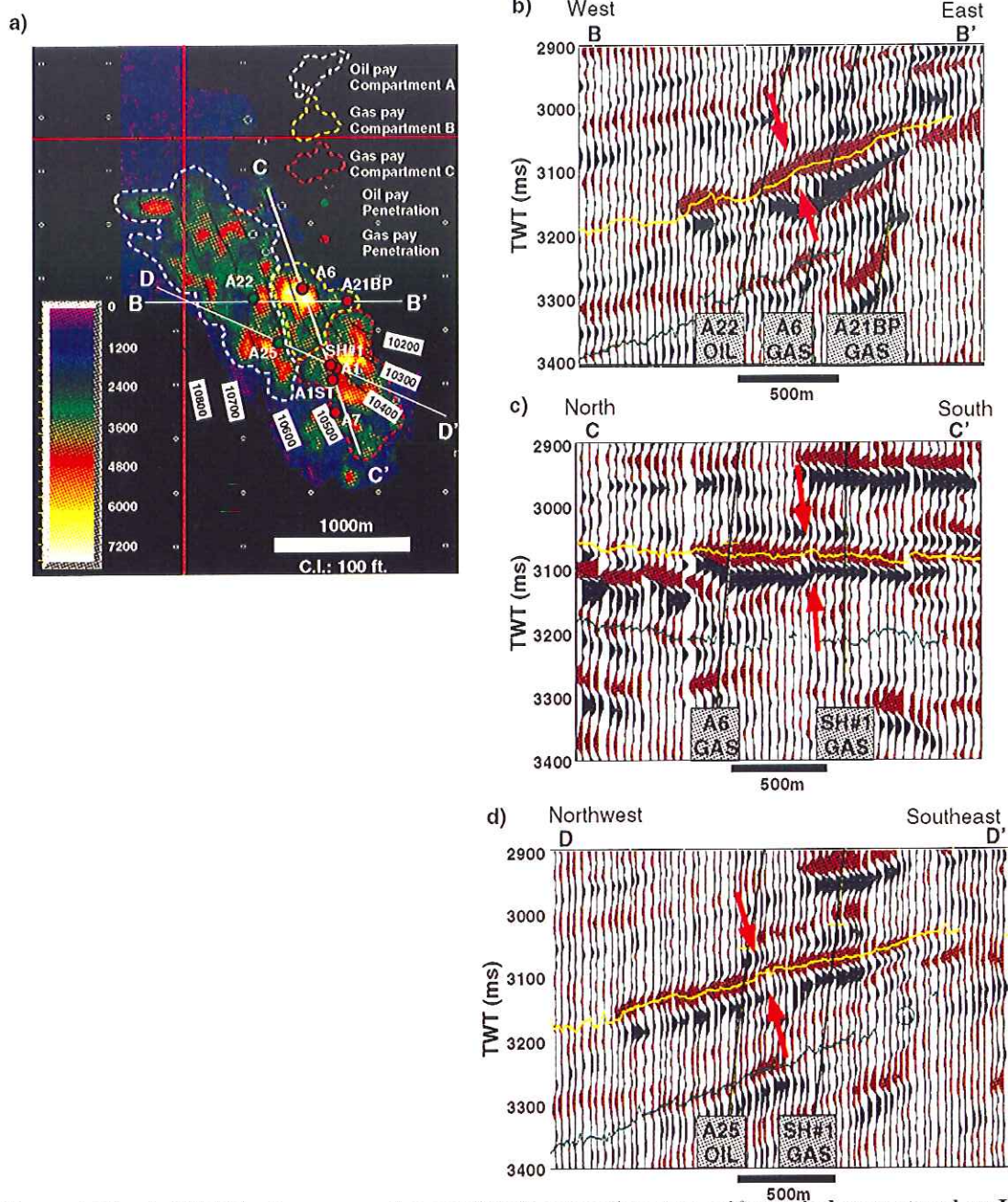
Figure A.10. a) 1994 Maximum negative amplitude extraction over a 10ms window centered on K8 horizon. Seismic profiles B-B', C-C', and D-D' are mapped with intersected wells. Interpreted reservoir compartments are outlined in white (A), magenta (B), and red (C). Compartment boundaries are highlighted in seismic profiles by red arrows. b) West-east seismic profile B-B' through A-22 (producer), A-6, and A-21BP wells. K8 is yellow horizon, K40 is mapped below in green. The change in wavelet character between A-22 and A-6 is interpreted as the boundary between compartments A and B. c) North-south seismic profile C-C' through A-6 and Shell #1 wells shows a change in wavelet character 700 feet north of Shell #1 well that is interpreted as the boundary between compartments B and C. d) Northwest-southeast seismic profile D-D' through A-25 and Shell #1 wells. Change in wavelet character 300 feet southeast of A-25 penetration is interpreted as boundary between compartments A and C.
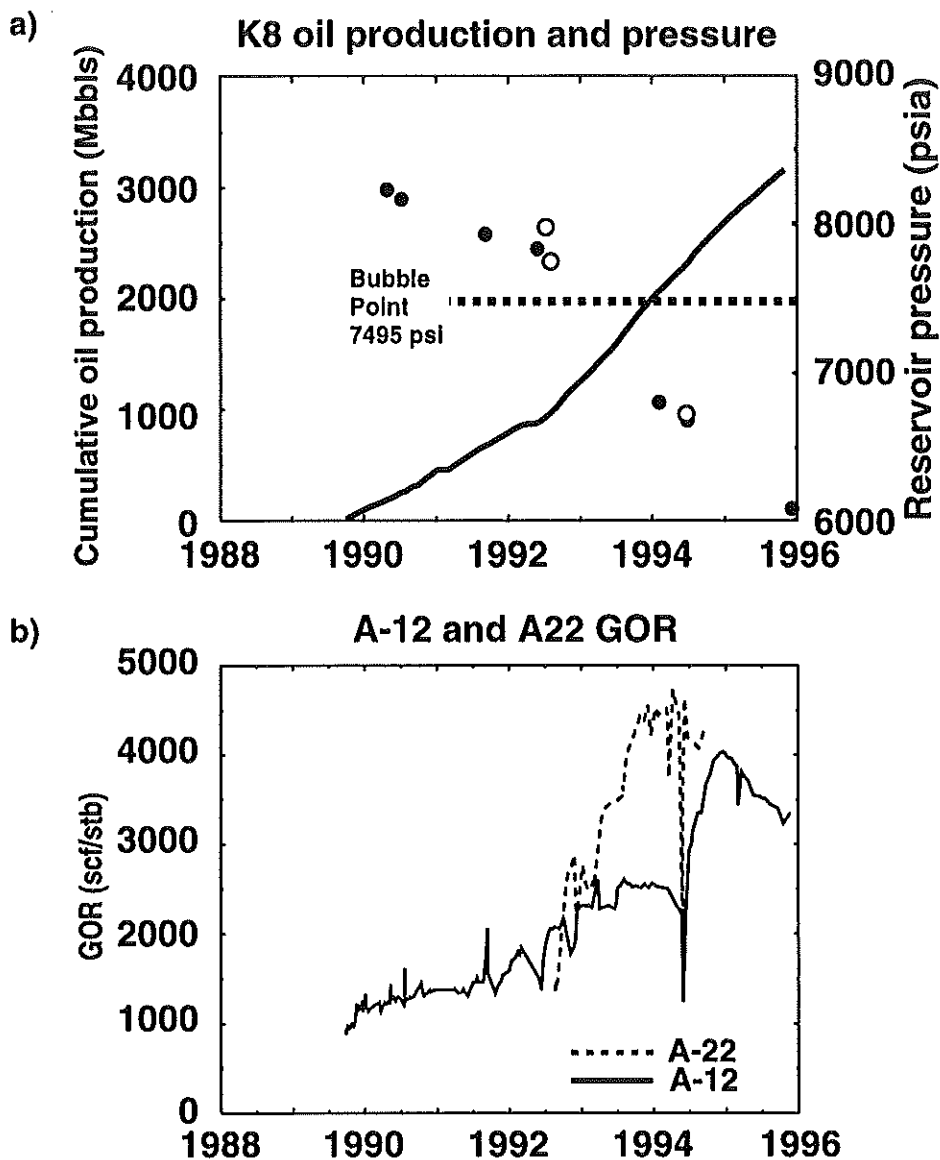
Figure A.11. a) Cumulative oil production and reservoir pressure measurements from A-12 and A-22 wells. Oil was initially undersaturated with bubble point of 7495 psia. Pressure values reflect estimated reservoir pressure, not local wellbore pressure, measured from A-22 (filled circles) and A-12 (open circles) and referenced to 10600 ft. subsea depth. a) Gas-oil-ratio from A-12 and A-22 wells measured in standard cubic feet gas per stock tank barrel oil (industry standard) increases with time, rising sharply with increased A-12 production in 1994.
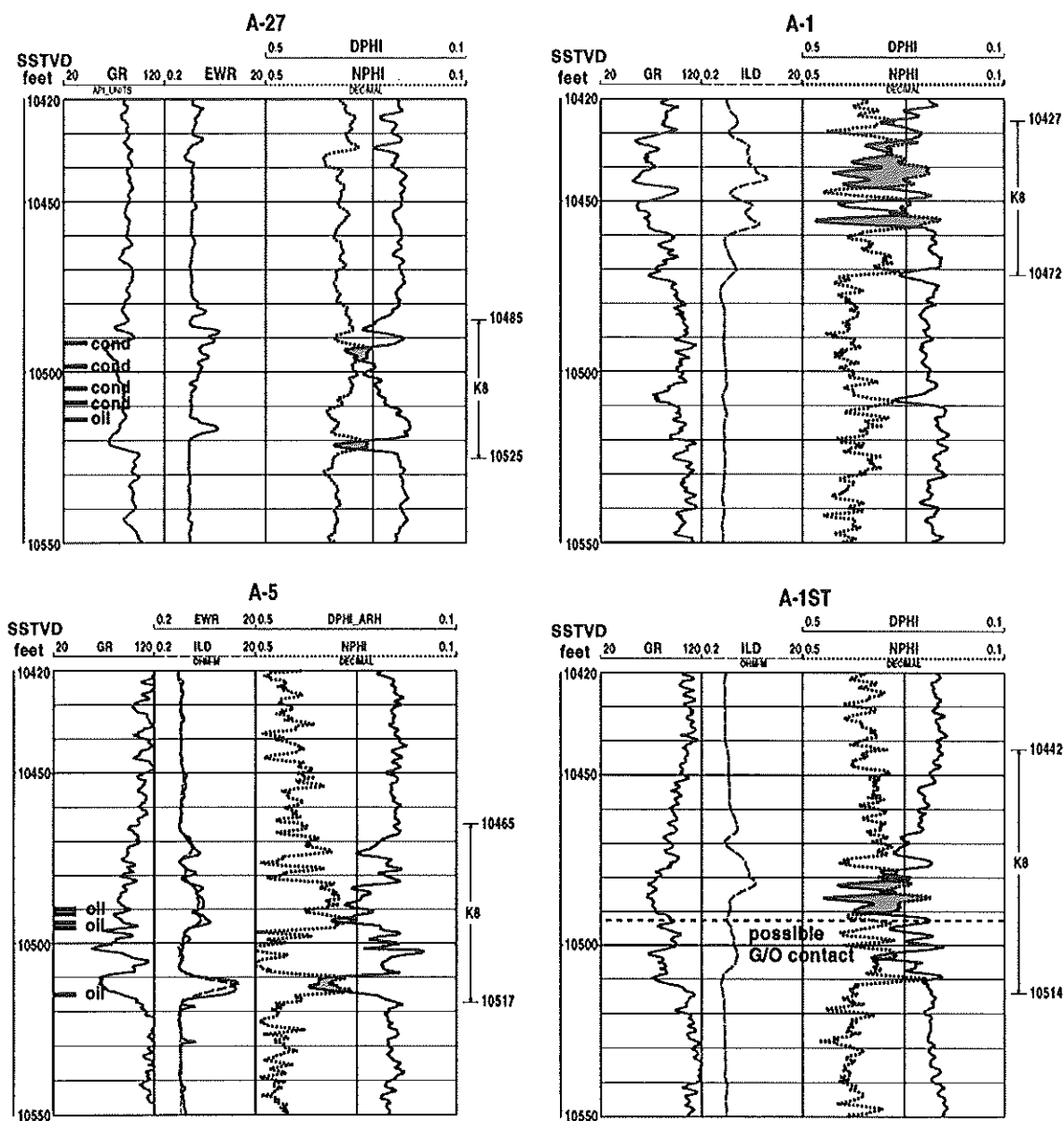
Figure A.12. Well logs of updip oil wells (A-27 and A-5) and southern gas wells (A-1, A-1ST): gamma ray (GR), EWR (resistivity logging-while-drilling tool), deep induction (ILD), neutron porosity (NPHI) and density porosity (DPHI). See Figures A.4, A.10, and A.13 for well locations. Crossover in neutron-density porosity logs does not clearly identify a gas-oil contact in the K8 reservoir. A-27 and A-5 wells show very little crossover only in the cleanest sands. A-1 and A-1ST show significant crossover in clean sands and gas inferred from crossover in the A-1ST appears to occur at the same level as oil in the A-5 well. A-5 response is somewhat ambiguous due to poor sand quality relative to the A-1ST at the same level. Potential gas-oil contact may be near 10500 ft. subsea depth below which A-1ST exhibits less crossover (although in poorer sands) and above which A-5 shows near-crossover in poor sands
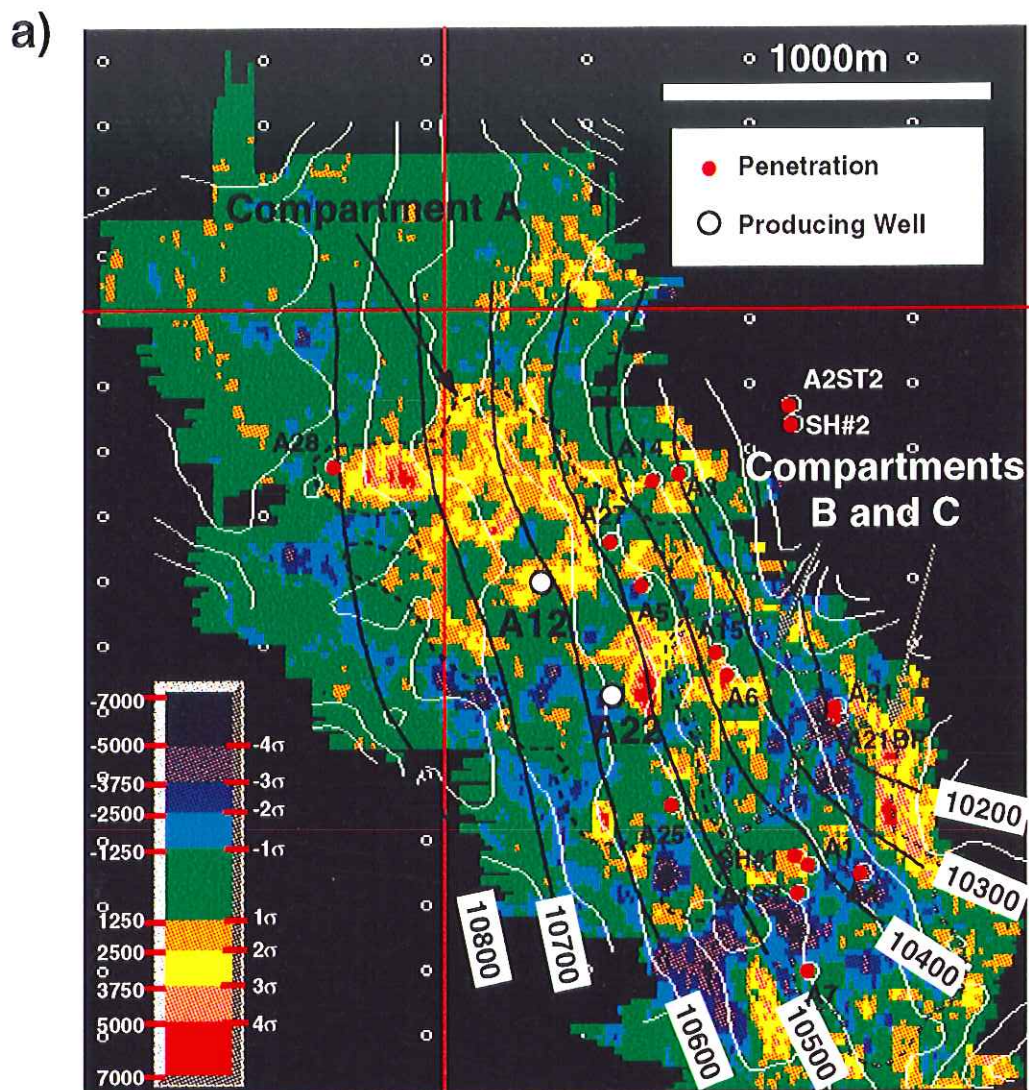
Figure A.13a. Seismic difference map: average values extracted from difference volume over a 10ms window centered on the K8 horizon. Inferred reservoir compartments are overlain, with dimming dominating the southern gas compartment (C), and brightening occurring over most of the oil compartment (A) and the northern gas compartment (B). Possible compaction acting in the gas compartments may be responsible for dimming with potential secondary migration (due to pressure gradient between compartments) causing brightening in oil compartment. Possible water influx may be responsible for the linear trend of dimming at the downdip limit of compartment A. This scenario is depicted schematically in Figure A.14a. Color bar is plotted in terms of standard deviations above or below the mean difference, which is zero.
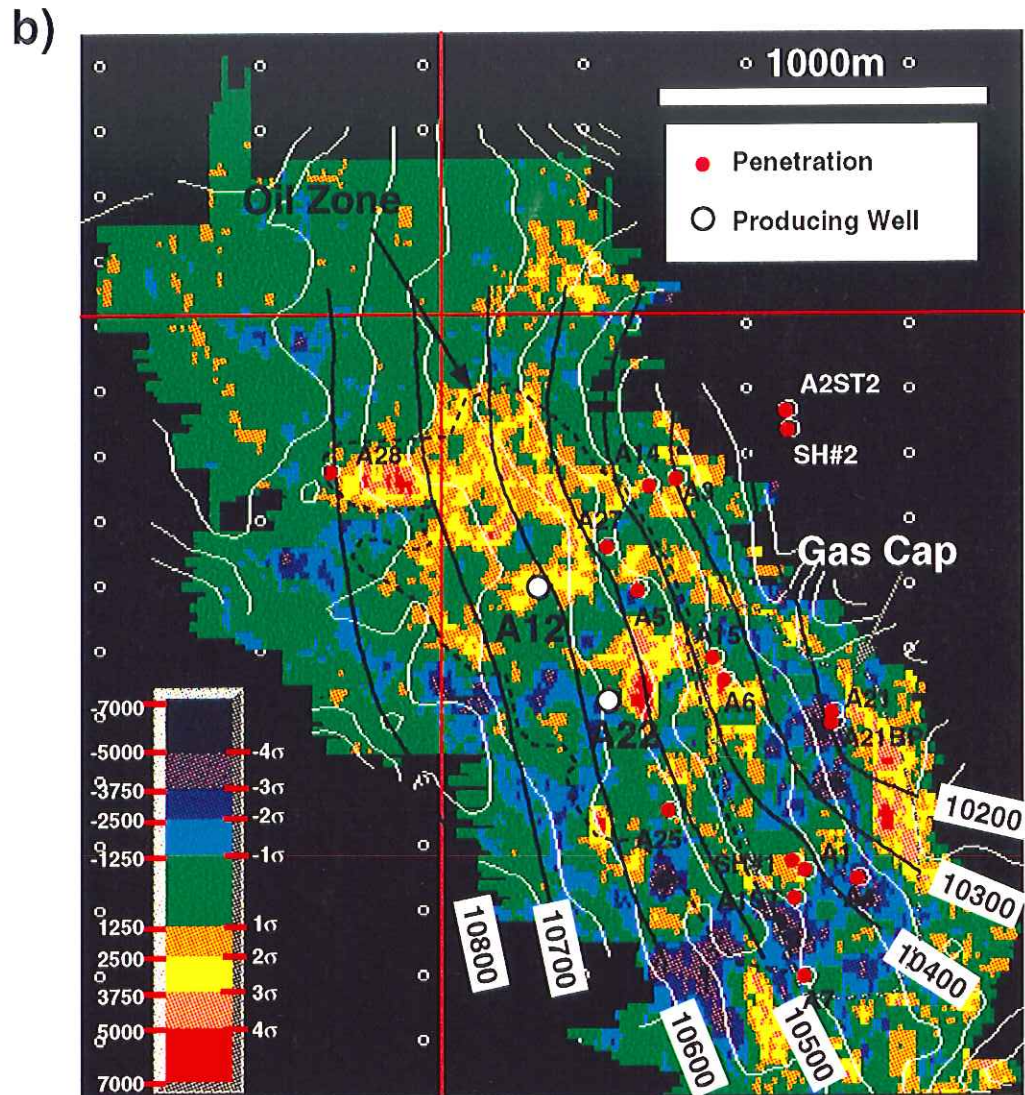
Figure A.13b. Seismic difference map on K8 horizon, same map as Figure A.13a, with outlines of possible oil leg and gas cap. The updip limit of the oil leg approximately follows structure. In our model, pressure decline produces reservoir compaction in the gas cap, brightening occurs over most of the oil leg due to gas cap expansion. This scenario is depicted in Figure A.14b. Trapped exsolved gas in the downdip oil zone may explain brightening in the oil compartment. We have no explanation for strong dimming in the south. As in Figure A.13a, dimming along western margin may possibly be due to water influx.
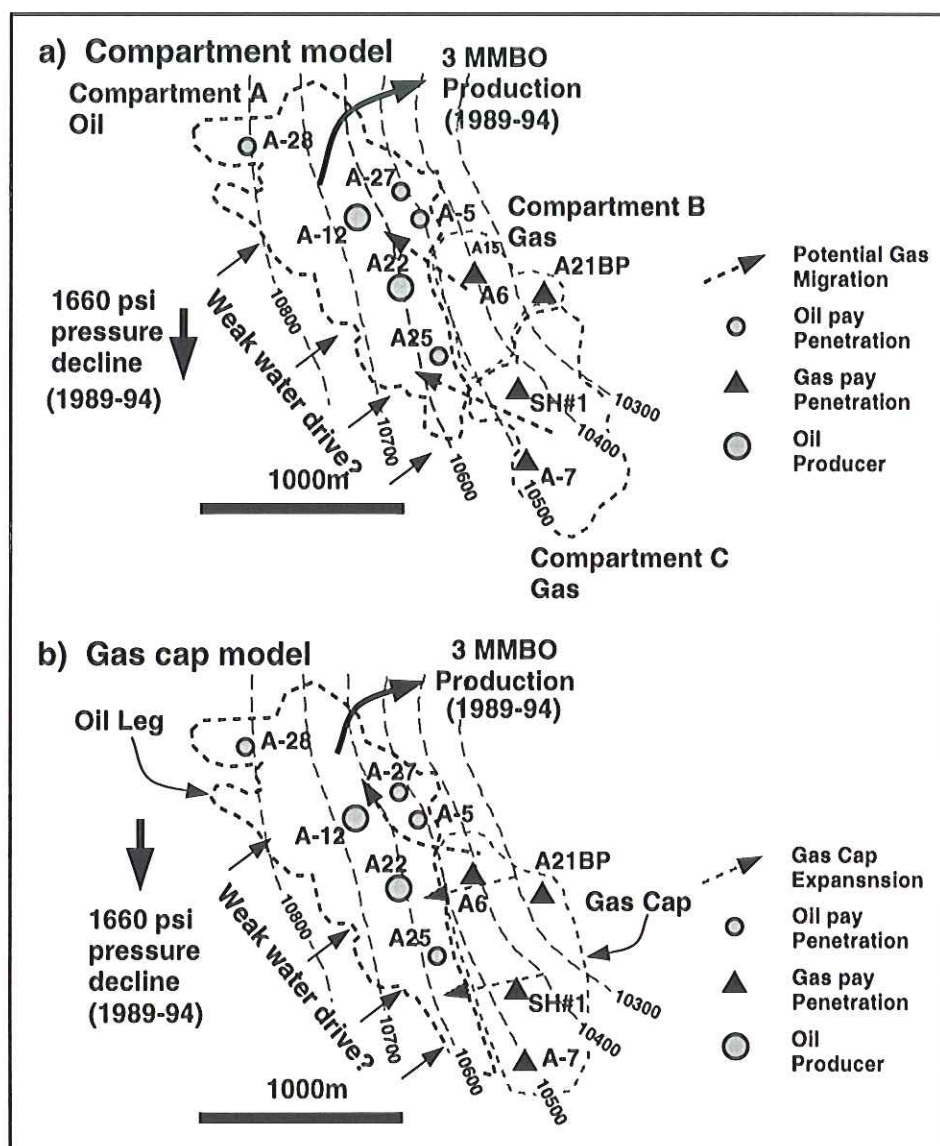
Figure A.14. Cartoon describing potential geologic models and possible mechanisms for producing seismic differences. a) Compartment model produces secondary gas migration from updip compartments due to pressure decline from oil production in compartment A. This could cause observed brightening in compartment A and dimming due to fluid loss and compaction in compartments B and C. Three compartments are outlined and arrows indicate potential gas migration. b) Gas cap model explains brightening in oil zone through gas cap expansion and gas exsolution. Trapped gas may cause brightening observed downdip in the vicinity of the A-28 well. As with the compartment model, compaction associated with pressure decline in the gas cap should produce dimming. Both models have potential water influx due to weak water drive along western margin of the reservoir.